Vol. 65 • No. 11
November 2022

Microwave Journal

IoT 6G 5G

horizon house®
Founded in 1958
mwjournal.com

DORADO JQL FERROCOM

HIGH POWER & BROADBAND CIRCULATORS

JQL introduces a new family of high power and broadband circulators with industry's best electrical performance. These units are designed to handle extremely high CW input power and significantly high peak power levels for shorter duration. Devices undergo 100% inspection under X-Ray and thermal imaging cameras. JQL has successfully incorporated advanced process and materials technology to handle extreme conditions and harsh environments necessitated by the RF & Microwave industry

Features & Benefits

- ✔ Superior electrical performance
- ✔ Compact size & Light weight
- ✔ Excellent repeatability
- ✔ SWaP-C incorporated
- ✔ RoHS compliant

Suitable For

- ✔ Test & Measurement equipment
- ✔ Medical instruments
- ✔ SATCOM uplink
- ✔ Military communication
- ✔ Electronic warfare
- ✔ Public safety systems

Hi-Σ Series Hybrid Drop in Circulator

- *2400 to 2500 MHz*
- *300 Watts CW Power*
- *0.18 dB Insertion loss*
- *over -40°C to +85°C*

X-Band Waveguide Circulator

- *2500 W Pulse power*

X-Band High Power SMT Circulator

- *250 W Pulse power*
- *5.9 mm diameter*

Octave Band Coaxial Circulator

- *2-4GHz 250W*
- *4-8GHz 150W*
- *8-18GHz 150W*

LEARN MORE, DROP US AN E-MAIL

MADE IN USA

1255 ARMOUR BLVD
MUNDELEIN, IL 60060
USA

+1-(888) 236-9828 (US)
+1-(630) 930-9917 (INTL)

JQLTECHNOLOGIES.COM
DORADO-INTL.COM
FERROCOMRF.COM

SALES@JQLTECHNOLOGIES.COM

1 MHZ TO 50 GHZ

Mesh Network Test Systems

Simulate Real-World Mesh Communication in Your Lab

- Port counts from 3 to N
- Independently controlled attenuation on every path
- Attenuation range up to 120 dB

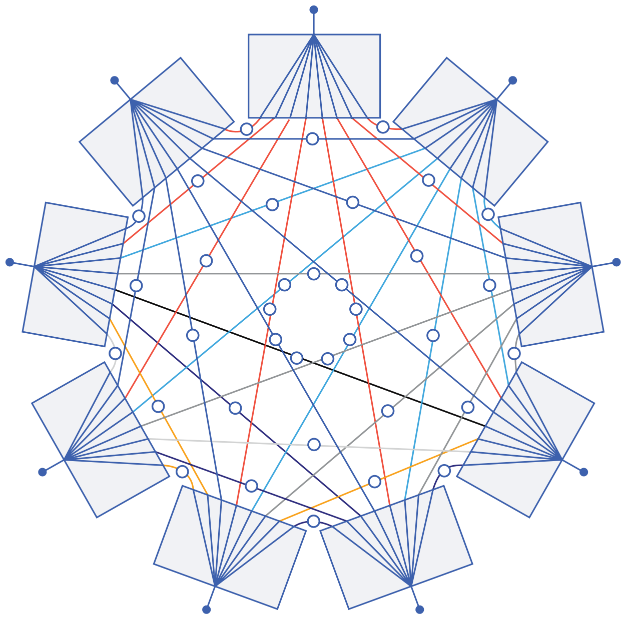

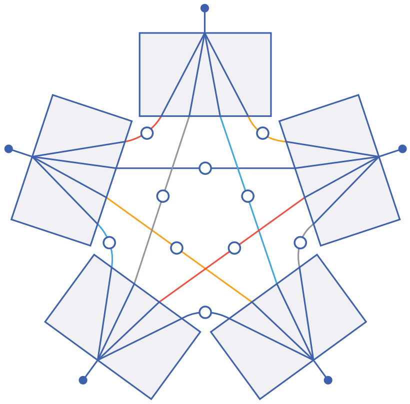

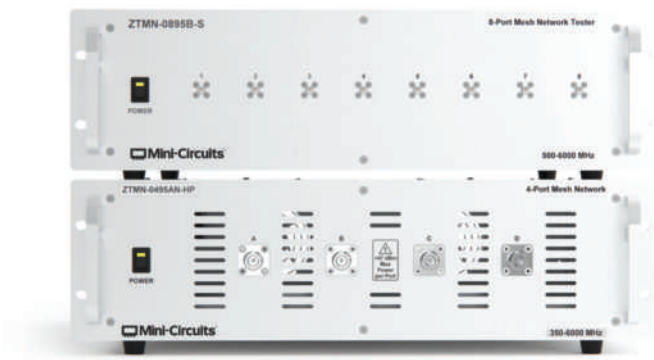

Ideal for testing receiver sensitivity, changes in range between devices, effects of interference on performance and more!

Common applications:

- R&D testing of wireless “smart” devices
- Bluetooth, Zigbee, Z-Wave, Wi-Fi, IoT
- Qualification / acceptance testing of military radios
- UHF / VHF band man-pack / vehicular systems
- PMR / TETRA

Mini-Circuits


RF-LAMBDA
THE LEADER OF RF BROADBAND SOLUTIONS
BROADBAND SSPA / EMC BENCHTOP
SOLID STATE POWER AMPLIFIER
0.1-22GHZ
ULTRA BROADBAND SSPA
RFLUPA01M22GA
4W 0.1-22GHZ
RFLUPA0218GB
20W 1-19GHZ
300W 6-18GHZ SOLID STATE BROADBAND
400W 8-11GHZ
SOLID STATE BROADBAND
0.1-6GHZ VHZ,
UHF, L, S, C BAND
RFLUPA02G06GC
100W 2-6GHZ
RFLUPA0706GD
30W 0.7-6GHZ
MADE IN USA
6-18GHZ C, X, KU BAND
RFLUPA08G11GA
50W 8-11GHZ
RFLUPA0618GD
60W 6-18GHZ
RFLUPA06G12GB
25W 6-12GHZ
18-50GHZ K, KA, V BAND
RFLUPA18G47GC
2W 18-47GHZ
RFLUPA27G34GB
15W 27-34GHZ
RFLUPA47G53GA2
10W 47-53GHZ
RFLUPA27G34GB
30W 18-40GHZ
BENCHTOP RF MICROWAVE SYSTEM POWER AMPLIFIER
RAMP00G06GA- 30W 0.01-6GHZ
RAMP39G48GA- 4W 39-48GHZ
RAMP01G22GA- 8W 1-22GHZ
RAMP27G34GA- 8W 27-34GHZ
www.rflambda.com
sales@rflambda.com
1-888-976-8880
1-972-767-5998
San Diego, CA, US
Carrollton, TX, US
Ottawa, ONT, Canada
Frankfurt, Germany

apitech™
We help you navigate the complexities of wireless test
From guidance to gear, get there with APITech
For more information vist:
apitech.com/wireless-test


AMPLICAL
Let Amplical
Jump Those Hurdles for You
with our Complete In-House Design, Manufacturing and Test Capabilities
Customers can depend on us for quick order fulfillment, competitive pricing and dedicated service.
Let us prove our commitment to you today.
High performance standard and custom Control Components and Amplifiers to 40GHz.
• EW Systems
• Communications Systems
• Radar
• Test
• Simulation
Products:
• Switches
• Attenuators
• Phase Shifters
• Limiters
• Switch Matrices
• Broadband Amplifiers
• Low Noise Amplifiers
• High Power Amplifiers
• Custom Components and Sub-assemblies
Phone: 973-386-1119
Fax: 973-386-1131
E-mail: info@amplical.com
web: www.amplical.com

BROADBAND LOW NOISE AMPLIFIERS

- Industry's Lowest Noise Figure up to 50 GHz
- Internal Voltage Regulation
- Gain & OP1dB values can be optimized to meet your requirement
- Internal Reverse Voltage Protection
- Unconditional Stability
- 2-IN-1 Dual Use Connectorized or Surface Mount
- Form, Fit, Function & Custom Package Designs
- Hermetic Sealing
- Military or Aerospace Screening

See more at: https://www.pmi-rf.com/categories/amplifiers

PLNA-30-10M20-292FF

PEAFS3-14-10M22G-292FF

LNA-0R518G-45-10DBM-SFF

PMI Model No.	Frequency Range (GHz)	Gain (dB)	Gain Flatness (dB)	Noise Figure (dB)	OP1dB (dBm)	Configuration Size (Inches) Connectors
PEAFS3-14-10M22G-292FF	0.01 - 22	14	±0.8	2.5	+14 (0.01 - 18 GHz) +13 (18 - 22 GHz)	0.53" x 0.70" x 0.26" 2.92mm (F) Removable
PLNA-30-10M20-292FF	0.01 - 20	28	±2.5	2.5	+14 (0.01 - 18 GHz) +13 (18 - 20 GHz)	0.53" x 0.70" x 0.26" 2.92mm (F) Removable
LNA-0R518G-45-10DBM-SFF	0.5 - 18	45	±2.0	2.95	+10	0.90" x 1.67" x 0.36" SMA (F) Removable

Noise Figure 10 MHz to 0.5 GHz

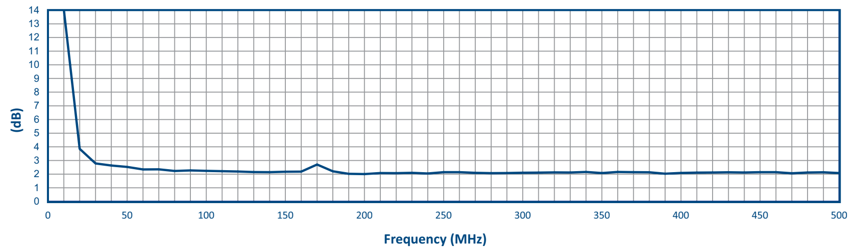

Noise Figure 0.5 to 18 GHz

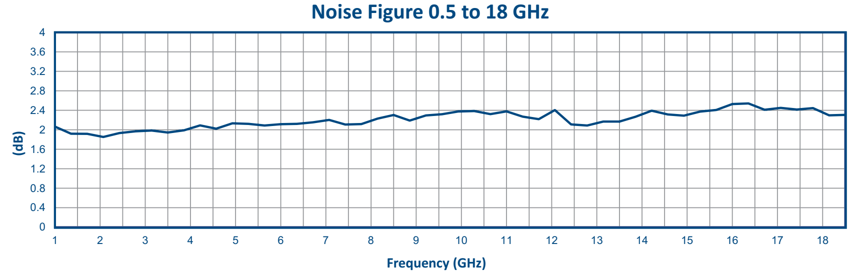

Noise Figure 18 to 22 GHz

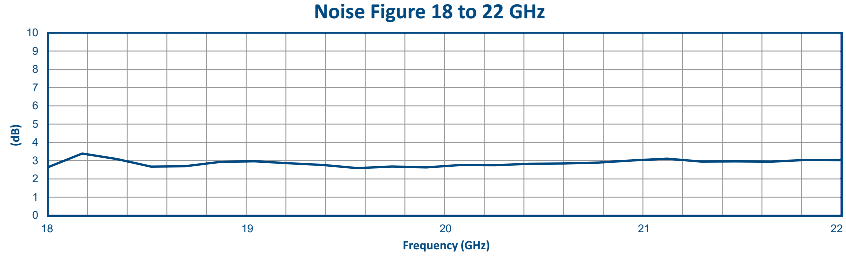

Typical data for PMI Model PEAFS3-14-10M22G-292FF

Quantic PMI
PLANAR MONOLITHICS

ISO 9001

West Coast Operation:
4921 Robert J. Mathews Pkwy, Suite 1
El Dorado Hills, CA 95762 USA
Tel: 916-542-1401, Fax: 916-265-2597

East Coast Operation:
7309-A Grove Road
Frederick, MD 21704 USA
Tel: 301-662-5019, Fax: 301-662-1731

sales@pmi-rf.com • www.pmi-rf.com

Quantic PMI
PLANAR MONOLITHICS

- Amplifiers - Solid State
- Attenuators - Variable / Programmable / Fixed
- Bi-Phase Modulators
- Couplers (Quadrature, 180°, Directional)
- Detectors - RF / Microwave
- Filters & Switched Filter Banks
- Form, Fit, Functional Products & Services
- Frequency Converters
- Frequency Sources
- Frequency Discriminators & IFM
- Frequency Synthesizers
- Gain & Loss Equalizers
- Integrated MIC/MMIC Assemblies (IMAs)
- IQ Vector Modulators
- Limiters - RF / Microwave
- Log Amps
- Miscellaneous Products
- Monopulse Comparators
- Multifunction Integrated Assemblies (IMAs)
- Phase Shifters & Bi-Phase Modulators
- Power Dividers/Combiners (Passive & Active)
- Pulse Modulators - SPST
- Rack & Chassis Mount Products
- Receiver Front Ends & Transceivers
- Single Side Band Modulators
- SMT & QFN Products
- Switch Matrices
- Switch Filter Banks
- Switches - Solid-State
- Systems - Radar Sense & Avoid
- Systems - Fly Eye Radar
- Threshold Detectors
- USB Products

Microwave Journal

November 2022
Vol. 65 • No. 11
5G/6G & IoT
mwjournal.com

CONTENTS

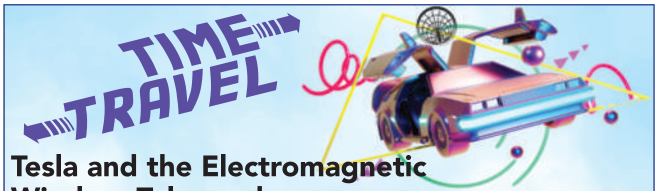

Cover Feature

Special Report

Technical Features

Special Report

Application Note

65 YEARS OF PUBLISHING EXCELLENCE

Microwave Journal CONTENTS

mwjournal.com

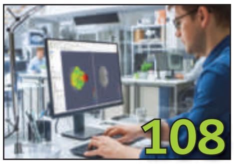

Product Feature

Tech Briefs

Departments

Microwave Journal (USPS 396-250) (ISSN 0192-6225) is published monthly by Horizon House Publications Inc., 685 Canton St., Norwood, MA 02062. Periodicals postage paid at Norwood, MA 02062 and additional mailing offices.

POSTMASTER: Send address corrections to Microwave Journal, PO Box 1028, Lowell, MA 01853 or e-mail mwj@e-circ.net.com. Subscription information: (978) 671-0446. This journal is issued without charge upon written request to qualified persons working in the RF & microwave industry. Other subscriptions are: domestic, $120.00 per year, two-year subscriptions, $185.00; foreign, $200.00 per year, two-year subscriptions, $370.00; back issues (if available) and single copies, $10.00 domestic and $20.00 foreign. Claims for missing issues must be filed within 90 days of date of issue for complimentary replacement.

STAFF

EXECUTIVE EDITORIAL OFFICE
685 Canton Street, Norwood, MA 02062
Tel: (781) 769-9750
FAX: (781) 769-5037
e-mail: mwj@mwjournal.com

EUROPEAN EDITORIAL OFFICE
16 Sussex Street, London SW1V 4RW, England
Tel: Editorial: +44 207 596 8730 Sales: +44 207 596 8740
FAX: +44 207 596 8749

SUBSCRIPTION SERVICES
Send subscription inquiries and address changes to:
Tel: (978) 671-0446
e-mail: mwj@e-circ.net

www.mwjournal.com

Printed in the USA


SM4234
SM4477

Microwave Journal ONLINE .COM

E LEARNING CENTER

Manufacturing Advantages of 3D-Printable Digital Foams Over Traditional Foam Cores for Very Low Dk Solid PCB Antenna Applications
Sponsored by: Fortify 11/30

Catch *Frequency Matters*, the industry update from *Microwave Journal*,
microwavejournal.com/FrequencyMatters

WHITE PAPERS

Copper Mountain Technologies — Near and Far-Field Antenna Measurement

ERZIA — Comparing Linearity Measurements in a GaN Ka-Band Satcom Power Amplifier

JFW — Supercharging your VNA with an RF Matrix Switch (VNA Port Extension)

Modelithics — Take Advantage of Ultra-Broadband Capacitor Models

Rohde & Schwarz, Make ideas real — Debugging Conducted Emissions with Oscilloscopes Made Easy

Rohde & Schwarz, Make ideas real — 5G NTN Takes Flight

Look for additional content from:

Coilcraft   Knowles Precision Devices

Executive Interviews

Jonas Ehinger, new CEO of **Gapwaves**, discusses the company's progress commercializing its waveguide technology, targeting growth and profitability from the automotive radar and mmWave 5G markets.

Todd Cates, co-owner of RF/microwave components distributor **HASCO**, describes trends in the industry and how HASCO is responding to serve the evolving needs of its customers, particularly the move to mmWave.

Join Us Online

Follow us
@Pathindle
@MWJGary
@MWJEditor

Join us at the RF and Microwave Community

Become a fan at facebook.com/microwavejournal

Visit us @ mwjournal.com

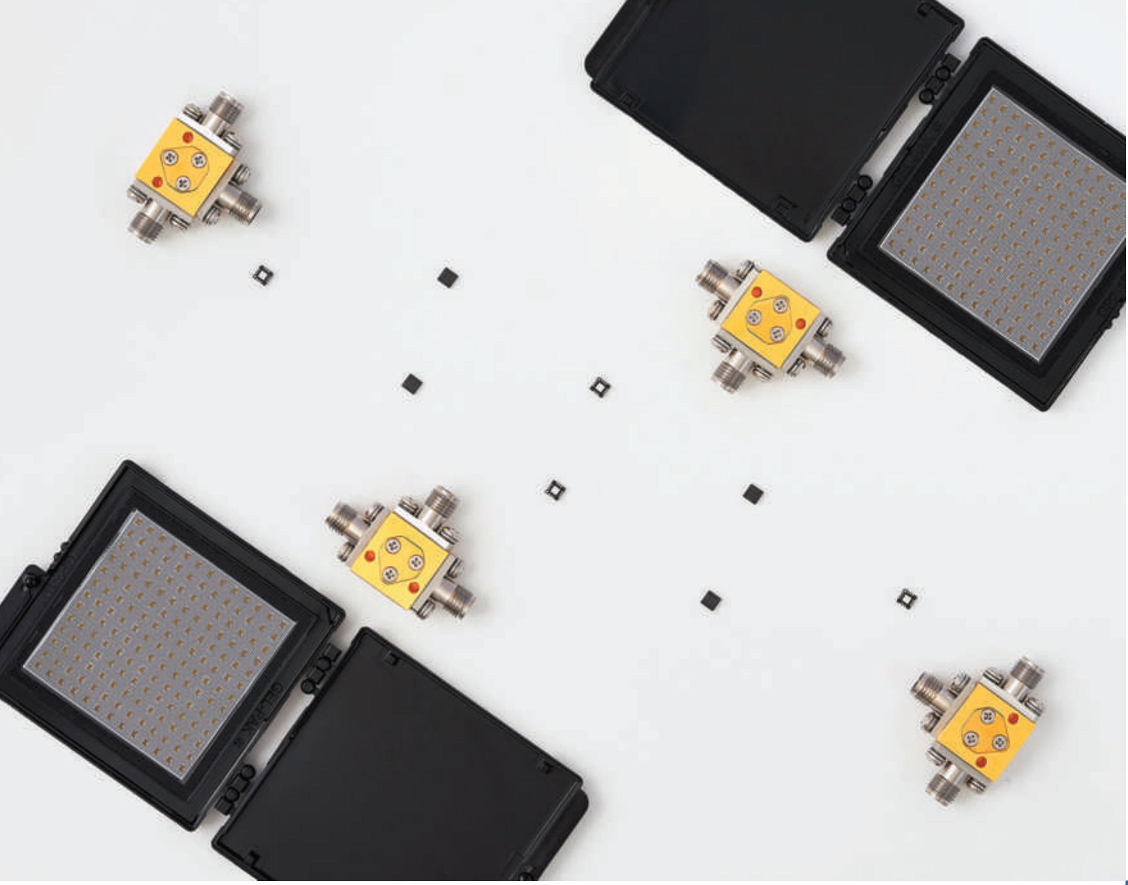

10 TO 65 GHZ

mmWave Mixers

Ultra-Wideband Frequency Conversion

- IF band as wide as DC-20 GHz
- Connectorized, SMT and die formats available
- LO to RF Isolation as high as 45 dB
- Conversion loss as low as 8.4 dB
- Useable as an up and down converter
- Suitable for 5G, WiGig, defense radar and communication, and more

Mini-Circuits®

STAY CONNECTED TO COMING EVENTS

MARK YOUR CALENDAR

NOVEMBER

15-17
Space Tech Expo Europe
Bremen, Germany
www.spacetechexpo.eu

15-17
Mobility Connectivity Conference
Bremen, Germany
www.spacetechexpo-europe.com/conference/mobility

15-18
electronica
München, Germany
https://electronica.de/en/

29-Dec. 2
APMC 2022
Yokohama, Japan & Online
www.apmc2022.org

DECEMBER

3-7
IEEE IEDM 2022
San Francisco, Calif. & Online
www.ieee-iedm.org

12-15
IEEE MAPCON 2022
Bangalore, India
www.ieeemapcon.org

JANUARY

5-8
CES
Las Vegas, Nev.
www.ces.tech

21-26
IPC APEX EXPO
San Diego, Calif.
www.ipcapexexpo.org

MEETINGS & COURSES January 21-26
CONFERENCE & EXHIBITION January 24-26
SAN DIEGO | CA

22-25
ARFTG
Las Vegas, Nev.
www.arftg.org

22-25
Radio Wireless Week
Las Vegas, Nev.
www.radiowirelessweek.org

31-Feb. 2
DesignCon
Santa Clara, Calif.
www.designcon.com/en/home.html

FEBRUARY

13-14
TOP Conference
London, U.K.
https://topconference.com

Call for Papers Deadlines

12/6	IMS2023
2/15	RFIC 2023
6/30	AMPC 2023

Online Panel

12/14
Upper mmWave and THz Communications Technology for 6G

FOR DETAILS VISIT MWJOURNAL.COM/EVENTS

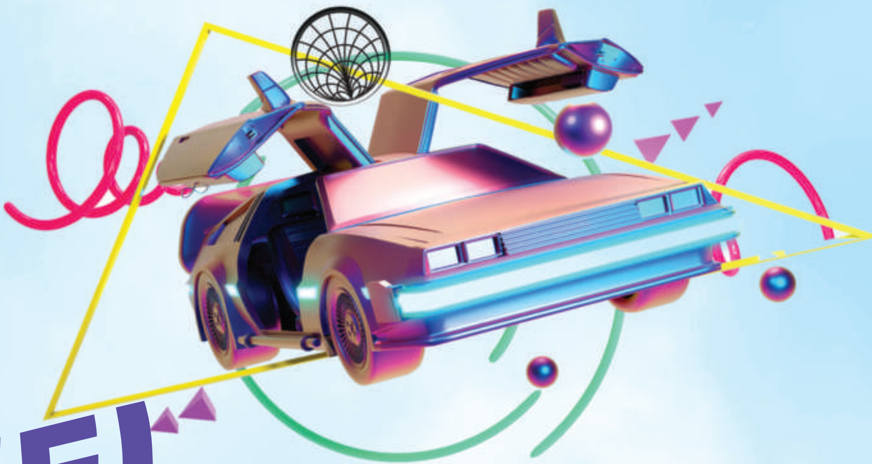

TIME TRAVEL

Excerpted from "History of Wireless"
Tapan K. Sarkar, Robert J. Mailloux, Arthur A. Oliner,
Magdalena Salazar-Palma and Dipak L. Sengupta

Tesla and the Electromagnetic Wireless Telegraph

The first wireless telegraphy patent, however impractical, was issued in the U.S. on July 20, 1872, to American dentist Mahlon Loomis, 15 years before Hertz. His patent, number 129,971, was for "Improvement in Telegraphing," and covered "aerial telegraphy by employing an `aerial' used to radiate or receive pulsations caused by producing a disturbance in the electrical equilibrium of the atmosphere."

Nikola Tesla was concerned with global views of telecommunication. Just like Loomis a few decades earlier, Tesla was convinced of the existence of a conducting layer in the atmosphere, and he tried to use it for transmitting information and electric energy over long distances.

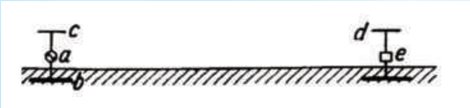

A figure from Tesla's patent for global wireless telegraphy.

Tesla started to consider the whole world as a resonator, whose basic resonance frequency he estimated as 6 Hz. Using rotating generators of his own design for carrier frequencies between the basic resonance and 20 kHz, with high towering antennas and ground electrodes (see Figure), he planned to create a "stationary wave" propagating from his transmitter to any point on the globe. In 1893, he filed a patent on such a system, which included the ideas of CW transmission with tuning and multiple phased radiators to increase and direct the radiated power.

After starting to build an expensive worldwide transmitter, he lost financial support because of Marconi's success with less costly equipment, and the grand plan was discontinued. His patent was later used in an American court against Marconi's patent.

When high-volume waveguide component testing looks like a high hurdle, Eravant gives you a leg up. Proxi-Flange™ waveguide segments make contactless waveguide connections a reality. Wave-Glide™ fixturing systems make contactless waveguide connections fast, easy, accurate, and repeatable. Both product families are compatible with Eravant's frequency extender systems, as well as all other frequency extenders commonly used today.

Stop worrying about how to test waveguide components and start harnessing Eravant's long history of producing and testing high-quality microwave and millimeter-wave components.

PROXI-FLANGE™

Contactless Waveguide Connections
Fast and Easy Component Testing
Accurate and Repeatable Test Results
Reduced Test System Maintenance
Frequency Coverage from 18 to 220 GHz

WAVE-GLIDE™

Effortless Connection of Components & amp; Test Systems
Configurable For a Wide Range of Components
Compatible with All Frequency Extenders
Supports Automated and Semi-Automated Testing

IoT 5G IoT 6G 6G

Cover Feature
Invited Paper

The Dual-Drive Power Amplifier: The Next Frontier in Power Amplification

Sanghoon Lee, James Kaney and Edgar Garay
Falcomm, Atlanta, Ga.

The first generation 30 GHz Dual-Drive™ power amplifier (PA) using a 45 nm silicon on insulator (SOI) process achieves 50 percent power-added efficiency (PAE) for a two-stage proof-of-concept, which is the highest efficiency ever achieved for a two-stage PA at 30 GHz on CMOS.

The world's dependence on wireless communications is ever increasing within our daily lives, spanning multiple industries such as automotive, health care, consumer products, space communications and travel, scientific and military. Powering these new opportunities in wireless communications is the PA, which enables wireless transmission of data around the world.

With a compound annual growth rate of ~12 percent, the $16 billion PA market is one of the main driving forces enabling the advancement in wireless communication systems.[1] Falcomm is working toward radically improving PA products for the wireless communications market.

Modern PAs are expected to support high-order modulation signals (e.g., 256-/1024-/4096-QAM) with OFDM, increasing peak-to-average power ratio (PAPR) specifications. Yet, these high PAPR levels can lead to less than desired average PAE at output back-off levels given current PA topologies. Therein lies the issue where the PA serves both as the enabler and the limiter for the desired implementation of advanced communication systems.

While the PA can service such high-order modulation schemes, it may inefficiently consume most of the power budget within a given wireless communication system, where most of the wasted energy is dissipated as heat. Given the ever increasing stringent communication protocols and requirements, high performance PAs are of paramount importance in the successful and rapid adoption of commercial next-generation communication networks.

Increasing the efficiency of PAs can greatly benefit the entire wireless communication market, which includes mobile devices, wearables, cellular base stations, cellphones, radar and other emerging markets.

For example, cost of ownership for cellular base stations is becoming a bigger concern for network operators as the deployment of 5G mmWave infrastructure takes place. In 2021, network operators spent about $120 billion for electricity in cellular base stations, where more than 50 percent of the energy consumption was from inefficient PAs. Therefore, increasing the efficiency of PAs will directly translate to reducing the electricity bill and carbon footprint of the wireless network infrastructure.

Another frontier for next-generation wireless communications systems is in space, where there is renewed interest and a desire to expand the robust low Earth orbital (LEO) economy and deploy a satellite infrastructure for reliable com-

munication networks (such applications are Wi-Fi from space, cellular access to remote locations and intra-space communication, to name a few) and maintain a constant human presence in LEO to facilitate the next generation of space travel.

While commercial spacecraft manufacturers like SpaceX have helped reduce rocket/payload launch costs to less than $2,000 per kilogram,[2] these costs still pose a high barrier to entry for companies with emerging new technologies, and they incur additional expenses to government agencies like NASA. Falcomm's customer interactions with satellite manufacturers found that battery and solar cell loads account for a significant portion of a satellite's weight. In some cases of Earth-to-space communication modules within satellites, the PA can be responsible for nearly 80 percent of the energy budget.

A more efficient PA can greatly ease thermal management requirements and reduce battery and solar cell sizes, but most importantly it can lower manufacturing and launch costs for satellites. For example, a micro-geostationary orbit (GEO) satellite manufacturer estimates that every 10 percent increase in PA efficiency will translate to $150,000 of launch cost savings per spacecraft due to the reduction in battery and solar cell weight. The estimated savings do not include the reduction in manufacturing and thermal management costs due to higher PA efficiency.

EXISTING PA TOPOLOGIES

The demand for more efficient and more linear PAs has driven extensive research to improve performance at the device level, for example increasing the f_{max}/f_t of the transistor.[3] In addition, improvements in the back end of the line processes such as thicker and lower-loss top metal layers have increased the performance of passive components, which has allowed a further increase in efficiency and output power.[4]

The increased f_{max}/f_t metrics of the transistor device, however, do not necessarily lend themselves to improved PA performance, as, typically, the smaller lithography nodes have reduced voltage supply overhead and smaller breakdown limits, making apparent the tradeoff in device performance and reliability.

With regard to circuit topology improvements, to this date, almost all PA designs rely on common-source or common-gate topologies and are mainly focused on increasing peak/power-back-off (PBO), PAE and maximum output power (P_{out}) by presenting multi-harmonic terminations to the output of the PA, as accomplished in the Class F, Class J and their inverse and continuous-mode operations.[5]

A topology that has gained popularity in recent years is the harmonic-tuned PA and its different variations. This topology takes advantage of adding load terminations at the fundamental frequency and at some of the harmonics to increase the maximum PAE of the amplifier. Most modern technology nodes exhibit an f_{max}/f_t between 100 and 300 GHz; therefore, at mmWave frequencies, the harmonic content might not be substantial enough to make a major improvement in efficiency. Additionally, passive networks that can provide harmonic tuning tend to be complex and lossy, further reducing the efficiency enhancement. Even though this technique shows low to moderate efficiency improvements, the beforementioned drawbacks hinder its adoption in commercial applications.

Recent efforts have also focused on further improving efficiency based on circuit topologies that can support complex modulation methods, such as stacked, outphasing, mixed-signal, reconfigurable and Doherty PAs.[6,7] However, in modern Si processes with nanometer sized technology nodes that employ supply voltages of less than 1 V per stacked transistor (2 V for cascode devices), these reported techniques see diminishing returns on PAE and P_{out} since the transistor knee voltage, V_{knee}, becomes a significant portion of the supply voltage. Moreover, an extra reduction in supply voltage is often observed

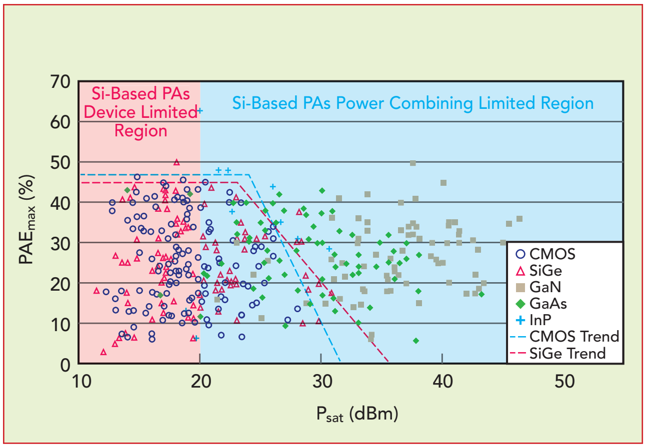

Fig. 1 **Published saturated output power vs. maximum PAE for 20 to 50 GHz PAs.**

in practical deployment to ensure device reliability.

This is especially relevant for mmWave array operations, where array element couplings result in substantial antenna impedance mismatches (VSWR) and undesired large PA output voltage/current swings. Although the reported techniques have improved overall PA efficiency at mmWave frequencies, their operating principles are incapable of theoretically surpassing the linear mode operation PA core efficiency of the Class B common-source topology without resorting to lower conduction angles or harmonic shaping.

Beyond solid-state technology, traveling wave tube (TWT) amplifiers have been commonly used in satellite transceivers due to their high-power capabilities and high efficiencies (greater than 90 percent). However, TWT amplifiers are extremely bulky with form factors spanning several tens of centimeters and cannot support modern communication systems due to the reduced antenna size and spacing requirements of array-based architectures at higher frequencies (greater than 1 GHz).

Therefore, ultra-efficient high-power millimeter-sized solid-state PAs are critical for the successful and rapid adoption of next-generation communication networks since they are superior to other alternatives in transceiver power efficiency, thermal management requirements and overall communications channel performance.

EFFICIENCY CONSIDERATIONS FOR PAS

Figure 1 shows P_{sat} versus PAE_{max} for previously published PAs ranging from 20 to 50 GHz.[8] There is an inherent tradeoff between P_{sat} and PAE_{max}. In addition, there exist two distinctive power/efficiency regions for PAs delimited by P_{sat}. In the red region, called the device limited regime, efficiency is limited by the technology or device performance characteristics and to some extent by the design topology.

In the blue region, called the circuits/combiner limited regime, an increase in power is attained by employing different power combining techniques and, therefore, efficiency is limited by the losses of the output combiner network. This shows a clear tradeoff between saturated output power and maximum efficiency.

Moreover, when considering energy efficiency in PAs, PAE can be characterized by the four independent factors shown in the following equations:

$$PAE = F_{Vmin} \times F_{Gain} \times F_{Matching} \times F_{Waveform} \quad (1)$$

$$F_{Vmin} \sim 1 - \frac{V_{min}}{V_{DD}} \quad (2)$$

$$F_{Gain} \sim 1 - \frac{1}{G} \quad (3)$$

$$F_{Matching} \sim \frac{Q_{ind}}{Q_{ind} + Q_{transformation}} \quad (4)$$

$$F_{Waveform} = 0.5 \sim 0.78 \quad (5)$$

where the first factor (F_{Vmin}) is associated with the maximum allowed output voltage swing, which is determined by the knee voltage of the device and the supply voltage; the second factor (F_{Gain}) is related to the gain of the device or the necessary driving power needed to saturate the PA; the third factor ($F_{Matching}$) relates to the passive efficiency of the output network and the last factor ($F_{Waveform}$) is a constant that depends on the PA gate biasing.

From these definitions we can conclude that the first two factors, F_{Vmin} and F_{Gain}, are limited by the device choice, while the last two factors, $F_{Matching}$ and $F_{Waveform}$, are limited by design choices. Previous topologies aimed at improving the maximum efficiency of the PA were limited to only increasing $F_{Matching}$ and $F_{Waveform}$ through design choices.

CLASS B PA THEORETICAL EFFICIENCY REVIEW

In Class B operation, the transistor is biased at the threshold voltage (V_{TH}) and only conducts current during half of the cycle. When the device is on, the drain current is proportional to ($V_{in} - V_{TH}$). Therefore, the drain current can be modeled as a half-wave rectified sine wave. Although the transistor drain current has large frequency content, the passive output network ensures that only the fundamental tone reaches the load. Using Fourier series analysis, we can define the maximum output power as:

$$P_{out} = \frac{V_{peak} \times I_{max}}{2} \quad (6)$$

The peak voltage swing at the load, V_{peak}, can be described in terms of the supply voltage, V_{DD}, and the knee voltage, V_{knee}, to include the effects of the device choice:

$$V_{peak} = V_{DD} - V_{knee} \quad (7)$$

The DC power dissipation of the transistor can be expressed using the maximum current going through the load, I_{max}, as shown in the following equations:

$$I_{DC} = \frac{2 \times I_{max}}{\pi} \quad (8)$$

$$P_{DC} = 2 \times V_{DD} \times I_{DC} \quad (9)$$

Finally, the maximum theoretical drain efficiency (DE) of an amplifier operating in Class B mode can be expressed by combining equations (6) through (9), as shown in equations (10) through (13).

UNMATCHED DYNAMIC RANGE.
UNMATCHED PERFORMANCE.

VDI's Mini VNAX modules are one-quarter the volume of standard modules making them well suited for probe station and antenna measurement applications.

BRIDGING THE THz GAP JUST GOT SMALLER.

VDI's VNA Extenders provide high performance frequency extension of vector network analyzers from 26GHz to 1.5THz. These modules combine high test port power with exceptional dynamic range and unmatched stability.

VDI's mini-modules are reduced in size, but yield the same industry leading performance as our original designs. The compact form factor and simplified power supply make them the recommended solution for most applications.

Mini-modules are currently available in standard waveguide bands for 26GHz to 1.1THz with higher frequency bands under development.

Waveguide Band (GHz)	WR28 26-40	WR19 40-60	WR15 50-75	WR12 60-90	WR10 75-110	WR8 90-140	WR6.5 110-170	WR5.1 140-220	WR4.3 170-260	WR3.4 220-330	WR2.8 260-400	WR2.2 330-500	WR1.5 500-750	WR1.0 750-1,100
Dynamic Range (BW=10Hz, dB, typ)	120	120	120	120	120	120	120	120	115	115	100	110	100	95
Dynamic Range (BW=10Hz, dB, min)	110	105	110	110	110	110	110	110	110	105	80	100	80	75
Magnitude Stability (±dB)	0.15	0.15	0.10	0.10	0.10	0.15	0.25	0.25	0.3	0.3	0.5	0.5	0.4	0.5
Phase Stability (±deg)	2	2	1.5	1.5	1.5	2	4	4	4	6	6	6	4	6
Test Port Power (dBm)	13	13	13	18	18	16	13	6	4	1	-10	-3	-16	-23

VDI

Virginia Diodes, Inc.
979 2nd St. SE, Suite 309
Charlottesville, VA 22902
434.297.3257

vadiodes.com

$$\eta_{class-B} = \frac{P_{out}}{P_{DC}} = \frac{V_{peak} \times I_{max}}{2 \times V_{DD} \times I_{DC}} \quad (10)$$

$$\eta_{class-B} = \frac{(V_{DD} - V_{knee}) \times I_{max}}{2 \times V_{DD} \times \left(\frac{2 \times I_{max}}{\pi}\right)} \quad (11)$$

$$\eta_{class-B} = \frac{(V_{DD} - V_{knee})}{2 \times V_{DD} \times \left(\frac{2}{\pi}\right)} = \frac{\pi}{4}\frac{(V_{DD} - V_{knee})}{V_{DD}} \quad (12)$$

$$\eta_{class-B} = \frac{\pi}{4}\left(1 - \frac{V_{knee}}{V_{DD}}\right) \quad (13)$$

Equation (13) shows the canonical Class B maximum efficiency of 78.5 percent when the V_{knee} is zero. In addition, Equation (13) also establishes the relationship between V_{knee} and the DE, $\eta_{class-B}$, as previously shown using the proportionality constant F_{Vmin} in Equation (1).

DUAL-DRIVE PA

The new patented Dual-Drive™ topology enables additional design freedom in improving PA performance by artificially reducing the knee voltage of the device, increasing the factor F_{Vmin} and in turn increasing the overall PAE_{max} of the PA. When a transistor is only driven at the gate, the device maximum efficiency is dictated by the device conduction angle and the knee voltage, V_{knee}. V_{knee} indicates the transition region between the linear and saturation region of a transistor and is a technology-specific physical parameter inherent to the physical device's fabrication process and size. Moreover, V_{knee} reduces the output voltage and drastically impacts the achievable DE and overall efficiency of a PA.

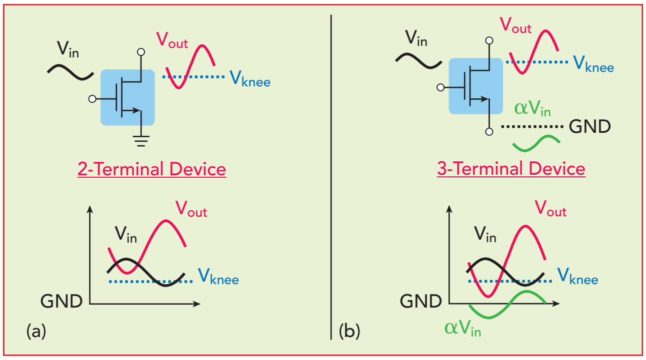

Fig. 2 Conventional common source (a) and Dual-Drive (b) topologies, showing gate, drain and source waveforms.

In the Dual-Drive™ topology, Falcomm exploits the transistor as a three-terminal device and drives both the gate and the source terminals with out-of-phase inputs V_{in} and αV_{in} ($0<\alpha<1$), as shown in ***Figure 2***. Assuming short terminations for all harmonics at the drain node, the source voltage now swings below ground while having an in-phase relationship with the drain voltage, increasing the maximum drain output voltage swing by αV_{in}. This increased output voltage swing can be attained without increasing the supply voltage, which means that the maximum DE is increased in the Dual-Drive™ topology by a factor greater than 1.

Falcomm demonstrated for the first time that through the Dual-Drive PA architecture they are able to artificially reduce/cancel out the knee voltage of the transistor, allowing for the maximum theoretical efficiency of a PA to be fundamentally increased beyond that of any PA class and topology as shown in Equation (14).

$$\eta_{Dual-Drive} = \eta_{class-B}\left(1 + \left(\frac{\alpha V_{in}}{V_{DD} - V_{knee}}\right)\right) \quad (14)$$

When the maximum voltage swing at the source is equal to the knee voltage of the transistor ($\alpha V_{in} = V_{knee}$), the theoretical maximum DE for the Dual-Drive PA will reach the maximum theoretical efficiency of the class B PA, $\frac{\pi}{4}$, as shown in Equation (15).

$$\eta_{Dual-Drive}(\alpha V_{in} = V_{knee}) = \frac{\pi}{4} \quad (15)$$

The strength of the source swing depends on α, which is a design con-

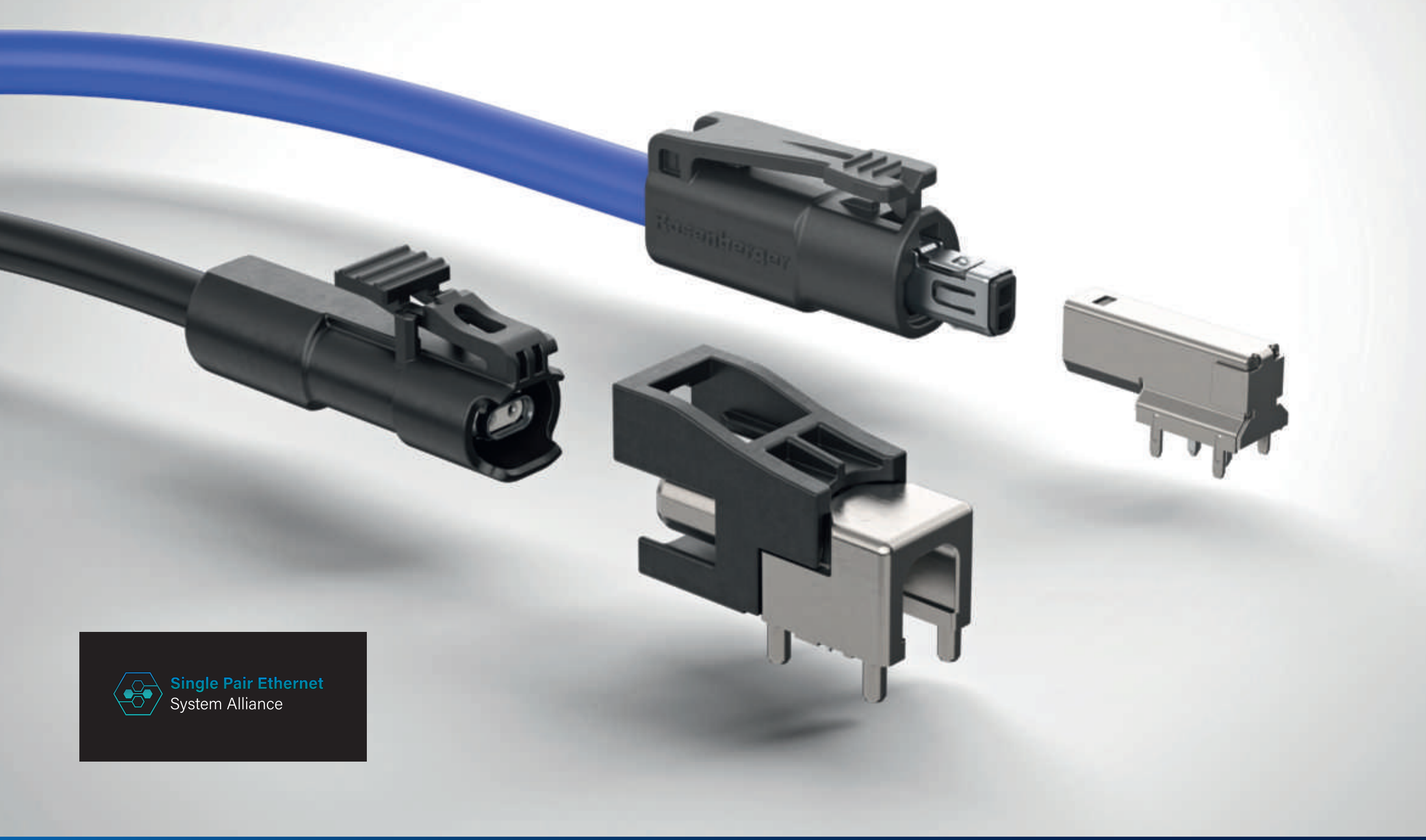

SINGLE PAIR ETHERNET

Single Pair Ethernet (SPE) Connectors

One wire pair – an infinite number of applications. Using power over data line (PoDL), parallel high-performance data and power transmission is supported via just one Ethernet wire pair.

Rosenberger provides two innovative SPE connector series

RoSPE-HMTD

- Space saving, lightweight and robust differential SPE connectors
- For Ethernet applications up to 15 GHz or 20 Gbps
- Based on H-MTD® automotive series with industrial housings

RoSPE-Industrial

- Industrial SPE connectors
- Developed in cooperation with leading manufacturers
- According to IEC 63171 up to 2.5 GHz

www.rosenberger.com/spe/

Rosenberger

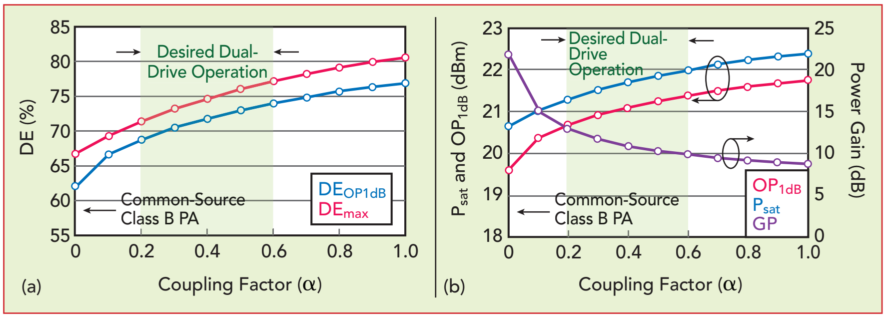

Fig. 3 Large-signal load-pull simulations of low voltage CMOS transistor: DE (a) and P_{sat}, $OP1_{dB}$ and power gain (b) vs. coupling factor.

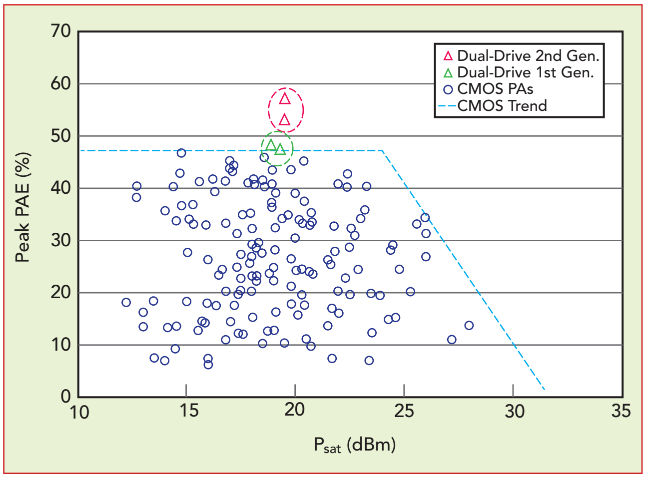

Fig. 4 Dual-Drive PA P_{sat} and PAE compared to CMOS PAs.

stant that can be adjusted. ***Figure 3*** shows that with varying α, there is a tuning tradeoff for PA designers to balance between power gain and the achievable efficiencies of the Dual-Drive PA transistor core. These results show that by employing the Dual-Drive architecture, the efficiency lost by the V_{knee} of the transistor can be recovered. In addition, Falcomm's analysis of the Dual-Drive PA is consistent with Equation (1).

BENEFITS OF THE DUAL-DRIVE PA

The benefits of the Dual-Drive PA topology are summarized as follows: first, increasing the source terminal coupling coefficient, α, can fundamentally increase the PA core DE beyond that of any other PA topology; second, higher DE can be maintained even at reduced supply voltages since the effect of V_{knee} under a lowered supply can be mitigated and third, the maximum output power can be increased while reducing the device modulation distortion, since the active device spends more time in its saturation region and less in triode.

Furthermore, the parallel input resistance of the transistor is reduced since the typically large device gate impedance is combined in parallel with its low device source impedance, aiding the design of broadband and low loss inter-stage matching networks without the need to implement lossy de-Qing resistors.

Finally, the Dual-Drive PA can mitigate the reliability issues of voltage peaking typically seen in complex harmonic-shaping PAs (Class J or continuous-mode Class F PAs). Therefore, the Dual-Drive PA is particularly suitable for high reliability space applications that mandate consistent operation in harsh environments while achieving ultra-high efficiency levels.

Initial efficiency measurement results from Falcomm's first and second generation low-power CMOS Dual-Drive PA prototypes in comparison with state-of-the-art PAs at the same frequency band are shown in ***Figure 4***. These initial results demonstrate that the Dual-Drive PAs are at least 25 percent more efficient than conventional PAs; which, based on estimates and discussions with one of Falcomm's potential customers building micro-GEO satellites, could translate into $350,000 in launching cost savings per satellite.

RF-LAMBDA

MADE IN USA

THE LEADER OF RF BROADBAND SOLUTIONS

EMC Broadband RF Power Amplifier

High Power Solid State

HUNDREDS IN STOCK

FAST SHIPPING

FREQUENCY UP TO 90GHZ

POWER UP TO 2KW CW

REMC06G18GG

6-18GHZ 300W

- AUTOMATIC BUILT IN SELF CALIBRATION AND BIAS ADJUSTMENT.
- OVER TEMPERATURE, CURRENT, INPUT POWER PROTECTION.
- VSWR MEASUREMENT AND OPEN CIRCUIT PROTECTION.
- USER FRIENDLY CONTROL INTERFACE.
- REMOTE ETHERNET CONTROL AND FIRMWARE UPDATE.
- HIGH POWER EFFICIENCY AND LIGHTWEIGHT.

RAMP42G47GA 42-47GHZ 8W

REMC02G06GE 2-6GHZ 500W

REMC08G11GE 8-11GHZ 400W

RAMP18G40GB-U 18-40G 20W

RAMP05M80GC 0.5-80GHZ

CoverFeature

DUAL-DRIVE PA SUPERIOR PERFORMANCE

The first technology demonstration was implemented using the GlobalFoundries 45 nm RFSOI. The chip occupies a total area of 1.3 × 1.2 mm^2 with a core area of 0.25 mm^2.[9] ***Figures 5*** and ***6*** summarize the Dual-Drive PA's continuous wave performance with different supply voltages (1.7 and 1.9 V), achieving a maximum OP_{1dB} of 19.1 dBm at 31 GHz with less than 1 dB variation from 23 to 34 GHz.

The Dual-Drive PA achieves a maximum PAE of 50 percent and maximum DE of 60 percent at 29 GHz. This is the highest reported efficiency for a two-stage CMOS PA in this frequency range. Moreover, a PAE greater than 40 percent is maintained across the entire bandwidth from 24 to 35 GHz.

The efficiency results are met with great linearity performance as well. For example, OP_{1dB} and P_{sat} are within 1 dB of each other, which translates to a maximum PAE at OP_{1dB} of 47.4 percent. Excellent linearity is demonstrated through extensive modulation measurements shown in ***Figures 7*** and ***8***. For example, for a 9 Gb/s 64-QAM signal without digital predistortion (DPD), the Dual-Drive™ PA achieves an average P_{out} of 15.1 dBm and average PAE of 30.2 percent with a -25 dB rms error vector magnitude at 30 GHz. The efficiency performance is maintained at supply voltage levels

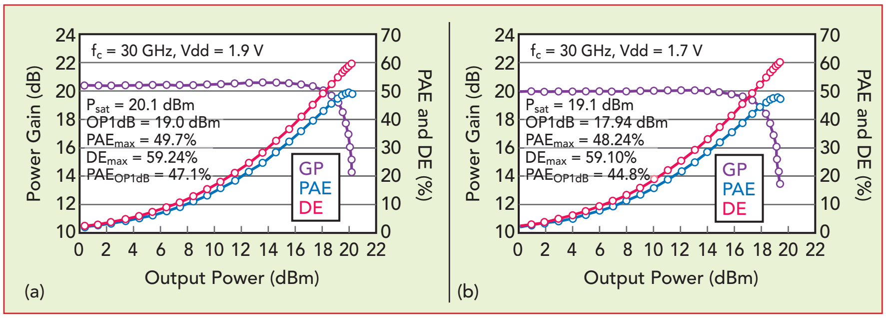

▲ Fig. 5 Measured power gain and efficiency vs. output power of the initial technology demonstration (version 0) of the Dual-Drive PA at 30 GHz, biased at 1.9 (a) and 1.7 (b) V.

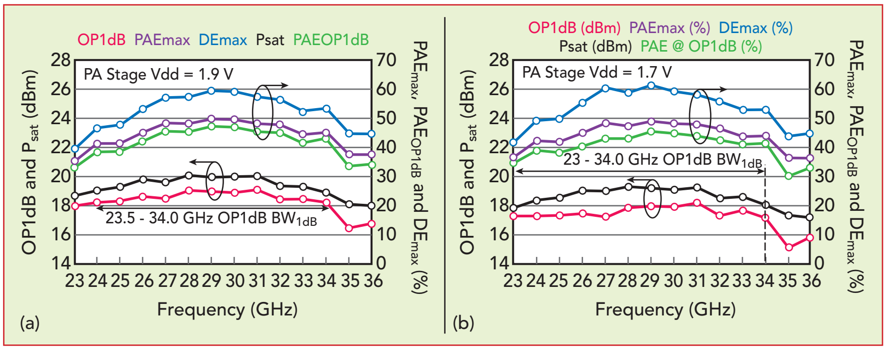

▲ Fig. 6 Large-signal CW measurements of the initial technology demonstration (version 0) of the Dual-Drive PA vs. frequency, biased at 1.9 (a) and 1.7 (b) V.

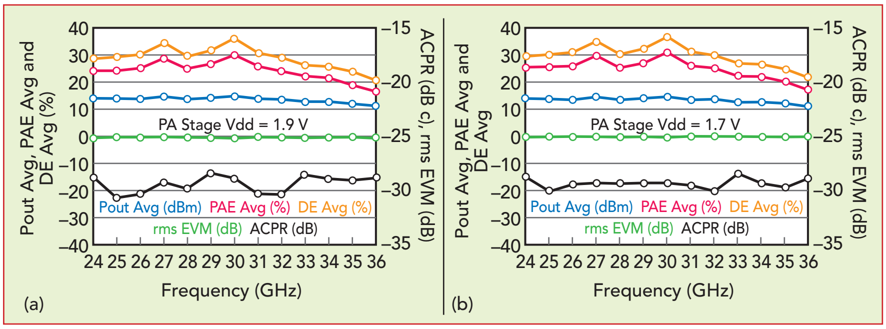

▲ Fig. 7 Measured single carrier, 64-QAM performance of the Dual-Drive PA, biased at 1.9 (a) and 1.7 (b) V.

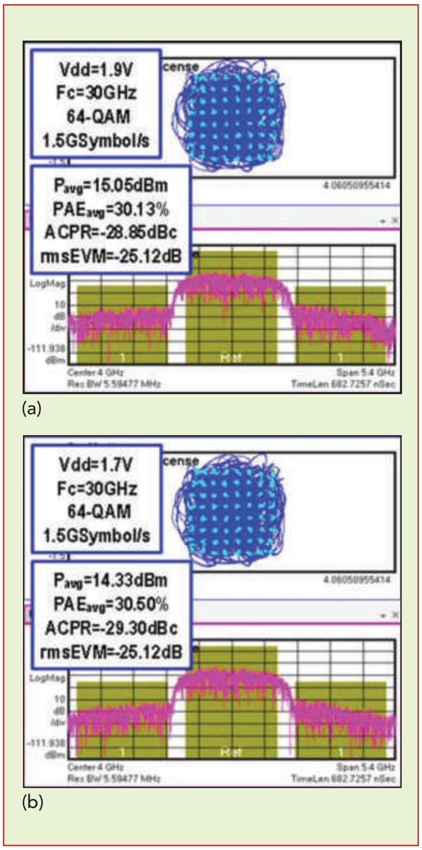

Fig. 8 Measured single carrier, 64-QAM constellation and spectrum performance of the Dual-Drive PA, biased at 1.9 (a) and 1.7 (b) V.

that are 20 percent lower than the rated supply voltage, which positions the technology for high reliability applications.

The first generation 30 GHz Dual-Drive PA using a 45 nm SOI process achieves 50 percent PAE for the two-stage proof-of-concept, which is the highest efficiency ever achieved for a two-stage PA at 30 GHz on CMOS. Falcomm has been further developing and maturing the technology and newer tested prototypes are reaching even higher efficiencies with PAE reaching the 55 percent mark for a two-stage PA and average PAE of 34 percent using a 9 Gb/s 64-QAM signal at 30 GHz, which is a higher average efficiency than a Doherty PA can offer but with half the Si area.

CONCLUSION

Falcomm is focusing on developing its core technology into a product catalog with PAs of different power levels, frequency ranges, gain and packaging that will bring a better value to satellite, base stations and handheld device manufacturers. Falcomm believes these results demonstrate that its technology will become the industry standard for PAs and, based on current design efforts, is confident that it can push the technology further. ■

References

1. "RF Power Amplifiers – Global Market Trajectories & Analytics," *Research and Markets*, April 2021, Web: www.researchandmarkets.com/reports/5141446/rf-power-amplifiers-global-market-trajectory.
2. I. Williams, "Boost-Phase Missile Defense Interrogating the Assumptions," *Center for Strategic and International Studies*, June 2022, Web: www.csis.org/events/boost-phase-missile-defense-interrogating-assumptions.
3. S. Lee, B. Jagannathan, S. Narasimha, A. Chou, N. Zamdmer, J. Johnson, R. Williams, L. Wagner and J. Kim, "Record RF Performance of 45-nm SOI CMOS Technology," *IEEE International Electron Devices Meeting*, December 2007, pp. 255–258.
4. O. Inac, M. Uzunkol and G. Rebeiz, "45-nm CMOS SOI Technology Characterization for Millimeter-Wave Applications," *IEEE Transactions on Microwave Theory and Techniques*, Vol. 62, No. 6, June 2014, pp. 1301–1311.
5. S. C. Cripps, P. J. Tasker, A. L. Clarke, J. Lees and J. Benedikt, "On the Continuity of High Efficiency Modes in Linear RF Power Amplifiers," *IEEE Microwave and Wireless Components Letters*, Vol. 19, No. 10, October 2009, pp. 665–667.
6. S. Hu, F. Wang and H. Wang, "A 28-/37-/39-GHz Linear Doherty Power Amplifier in Silicon for 5G Applications," *IEEE Journal of Solid-State Circuits*, Vol. 54, No. 6, June 2019, pp. 1586–1599.
7. E. F. Garay, D. J. Munzer and H. Wang, "26.3 A mm-Wave Power Amplifier for 5G Communication Using a Dual-Drive Topology Exhibiting a Maximum PAE of 50 Percent and Maximum DE of 60 Percent at 30 GHz," *IEEE International Solid-State Circuits Conference*, February 2021, pp. 258–260.
8. H. Wang, T. -Y. Huang, N. Sasikanth Mannem, J. Lee, E. Garay, D. Munzer, E. Liu, Y. Liu, B. Lin, M. Eleraky, H. Jalili, J. Park, S. Li, F. Wang, A. S. Ahmed, C. Snyder, S. Lee, H. T. Nguyen and M. E. D. Smith, "Power Amplifiers Performance 2000-Present," *Georgia Tech Electronics and Micro-System Lab (GEMS)*, August 2021, Web: https://gems.ece.gatech.edu/PA_survey.html.
9. E. F. Garay, D. J. Munzer and H. Wang, "A 150 GHz Lens-Free Large FoV Regenerative 2 × 2 Transceiver Array With 31 Percent DC-to-EIRP Efficiency and −70 dBm Sensitivity for a 70 cm Bidirectional Peer-to-Peer Link," *IEEE Journal of Solid-State Circuits*, Vol. 57, No. 7, July 2022, pp. 2102–2113.

Lockheed Martin, Verizon Demonstrate 5G-Powered ISR Capabilities for the Department of Defense

In recent demonstrations, Lockheed Martin and Verizon flew 5G-enabled drones to capture and securely transfer high speed, real-time intelligence, surveillance and reconnaissance (ISR) data from aircraft in flight to geolocate military targets. "We are positioning ITT to support our customers' emerging technology needs, while also greatly enhancing our ability to stake out new markets," said Steve Loranger, ITT's chairman, president and chief executive officer. "We believe this move will also allow ITT to achieve greater operating efficiencies and optimize our cost structure, which will help drive successful business strategies for continued top-line growth."

The companies demonstrated two key advances in technology that can provide critical applications for the Department of Defense (DOD):

- First, real-time ISR RF and streaming video data was transmitted over 5G mmWave links to allow advanced signal processing algorithms to be executed at the tactical edge. The data was displayed in a livestream video feed. This capability will provide enhanced levels of situational awareness and command and control for commanders and service members in the field.
- Second, the technology passively detected and geolocated RF signals that could be used for communications, sensing or jamming. This will enable the DOD to detect and target adversarial assets in a military environment.

Dan Rice, vice president of 5G.MIL Programs at Lockheed Martin said, "To stay ahead of our adversaries, military decision-makers need the timely and accurate information that 5G.MIL delivered in this demonstration. By blending advanced commercial 5G capabilities with military capabilities using secure, open standards, we are helping to make the DOD's vision for integrated deterrence a reality."

Srini Kalapala, senior vice president for Technology and Product Development at Verizon stated, "Verizon is the network America relies on, and our Private 5G Ultra-Wideband networks provide the security, reliability, capacity and low latency that the defense sector depends on. By demonstrating the mission critical connectivity that our network provides, we are demonstrating how 5G and edge computing can help the DOD address their strategic priorities and continue to develop advanced solutions."

These demonstrations, held in May and September 2022, are part of an ongoing 5G collaboration announced by the companies last year focused on faster delivery of cutting-edge technologies to the DOD.

Future demonstrations between Verizon and Lockheed Martin are expected to expand ISR test scenarios to include precision geolocation of moving RF emitters. The companies plan to extend public-private network collaboration securely using 5G.MIL hybrid networks with military data links.

USAF Selects Raytheon Missiles & Defense, NGC to Deliver First Hypersonic Air-Breathing Missile

Raytheon Missiles & Defense, a Raytheon Technologies business, in partnership with Northrop Grumman Corporation, has been selected to develop the Hypersonic Attack Cruise Missile (HACM) for the U.S. Air Force (USAF). HACM is a first-of-its-kind weapon developed in conjunction with the Southern Cross Integrated Flight Research Experiment (SCIFiRE), a U.S. and Australia project arrangement.

Under this contract, the Raytheon Missiles & Defense and Northrop Grumman team will deliver operationally ready missiles to the USAF.

"Raytheon Missiles & Defense continues to be at the forefront of hypersonic weapon and air-breathing technology development," said Wes Kremer, president of Raytheon Missiles & Defense. "With advanced threats emerging around the globe, the HACM will provide our warfighters a much-needed capability."

The HACM is an air-breathing, scramjet powered munition. Scramjet engines use high vehicle speed to forcibly compress incoming air before combustion, which enables sustained flight at hypersonic speeds, Mach 5 or greater. By traveling at these speeds, hypersonic weapons, like the HACM, can reach their targets more quickly than similar traditional missiles, allowing them to potentially evade defensive systems.

"The HACM creates a new class of strategically important weapons for the U.S. military," said Mary Petryszyn, corporate vice president and president, Northrop Grumman Defense Systems. "Our scramjet propulsion technology is ushering in a new era for fast-

HACM (Source: Northrop Grumman)

For More Information Visit mwjournal.com for more defense news.

er, more survivable and highly capable weapons."

Raytheon Technologies and Northrop Grumman have been working together since 2019 to develop, produce and integrate Northrop Grumman's scramjet engines onto Raytheon's air-breathing hypersonic weapons. Their combined efforts enable both companies to produce air-breathing hypersonic weapons, the next generation of tactical missile systems.

BAE Systems to Develop Filter Technology to Improve Radar, Communications and Electronic Warfare Capabilities

The Defense Advanced Research Projects Agency (DARPA) has awarded BAE Systems' FAST Labs™ research and development organization a $6.5 million contract for the COmpact Front-end Filters at the ElEment-level (COFFEE) program. COFFEE aims to provide filter technology to improve performance of critical DOD RF and microwave systems with stringent power and size constraints such as digital active electronically scanned arrays.

Highly integrated and high channel-count RF systems are pervasive for DOD applications. The COFFEE program aims to provide elemental-level protection for these systems against interferers that could adversely impact the operation in congested environments.

> Filtering technology to protect systems and make them more robust and resistant to interference.

"Wideband, highly integrated RF systems are essential to enable mission critical operations; however, high bandwidth receivers often have limited dynamic range that can leave them vulnerable to electronic jamming," said Chris Rappa, chief technologist at BAE Systems' FAST Labs. "COFFEE will provide filtering technology to protect systems and make them more robust and resistant to interference."

BAE Systems will develop filter technology that can address a broad microwave frequency range that DOD radio systems generally operate in, with element-level integration and without sacrificing performance. The company will ensure the filters are manufacturable with reproducible performance.

BAE Systems' work on the COFFEE program is a part of DARPA's Electronics Resurgence Initiative, a five-year, upwards of $1.5 billion investment in the advancement of the U.S. semiconductor industry.

MMWAVE FILTERS

LTCC Meets 5G

The World's Widest Selection

- Band pass filters optimized for n257, n258, n260 and n261 5G bands
- Low pass filters with passbands up to 30.5 GHz
- High pass filters fco from 28 to 36 GHz
- Rejection up to 40 dB
- Proprietary material systems and distributed topologies
- Pick-and-place standard case styles

Mini-Circuits®

CommercialMarket

Cliff Drubin, Associate Technical Editor

By 2025, More than 10M Vehicles Will Be Capable of Short-Range V2X Communication

According to ABI Research more than 10 million vehicles will be capable of short-range vehicle-to-everything (V2X) communication by 2025. However, indirect communication via the cellular network (e.g., V2N2X, I2N2V) still constitutes the most significant yet untapped V2X opportunity. Cellular connectivity will be available in 346 million vehicles by 2025 and smart city cellular connections will exceed 165 million.

In 2021, Europe was the region with the largest fleet of short-range V2X communication-enabled cars, but all from a single automaker, Volkswagen. "Given the lack of commitment of more automakers so far, by 2023, China alone will overtake Europe. The inauspicious scenario in Europe is leading industry players to place more emphasis on cellular network tests for the time being. However, there are still fundamental business model challenges to be overcome with this route. Although a truck and a private vehicle OEM may deploy ITS-G5 in 2023, the crucial market driver for mass adoption will be the V2X inclusion in the Euro New Car Assessment Program (NCAP) scoring, as is currently happening in China. Lagging, the U.S. now has a solid regulatory framework for C-V2X, paving the way for deployments," explained Maite Bezerra, smart mobility and automotive industry analyst at ABI Research.

There are suggestions in the industry that the V2X inclusion in the 2025 Euro NCAP rating scheme will be delayed to 2027 due to insufficient time to develop new test protocols. This includes establishing enough labs and validating new vehicle capabilities. While the NCAP has not officially confirmed any changes, there is consensus that if the 2025 timeframe is maintained, it will focus on Day One use cases. There is also consensus that 2027 will be the inflection point for mass adoption because a complete range of Day Two use cases will become part of the Euro NCAP scoring.

The recent dismissal of the appeal against the FCC's 5.9 GHz spectrum proceedings means that C-V2X has a clear path in the U.S. and should spur the FCC to grant the existing C-V2X waiver requests faster. On the downside, the U.S. may not have enough spectrum for some advanced cooperative perception/Day Two use cases in the future. In China, C-V2X is currently found in low volume premium vehicle models, but there are at least 25 OEMs in different stages of V2X production in the country. COVID-19 lockdowns and discussions about the GNSS positioning standard slowed down deployments in 2022. However, shipments of vehicles with C-V2X will grow exponentially in 2023, surpassing one million as carmakers prepare for China NCAP 2025.

IoT Cellular Connections Continue Double-Digit Growth, Despite Global Uncertainties

According to Waseem Haider, principal analyst, enterprise IoT at Strategy Analytics and author of the report, "IoT Cellular Connections by Air Interface by Region: 2022-2030 Forecast Update," "the latest forecast update looks at the historical data as far as 2013 and forecasts IoT connections by air interface technology (2G, 3G, 4G, 5G) and by region (Asia Pacific, North America, Western Europe, Central & Eastern Europe, Caribbean & Latin America and Middle East & Africa). Over the forecast period, North America and Asia Pacific are expected to achieve the highest compound annual growth rate of 16 and 14 percent, respectively."

Between 2022-2030, the mix by technology will change with 5G making strong inroads replacing 4G connections, from 4G comprising 71 percent of connections in 2022 to only 49 percent in 2030, although a year-over-year decline in IoT cellular connections in 2022 is expected due to the COVID-19 lockdown in China, chip shortage/supply chain disruption and geopolitical conflicts. Overall IoT cellular connections will grow at 14 percent throughout the forecast period.

The outlook for IoT cellular connections is clear: 4G will continue to dominate overall, driven by 2G replacements, especially in China, but also elsewhere. 3G phases out with most connections moving to 4G. 5G is expected to reach 47 percent of the connections mix by 2030, while 4G will remain the dominant technology at 49 percent.

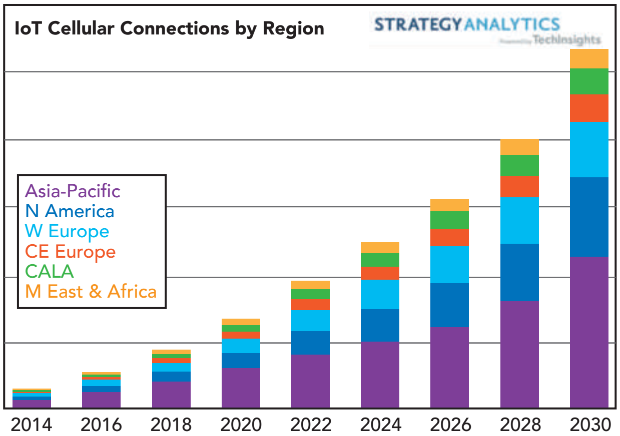

Source: Strategy Analytics

6G's Deployment in 2029 and Widespread Commercialization in 2032 Will Require Investment in Distributed Computing and AI

As 5G's commercial rollout continues, the deployment of distributed computing has become progressively more important. Distrib-

For More Information Visit mwjournal.com for more commercial market news.

uted computing, or 'edge-to-cloud' compute, is the use of disaggregated resources to perform compute operations. But in the 5G era, distributed computing has played a supportive role, while, as enterprises and service providers transition to 6G, distributed computing will be given a leading role. According to ABI Research, a sound distributed computing and artificial intelligence (AI) strategy will underpin successful 6G commercial deployment and enterprise use case enablement.

"End users in the 6G-era will not be concerned about merely connecting devices and creating data, but instead, they will want to extract valuable information from this data to make real-time operational decisions. Enterprise network expectation progression will mean that with the 6G rollout, the role of distributed computing is likely to change drastically," said Reece Hayden, distributed and edge computing analyst at ABI Research. "6G networks will need to be deployed across distributed computing domains with integrated edge AI resources to provide effective services for enterprise applications."

The shift toward 6G will lead to greater convergence of technologies and a more prominent role for distributed computing integrated with edge AI. Three core 6G expectations will lead to this growth in distributed intelligence: technology, commercialization, and society:

- Technology: 6G is expected to be built in the subterahertz spectrum, meaning that deployment will be denser, while higher speeds will mean more data. Both factors mean the network will need to be built on top of a cloud-native, highly disaggregated, agile, distributed computing architecture that can intelligently scale to meet real-time deployment requirements while supporting revolutionary enterprise use cases.
- Commercialization: use case enablement, data value extraction and end-to-end network service expectations will mean that best-effort service level agreements (SLAs) are no longer acceptable. Instead, distributed intelligence resources will be required to provide real-time data computation and value extraction support, achieve guaranteed SLAs and support telco network monetization through ubiquitous network slice deployment.
- Society: 6G is expected to drive sustainability and eliminate the digital divide. Distributed computing integration will aid data localization, limit backhauling, lower network power consumption and put social value at the forefront.

Achieving the necessary integration of distributed computing and AI will not be simple. Hayden stated, "Market standardization through increased cooperation and openness will be essential to overcoming the knowledge gaps and investment costs that could trouble telco-led technological convergence."

Around the **Circuit**

Barbara Walsh, Multimedia Staff Editor

MERGERS & ACQUISITIONS

VIAVI Solutions Inc. announced it has completed the acquisition of **Jackson Labs Technologies**, a leader in position, navigation and timing (PNT) solutions for critical infrastructure serving both military and civilian applications. Jackson Labs develops and supplies modules, subsystems and box-level solutions that include front-end receivers, transcoders, rack-mounted equipment and patented retrofit technology. Their broad customer base includes armed forces, defense contractors, energy distribution infrastructure, low Earth orbit operators and 5G service providers. Jackson Labs' next-generation M-Code solutions complement and advance VIAVI's timing and synchronization portfolio at a time when PNT requirements for defense, space, commercial aviation, transportation and telecommunication networks are expanding and becoming increasingly critical.

A merger between **Curvalux UK Ltd** and **Cambridge Broadband Networks Group (CBNG)** was completed to achieve the technology innovation required to realize the ever-increasing global demand for high speed Fixed Wireless Access (FWA). The merger will combine the experienced heritage of CBNG with Curvalux's technology for the timely delivery of disruptive 5G solutions worldwide. The two companies will remain independent with CBNG becoming a subsidiary of Curvalux UK Ltd. Curvalux's patented antenna design for FWA enables telecom operators to extend services to unserved and underserved remote areas with a faster deployment time and much lower total cost of ownership than fiber installation.

Trexon, a portfolio company of Audax Private Equity, announced that it has completed the acquisition of **Intelliconnect**, a supplier of RF connectors, adapters and cable assemblies. Founded in 2003 and based in Chelmsford, U.K., Intelliconnect has grown rapidly since its inception, becoming a market leader in design-led RF components.

COLLABORATIONS

Renesas Electronics Corp. announced a strategic partnership with **Jariet Technologies Inc**. As part of the partnership, Renesas is investing US$7 million into Jariet's new round of funding. Based in California, U.S., Jariet is a high-growth start-up uniquely capable of leveraging deep sub-micron process nodes to deliver unprecedented performance and integration for next-generation communication networks, such as cellular, connectivity and satellite communications.

ThinKom Solutions Inc. and **Inmarsat Government** announced a collaboration to deliver more efficient and reliable satellite communications (satcom) for tactical operations. The pair will combine ThinKom's ThinAir® Ka2517 antenna with Inmarsat Government's G-MODMAN II and G-MODMAN Open Platform modem managers to support Department of Defense (DOD) connectivity around the globe. The solution enables the vision of Advanced Battle Management System contribution to joint all domain command and control (JADC2) operations. This unique combination delivers on many facets of the U.S. government's tactical edge efforts. By enabling cloud-based computing, seamless data sharing, intelligent operations or autonomous use cases, the innovative solution reduces decision-making timelines for intelligent assets supporting troops in the field.

The China Mobile Research Institute and **Rohde & Schwarz** have joined forces to research and validate joint communication and sensing (JCAS). They plan to use the latest R&S AREG800A automotive radar echo generator from Rohde & Schwarz as an object simulator in a JCAS testing solution, thereby accelerating the research and development of JCAS and readying it for industrialization. The JCAS testing solution has the latest R&S AREG800A as an object simulator.

Altum RF announced a new grant and collaboration with **Industrial Technology Research Institute** (ITRI) and **TMY Technology Inc.** (TMYTEK). Altum RF, ITRI and TMYTEK will collaborate on an antenna and semiconductor integrated modules project for satcom systems. The grant comes from the Eureka Globalstars Taiwan framework. The project began in August 2022 and is slated to continue for two years.

NEW STARTS

The Institute for the Wireless Internet of Things at **Northeastern University** has announced the creation of Open6G, a new **U.S. DOD**-supported industry-university cooperative research center focused on future open, programmable and disaggregated 6G systems. Open6G is led by an anchor award under the auspices of the Innovate Beyond 5G thrust within the 5G-to-xG Initiative, Office of the Under Secretary of Defense (Research and Engineering). The new Open6G facility will occupy approximately 4600 square feet at the Innovation Campus in Burlington, Mass.

SnapEDA has launched the **SnapEDA Syndication Network**. This ecosystem of over 30 distribution partners includes electronic component distributors, printed circuit board tool makers and engineering media sites. The SnapEDA Syndication Network connects the electronic designers and engineers who are at the heart of the electronic industry with design content for millions of electronic components.

CONTRACTS

The U.S. Air Force awarded **Raytheon Missiles and Defense** a $985,348,124 contract to develop and demonstrate Hypersonic Attack Cruise Missile (HACM) prototypes, underscoring the Air Force's focus on increasing

For More Information For up-to-date news briefs, visit mwjournal.com

HIGH POWER COUPLERS

5 - 500 Watts

Model #	Frequency (MHz)	Coupling (dB) [Nom]	Coupling Flatness (dB)	Mainline Loss (dB) [Typ./Max.]	Directivity (dB) [Typ./Min.]	Input Power (Watts) [Avg.]
SDCHP-125	10 - 250	18.5	0.5	0.1 / 0.4	24 / 19	30
SDCHP-140	10 - 400	18.75	1	0.5 / 0.85	27 / 22	25
SBCHP-1100	10 - 1000	10	0.5	1.2 / 1.4	17 / 15	5
KBK-HP-1100	10 - 1000	10	0.5	1.2 / 1.4	17 / 15	5
KDK-HP-255	20 - 550	20	0.4	0.25 / 0.35	23 / 18	27.5
SDCHP-255	20 - 550	20	0.4	0.25 / 0.35	23 / 20	27.5
SDCHP-335	30 - 350	20.1	0.85	0.24 / 0.32	24 / 20	75
SDCHP-484	40 - 840	19.2	0.9	0.3 / 0.4	24 / 20	30
SCCHP-560	50 - 560	14.6	0.7	0.48 / 0.65	23 / 20	75
SCCHP-990	90 - 900	15.2	0.6	0.52 / 0.64	20 / 17	38.3
SBCHP-2080	200 - 800	12.3	0.7	0.64 / 0.80	24 / 18	48.3
SBCHP-2082	200 - 820	11.0	0.5	0.74 / 0.9	22 / 19	22.5
KDS-30-30-3	27 - 512	27.5	0.75	0.3 / 0.4	23 / 15	50
KDS-30-30	30 - 512	27.5	0.75	0.3 / 0.4	23 / 15	50
KBK-10-225	225 - 400	11	0.5	0.6 / 0.7	25 / 18	50
KBS-10-225	225 - 400	10.5	0.5	0.6 / 0.7	25 / 18	50
KDK-20-225	225 - 400	20	0.5	0.2 / 0.4	25 / 18	50
KDS-20-225	225 - 400	20	0.5	0.2 / 0.4	25 / 18	50
KEK-706H	500 - 2500	31.5	2.5	0.28 / 0.4	18 / 12	100
SCS-8012D	800 - 1200	20	0.6	0.22 / 0.25	22 / 18	100
KEK-704DH-2	850 - 1250	30	0.25	0.20 / 0.30	28 / 25	500
KEK-704H	850 - 960	30 5	0.25	0.08 / 0.20	38 / 30	500
SCS100800-10	1000 - 8000	10.5	2	1.2 / 1.8	8 / 5	25
SCS100800-16	1000 - 7800	16.8	2.8	0.7 / 1	14 / 5	25
SCS100800-20	1000 - 7800	20.5	2	0.4 / 0.75	12 / 5	25
SCS-1522B	1500 - 2200	10	--	0.65 / 0.75	23 / 18	100
SCS-1522D	1500 - 2200	20	--	0.32 / 0.38	23 / 20	100
SCS1701650-16	1500 - 15500	17	2.5	1 / 1.4	16 / 5	25
SCS1701650-20	1700 - 15000	21	2.5	0.9 / 1.3	10 / 7	25
SDC360440-10	3600 - 4400	8.6	0.25	0.7 / 1.4	18 / 10	10
SDC360440-20	3600 - 4400	19	0.25	0.7 / 1.2	16 / 10	10

New Models!

Talk To Us About Your Custom Requirements

SYNERGY® MICROWAVE CORPORATION

Phone: (973) 881-8800 | Fax: (973) 881-8361
E-mail: sales@synergymwave.com | Web: www.synergymwave.com
Mail: 201 McLean Boulevard, Paterson, NJ 07504

interoperability with allies and partners to stay ahead of strategic competitors. HACM is an air-launched, scramjet-powered hypersonic weapon designed to hold high-value targets at risk in contested environments from standoff distances.

Orolia Defense and Security has received initial production authorization to provide PRSS1b Personnel Recovery Devices to the **U.S. Army**, shipment began in September 2022. The order will fulfill the first line item complying with the current indefinite delivery/indefinite quantity contract. Orolia's PRSS1b PRD will be the first device of its kind to provide second-generation Cospas-Sarsat signaling that delivers faster and greater location accuracy than any other previously fielded tactical location device. Cospas-Sarsat is an international, humanitarian search and rescue system that uses space-based technology to detect and locate 406 emergency beacons carried by ships, aircraft or individuals venturing into remote areas, often inaccessible by mobile phone.

PEOPLE


▲ *Christine Dunbar*

IQE plc has appointed **Christine Dunbar** as vice president of U.S. sales. The decision to appoint Dunbar follows an extensive search process led by Wayne Johnson, executive vice president of sales and business development. With over two decades of experience working with multinational technology companies in the semi conductor industry, Dunbar has the expertise required to lead execution of IQE's U.S. sales strategy.

Mercury Systems Inc. announced that **Allen Couture** joined the company as senior vice president of execution excellence. In this customer-centric role reporting to Mercury CEO Mark Aslett, Couture will have a matrixed responsibility for engineering, supply chain, operations, quality and program management to ensure Mercury has systems, processes and talent that can scale to support Mercury's growth strategy. Couture has spent the last 10 years in leadership roles with Raytheon Technologies, most recently serving as vice president of operations and security at Raytheon Missiles & Defense.

Kymeta announced the addition of retired Boeing executive **Nicole Piasecki** to its board of directors. The news comes in light of **Steve Spengler**'s retirement from the board after serving for five years. Piasecki is a seasoned executive with over 35 years of experience in both rotary and fixed wing air-


▲ *Nicole Piasecki*


▲ *Lt. General (retired) Fran Beaudette*

Qorvo® Ultra-Wideband

Enabling Seamless & Secure Ecosystems

Ultra-Wideband has been adopted into **40+** verticals across mobile, consumer, automotive & industrial

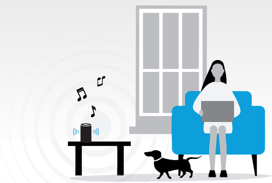

Spatial Awareness

Safety

Secure Transactions

Location Services

Why Qorvo?

- **We can help you** with expertise across 100s of applications in mobile, automotive, consumer and industrial
- **We have turnkey solutions and software** including low-latency/low power chips
- **We will take you to the next level,** investing in UWB R&D to enable your future applications and use cases
- **Join our tech forum,** the largest UWB technical community, with 3500+ engineers

Resources

Brochures & Ebooks
- Ultra-Wideband Brochure
- Ultra-Wideband For Dummies® Ebook

Blogs
- How Does Ultra-Wideband Work? Learn from Qorvo Experts
- Lights, Camera, Action! UWB is the Star Supporter in Le Premier Royaume
- Bringing the Bible to Life with Ultra-Wideband
- Location, Location, Location: The Road to Ultra-Wideband

Videos
- A Future Enabled by Ultra-Wideband
- UWB for Automotive: An Engineering Primer
- The Future is Ultra-Wideband

White Papers
- Getting Back to Basics with Ultra-Wideband

To learn more, visit **www.qorvo.com/go/uwb**

qorvo®

craft at Boeing and United Technologies. In addition to welcoming Piasecki, Kymeta has added **Lt. General (retired) Fran Beaudette** to the company's board of advisors. General Beaudette spent 32 years in the U.S. Army, most recently as the head of USASOC, a 36,000-soldier command responsible to man, train, organize and equip the U.S. Army's Special Operations.

▲ *Donna Vareha-Walsh*

Indium Corp. announced that its director of global supply chain and international trade compliance, **Donna Vareha-Walsh**, has been elected to the American Tin Trade Association board of directors. In her role at Indium Corporation, Vareha-Walsh oversees the company's global supply chain and trade compliance functions which includes all inventory, quality, sourcing, logistics and supply chain strategies. She leads a global team to ensure Indium Corporation's global business has a secure supply chain with quality partner suppliers. Vareha-Walsh has more than 20 years of metals market experience from numerous roles and responsibilities, including director of Global Procurement for a global premium alloy company and director of Metallurgical Operations and Procurement for a global tungsten-based business.

REP APPOINTMENTS

HyperLabs of Louisville, Colo., announced the addition of **Ward Davis Associates** as their newest U.S. sales representative covering the state of California. HyperLabs is a provider of high performance components and test equipment with a focus on high speed data and time domain applications. HyperLabs develops ultra-broadband baluns, pickoff tees, bias tees samplers, amplifiers (and more) to 110 GHz. Focusing heavily on cutting-edge yet budget-conscious designs, HyperLabs also offers a range of benchtop pulse/impulse generators, TDR, TDT and signal path analyzers.

Modelithics introduced **EMA Design Automation Inc.** as a Modelithics Reseller. As a reseller of Modelithics, EMA will be able to meet the needs of design engineers globally by offering highly accurate RF and microwave active and passive simulation models for Modelithics' premium product, the Modelithics COMPLETE Library, which includes over 825 models representing more than 25,000 components from over 70 vendors.

TTM Technologies' Radio Frequency & Specialty Components Business Unit (formerly known as Anaren) entered into a distribution agreement with **RFMW**. TTM will be offering its complete line of RF&S products through RFMW, including its proven signature lineup of Xinger® brand products. The distribution services will include opportunity identification and development, technical sales support and distribution. TTM components will also be available on the RFMW online store.

INVITED PAPER

InP + CMOS Heterogeneous Integration for The Next Generation of Wireless

Nadine Collaert and Michael Peeters
imec, Leuven, Belgium

Early discussions of the capabilities that will enable 6G envision materials and devices operating above 100 GHz. Indium phosphide (InP) is one semiconductor technology with the characteristics to achieve the required speed, efficiency and output power for sub-THz frequencies. To serve global wireless markets, InP process technology must be commercialized to maintain the performance advantages while able to be mass produced at the requisite prices to meet market needs. To develop InP into a mature technology, imec is researching nano-ridge engineering to grow InP on Si. Then, to integrate all the semiconductor components into a multi-function communications circuit, imec is exploring printed circuit board (PCB), 2.5D and 3D packaging technologies.

Every 10 years heralds a new generation of mobile communications. Over the generations, the number of subscribers has grown tremendously, each subscriber consuming an ever-increasing amount of wireless data. In the beginning, we were happy to send a text message. Today, 5G has achieved more than 1 billion human-to-machine and machine-to-machine connections with peak data rates of 10 Gbps. 5G is also an inflection point: in addition to needing more connections with data rates at ever higher speeds, the technology has the potential to enable new applications such as autonomous driving and holographic presence. These demands on the radio technology will drive 6G, envisioned for launch in 2030. By then, we will expect peak data rates greater than 100 Gbps with extreme coverage, pervasive connectivity and capabilities undefined today.

GENERATING EFFICIENT POWER ABOVE 100 GHZ

To enable these very high data rates, the telecom industry has been increasing channel bandwidth, which pushes operating frequencies higher. The vision for 6G is that the frequencies above 100 GHz will be tapped, starting with D-Band around 140 GHz. The biggest semiconductor challenge for circuits above 100 GHz is achieving sufficient gain, output power and efficiency. For both CMOS and SiGe amplifiers, the saturated output power at D-Band does not exceed 15 dBm, with efficiency typically below 10

PRECISION DEVICES knowles

Check out our complete range of RF and microwave solutions that support applications from VHF to Ka band.

PRODUCT HIGHLIGHTS

SMT Cavity Filters at C Band

- Solder Surface Mount Assembly Cavity Filters
- 1-5% Bandwidth

V80 SLC

- Highest capacitance in the smallest footprint
- Excellent high frequency response

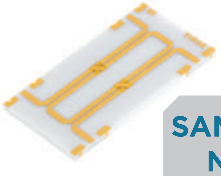

SAMPLING NOW!

SMT Quadrature Hybrid Couplers, C to K band

- Capability from C to K band
- Inherently wide band
- Surface Mount Assembly

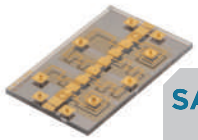

SAMPLING NOW!

2-18GHz Highpass and Bandpass Filters

- Very wide band, L to Ku
- Low Insertion Loss
- Temperature Stable

RfMW® It's who we are It's what we do

>> Learn more: rfmw.com/dielectric

Contact us today to explore a range of catalog and custom design options: **sales@rfmw.com**

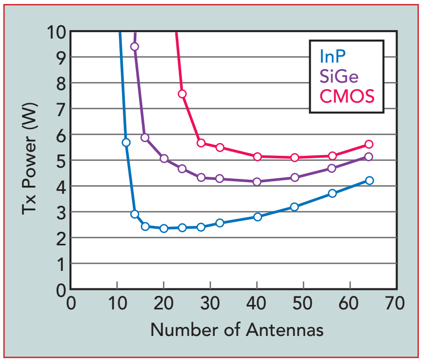

Fig. 1 PA Tx power vs. number of antenna elements for a constant array EIRP, comparing InP, SiGe and CMOS PAs.

percent. This is very low for communications systems using popular modulation schemes like 64-QAM. To achieve the required linearity, the power amplifier (PA) is backed off more than 6 dB below its saturated output capability. As the output power is reduced, efficiency drops more than linearly.

InP offers much better performance at these frequencies: output power greater than 20 dBm with efficiencies above 20 percent—even to 30 percent. For arrays where the transceiver footprint is restricted to a half-wavelength or the number of antenna elements is limited, InP enables 2× lower power consumption and 2× smaller footprint (see ***Figure 1***).[1]

BRINGING INP TO MATURITY

Creating InP heterojunction bipolar transistors (HBTs) for 100 GHz and higher frequency systems requires, first, a mature and cost-efficient InP technology and, second, an approach to integrate InP and Si components into a complete system. To meet both challenges, heterogeneous integration of a III-V material such as InP with CMOS is key. CMOS will be the predominant technology used for calibration, control, beamforming and data conversion.

To meet the speed, efficiency and output power needed for these wireless systems, imec envisions InP HBTs fabricated on a 300 mm (12 in.) Si wafer platform. Today, compared to Si, InP wafers are small—under 6 in.—and devices are fabricated using serial processes such as e-beam for gate lithography, and the contact metallization is gold-based. InP is brittle, one of the most prominent challenges. None of these are compatible with CMOS fabrication.

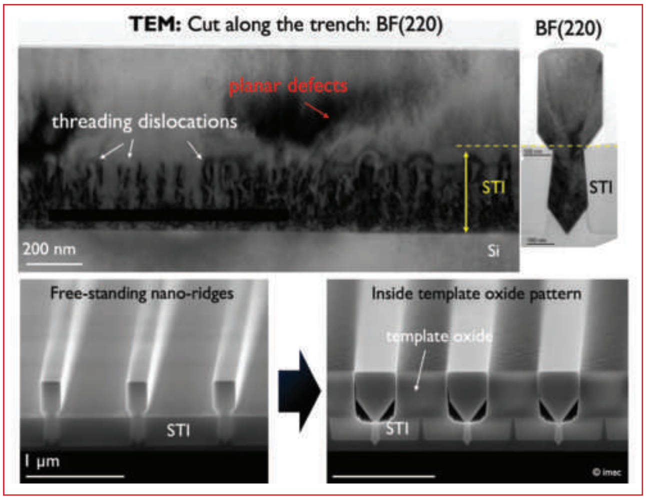

Fig. 2 Nano-ridges fabricated with InGaAs.

To use InP with Si, imec is researching ways to transfer III-V materials onto Si. Due to the large lattice mismatch between both materials, growing InP on Si usually introduces defects, mainly threading dislocations and planar. These induce leakage currents that can dramatically deteriorate device performance or impair reliability because the defects capture and release carriers at RF frequencies. To address the defects generated when directly growing InP on Si, imec is developing a fabrication process called nano-ridge engineering, which selectively grows the III-V material in pre-patterned structures or trenches in the Si (see ***Figure 2***). These high aspect-ratio trenches are very effective, trapping the defects in the narrow bottom part and growing high-quality, low defect material out of the trench. At the same time, overgrowing the nano-ridge widens it near the top, forming a solid base for a device stack. Reducing the pitch between nano-ridges enables them to merge to create a local plate of III-V material.

Recently, imec demonstrated box-shaped nano-ridges fabricated with 53 percent InGaAs, which efficiently trapped the threading dislocations in the trench. The nano-ridges were successfully grown both standalone and in a guided template. imec is using the same approach—combining InGaAs nano-ridge engineering with insights from earlier demonstrations of InGaP/GaAs nano-ridge HBTs—to develop a heterostructure stack for 140 GHz applications.

Other than direct growth such as nano-ridge engineering, InP can also be placed on Si using small InP substrates as the starting material. Called wafer reconstitution, high-quality InP substrates would be diced and sorted into non-patterned tiles during wafer fabrication, with the tiles subsequently attached to a Si wafer, planarized and processed in the fab. ***Table 1*** assesses the performance, cost and heterogeneous integration potential of the direct growth and wafer reconstitution options compared to native InP substrates.

TABLE 1

NATIVE INP VS. INTEGRATION TECHNIQUES FOR INP ON SI

	Native InP Substrates	Nano-Ridge Engineering	Wafer Reconstitution
Performance	High f_t/f_{max} and Excellent PA Performance	Requires Defects < 5M	Similar to Native InP, Not Demonstrated
Cost	High	Further Reduction: Increase III-V Area Through Pitch Scaling	Further Reduction: Reusability and Increase III-V Area
Heterogeneous Integration	Needs Back-End Adaptation of Gold-Compatible 2.5D/3D Approach	Back-End Multi-Level Copper Possible	Back-End Multi-Level Copper Possible

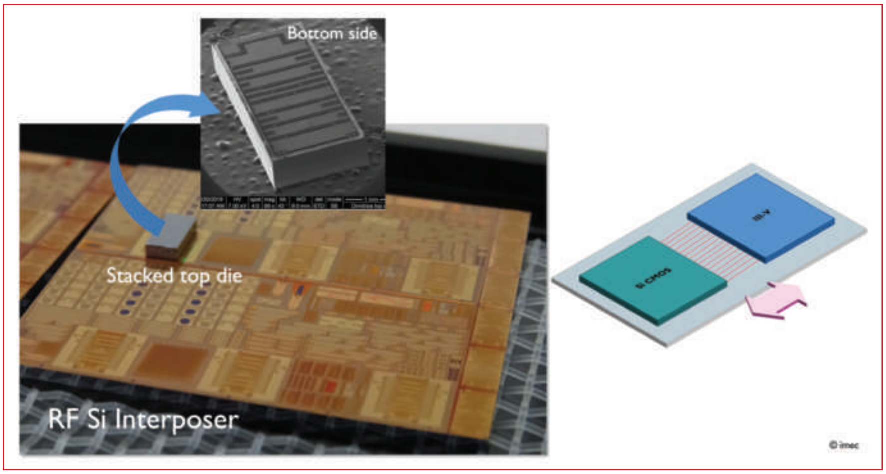

Fig. 3 Top view of an RF interposer with a Si stacked top die.[2]

SYSTEM LEVEL CO-INTEGRATION

Obtaining a mature and cost-efficient InP technology through direct growth or wafer reconstitution is only part of the challenge, however. The resulting components need to be integrated into a complete system comprised of various building blocks in III-V and CMOS technologies, such as InP HBTs for PAs or CMOS for the beamforming transceiver. This poses a set of integration challenges. imec is looking into monolithic (2D) integration of III-V and Si devices in the same plane and 2.5D and 3D integration approaches for heterogeneous integration.

State-of-the-art PCB technology is continually being optimized to support higher frequencies, including reducing the pitch and optimizing materials and layout. 2.5D integration uses Si interposers—a chip or layer with lithography-defined connections and possibly through Si vias—to connect III-V and Si die. While this technology has been optimized for high speed digital applications (see ***Figure 3***), it requires development to optimize it for RF. imec is evaluating dielectrics and various thicknesses of the metal layers to achieve low loss, high frequency interconnects. Options include high resistivity Si substrates or thick dielectric layers to distance the metal layers from the lossy substrate; also, a very thick redistribution layer, an extra metal layer to reduce metal loss. imec is also developing the capability to integrate high-quality passives for certain circuit applications.

2.5D AND 3D: KEY FOR HETEROGENEOUS INTEGRATION

Why 3D integration? As frequency increases, wavelength decreases and the area of an antenna array shrinks accordingly. Above 100 GHz, the antenna pitch gets smaller than the front-end circuit pitch, as the area of mmWave RFICs hardly shrinks. So the footprint of the antenna array sets the size constraints; to fit everything underneath the antenna, heterogeneous integration using the third dimension becomes necessary.

Over the last decade, tremendous progress has been made with 3D interconnects, particularly reducing the interconnect pitch for wafer-level applications—i.e., wafer-to-wafer, die-to-wafer (see ***Figure 4***).[3] For wafer-to-wafer or hybrid bonding, imec has achieved pitches below 1 µm and can push this down to below 500 nm. The same trend to reduce the pitch holds for die-to-wafer bonding and die stacking using micro-bumps.

Several challenges are shared between the two integration schemes for >100 GHz cases. First, they both rely on having a fine via or micro-bump pitch below 100 µm. Second, they must accommodate large numbers of connections for routing

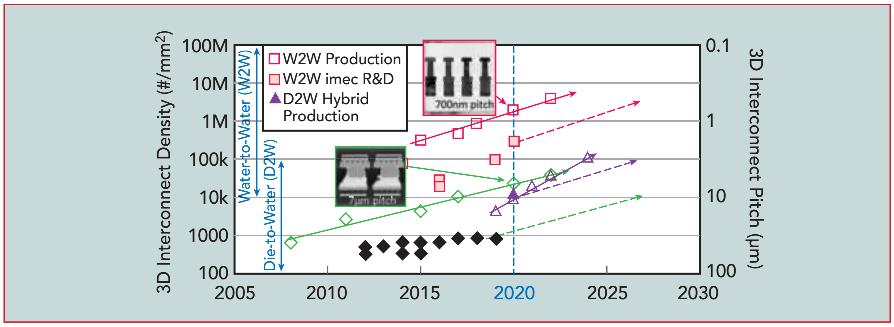

Fig. 4 3D interconnect technology roadmap. Includes data from H.-S. Philip Wong, et al.[4] and Techinsights.

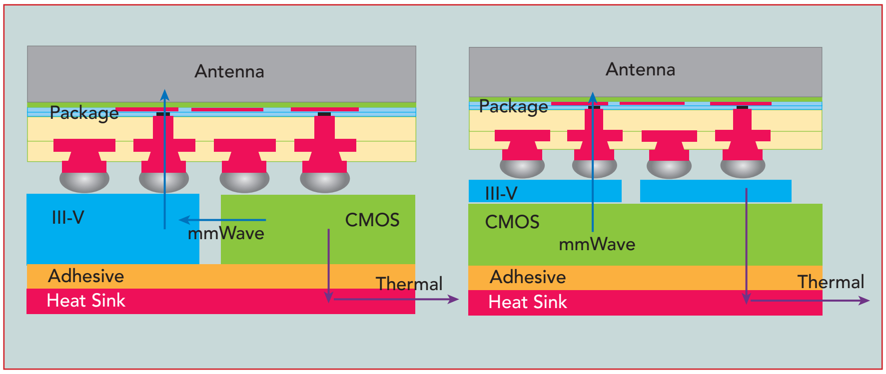

Fig. 5 2/2.5D integration using a Si interposer to connect the III-V and Si die (a). 3D integration where the III-V die are stacked on the Si (b).

the RF, DC, IF and digital signals. Finally, both the trace and space dimensions need to be much smaller than 50 µm, preferably between 5 and 10 µm.

There are also differences between the two schemes (see ***Figure 5***). In the case of 2D or 2.5D integration, the III-V device sits next to the CMOS IC, enabling better thermal management because both die can be in direct contact with a heat sink. The disadvantage is that the footprint may need to be extended in one dimension for some applications, meaning this architecture only enables 1D beam steering. In comparison, 3D integration enables all the die and circuits to fit under the antenna and enables 2D beam steering across a hemisphere. 2D beam steering is necessary for 5G and similar applications to minimize penetration losses and increase reach. With 3D, thermal management is more challenging and, of course, 3D integration is more complex, having unique processing challenges.

SYSTEM TECHNOLOGY CO-OPTIMIZATION

The choice of integration and packaging solutions ultimately depends on the application. Because so many options are available, imec has launched a system technology co-optimization (STCO) program to guide the technology choices at the system level. The STCO methodology uses architecture and application constraints, assessing signal loss, bandwidth, heat dissipation, mechanical stability and cost. Considering these parameters together enables trade studies to determine the appropriate technology and device designs for 6G. ■

References

1. C. Desset et al., "InP/CMOS Co-integration for Energy Efficient sub-THz Communication Systems," *IEEE Global Communications Conference*, December 2021.
2. X. Sun et al., "Cost-Effective RF Interposer Platform on Low-Resistivity Si Enabling Heterogeneous Integration Opportunities for Beyond 5G," *IEEE 73rd Electronic Components and Technology Conference*, June 2022.
3. E. Beyne, "3D System Integration: Technology Landscape and Long-Term Roadmap," *Roadmap on 3D Interconnect Density Forum, International Solid-State Circuits Conference*, February 2021.
4. H.-S.P. Wong et al., "A Density Metric for Semiconductor Technology," *Proceedings of the IEEE*, Vol. 108, No. 4.

Nxbeam

Ka-Band Power

27 TO 31 GHz

Maximized performance for linear power applications

GaN MMIC's to 40W

Nxbeam's suite of Ka-band PA MMICs offers customers an unparalleled combination of power, gain, and efficiency with proven reliability.

PRODUCTS:
NPA2001-DE
NPA2002-DE
NPA2003-DE
NPA2030-DE

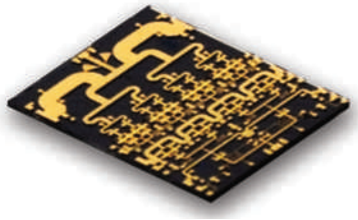

Packaged MMICs to 35W

Nxbeam offers its Ka-band MMICs in leaded flange packages for easier system integration

PRODUCTS:
NPA2001-FL
NPA2002-FL
NPA2003-FL
NPA2030-FL

Module Products to 60W

For higher levels of power and integration, Nxbeam offers modules that combine multiple Nxbeam MMICs to achieve higher performance in an easy-to-use form factor. Custom designs available

PRODUCTS:
NPM2001-KW
NPM2002-KW
NPM2003-KW

Chipless RF Identification Tags with Microstrip Patch Resonators

Kawther Mekki and Ali Gharsallah
University of Tunis El Manar, Tunis, Tunisia

Omrane Necibi
University of Jouf, Jouf, Saudi Arabia

Hugo Dinis and Paulo Mendes
University of Minho, Braga, Portugal

An RF identification (RFID) coding approach is based on the radar cross section (RCS) of a multi-patch chipless RFID tag. Combined with classical frequency coding, this increases the coding capacity. This work describes a six-resonator RFID tag using microstrip patches that has a high data capacity and low-cost. It can be directly printed on products such as personal IDs, credit cards, paper and textiles because it needs only one conductive layer. It is designed to operate over the range of 4.5 to 6.2 GHz, at frequencies allocated for RFID systems.

For several years, RFID technology has brought many innovations in the field of automatic identification of people and goods; however, for consumer product identification the barcode is still dominant.[1] An RFID system consists of RFID tags and an RFID reader.[2,3] RFID tags are attached to objects to be identified. Each RFID tag contains a unique tag identification number (tag-ID). The RFID tag contains electronic circuitry that stores the tag-ID and communicates wirelessly with the RFID reader. The RFID reader transmits an interrogation signal, which communicates with the RFID tag to obtain its unique tag-ID. The tag either actively transmits an RF response signal or passively reflects (backscatters) the interrogation signal. The tag response is captured by the RFID reader antenna and processed by the reader to extract its tag-ID.[4-7]

Chipless technology is of interest since its cost is lower than technologies with active chips and it enables operation under adverse environmental conditions where electronic chips can be easily destroyed. There has been much research focused on high performance chipless RFID tags.[8,9] Numerous resonant topologies have been proposed, such as U-shape,[10] L-shape,[11] octagonal,[12] slot,[13] triangular patch,[14] microstrip line[15] and shorted dipoles oriented at 45 degrees.[16]

According to the encoding method, chipless RFID tags can be grouped into two main categories: 1) frequency signature based[17-20] and 2) time domain reflectometry based chipless RFID.[7,21-23]

Recent development in the era of low-cost and compact communication systems has largely been due to the advent of small weight and size antennas that can provide good performance over a broad frequency range. The rectangular microstrip patch is an attractive choice. Its theory of operation is computationally simple. It is low-cost, easy to fabricate and is conformable. It enables low-profile structures of compact size that assure reliability, mobility and good efficiency.

This work describes a chipless tag comprising six patch resonators with coding based on control of its RCS magnitude over a 1.6 GHz bandwidth from 4.5 to 6.2 GHz. The effects of mutual coupling are also explored. Phase, along with frequency coding, enables increased coding capacity. Measurements validate simulation.

MICROSTRIP PATCH RESONATOR DESIGN

The microstrip patch is designed to operate over a narrow band. In the design of RCS magnitude-based chipless tags, resonant behavior is desirable. The design procedure is described by Karmakar.[24] It is fabricated on a 0.76 mm thick Rogers RO4350B substrate (see ***Figure 1***).

The width W_p and length L_p are

given by the following equations:[25]

$$W_p = \frac{c}{2f_0\sqrt{\frac{(\varepsilon_r+1)}{2}}} \quad (1)$$

where

$$L_p = L_{eff} - 2\Delta L \quad (2)$$

$$L_{eff} = \frac{c}{2f_0\sqrt{\varepsilon_{reff}}} \quad (3)$$

And ΔL is determined by

$$\Delta L = 0.412h\frac{(\varepsilon_{eff}+0.3)\left(\frac{W}{h}+0.264\right)}{(\varepsilon_{eff}-0.258)\left(\frac{W}{h}+0.8\right)} \quad (4)$$

Where c is the speed of light in a vacuum, h is the substrate thickness and ε_{reff} is the effective permittivity given by the equation:

$$\varepsilon_{reff} = \frac{\varepsilon_r+1}{2} + \frac{\varepsilon_r-1}{2}\left[1+12\frac{h}{W_p}\right]^{-\frac{1}{2}} \quad (5)$$

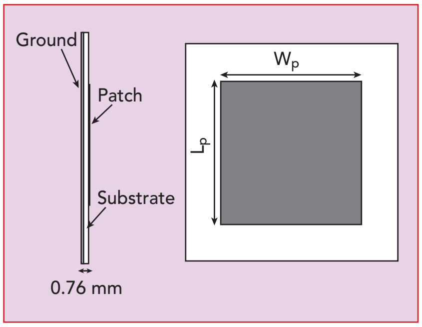

Fig. 1 Microstrip patch antenna geometry.

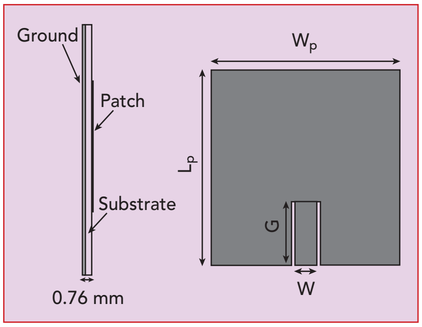

Fig. 2 Geometry of the chipless RFID tag using slots to reduce size. L_p = W_p = 16.5, W = 1.2 and G = 6 mm for a patch resonant at 4.6 GHz.

PARAMETRIC STUDY

The microstrip antenna's patch length L_p and width W_p are calculated theoretically to be 17.2 and 21.7 mm, respectively, for resonance at 4.6 GHz, the target frequency of the lowest frequency patch. A parametric study of the dimensions of the patch antenna with slots (see ***Figure 2***) is done to optimize performance and reduce size (L_p = W_p = 16.5 mm).

The parameter sweep section of the CST Studio Suite is used to optimize the various patch parameters. Changes to W_p, L_p and slot dimensions W and G have a significant impact on RCS. ***Figure 3a*** shows the resonant frequency as a function of L_p and W_p. The initial result, using dimensions analytically derived show resonance at f = 3.6 GHz. After optimization, resonance is achieved at f = 4.6 GHz with $L_p$and W_p both equal to 16.5 mm. For best results, W = 0.9 to 1.5 mm and G = 4 to 8 mm, as shown in ***Figure 3b***. ***Figure 4*** shows


RF Test Solutions
Real-Time Spectrum Analyzers
RSA3000 & 5000 Series
NEW!
RF Signal Generator
DSG5000 Series
• 3 to 6.5GHz Models
• 1ms Sweep
• 1Hz RBW
• 7 Visualization Modes
• Available Tracking Generators
• Vector Network Analysis
• 3.5" Touch Screen
• Frequencies to 20GHz
• Up to 8 Channels
• Long Term Phase Stability +/- 1°
• Amplitude, Frequency, Phase & Pulse Modulations
Discover RIGOL's Powerful RF Test Solutions
RIGOL
www.RIGOLna.com

the final magnitude and phase response of the 4.6 GHz patch.

A similar procedure is used to determine the dimensions of the other patches in the multi-bit tag.

CHIPLESS RFID DESIGN SIMULATION AND MEASUREMENT

Four-Bit Patch Tag

In the case of a multi-patch tag, an array of narrowband patches performs the functions of signal reception, tag-ID data encoding and transmission of backscattered signals. The individual patches each have a different resonant frequency and backscatter. A unique frequency signature is produced by the array in the total backscattered signal. The RCS of the tag presents the frequency signature encoding the tag-ID data.

Two multi-patch tag designs are considered. The first is composed

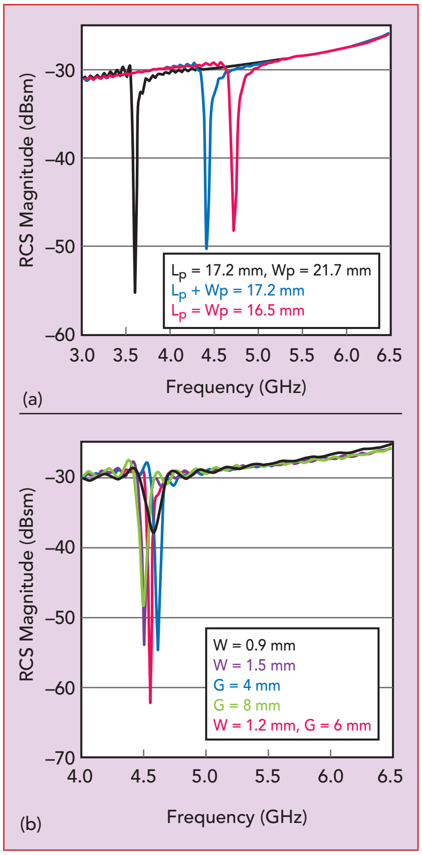

▲ Fig. 3 RCS magnitude over frequency vs. L_p and W_p (a) and W vs. G (b).

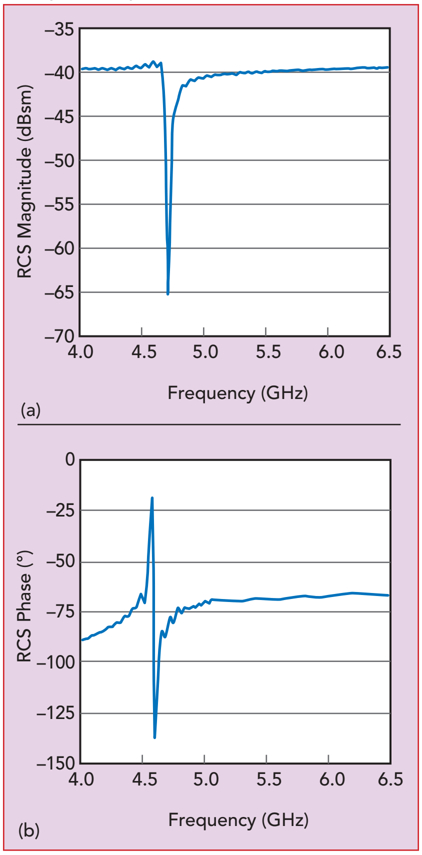

▲ Fig. 4 RCS magnitude (a) and phase (b) of the optimized 4.6 GHz design.

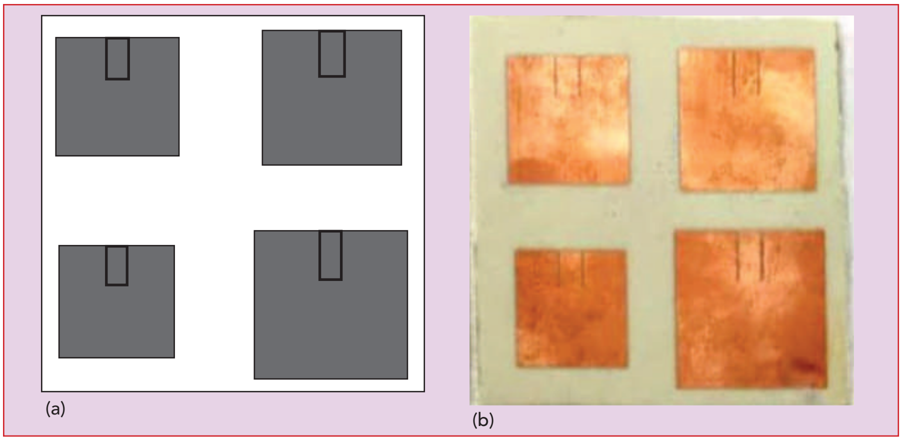

Fig. 5 Layout (a) and manufactured (b) patch tags returning the ID 1111.

of four rectangular microstrip patch resonators. The four patch resonators have lengths L_p of 12, 13.5, 15 and 16.5 mm and resonate at 6.1, 5.7, 5.1 and 4.6 GHz, respectively (see ***Figure 5***). Measurements are made in an anechoic chamber using a Keysight PNA-N5221A vector network analyzer (VNA) as shown in ***Figure 6***. The horn antennas are separated by e = 30 cm. All resonant peaks up to r = 30 cm can be extracted. Simulated and measured results are shown in ***Figure 7***.

One or more rectangular patches can be printed on a tag, and one or more of these patches can be shorted, nulling its corresponding frequency. A data bit 1 or 0 is encoded according to the presence or absence of a notch in the spectral response, respectively. Four notches appear in the magnitude response as four 1's of the tag with ID "1111," while three notches appear for three 1s, with no notch for the 0 in the magnitude response of the tag with ID "1101" (see ***Figure 8a***). Four phase transitions are seen in the phase response for the tag with ID "1111," but no phase transition appears in the 0 for the tag with ID "1011" (see ***Figure 8b***).

Six Bit Patch Tag

Data capacity can be achieved by adding more resonators. Six resonators with L_p = 12, 13.5, 14.5, 15.5, 16.5 and 17.5 mm create six notches in the spectrum corresponding to six resonant frequencies at 6.1, 5.7, 5.4, 5.1, 4.7 and 4.4 GHz. The simulated and the manufactured structures are shown in ***Figure 9***. Simulation and measurement results are shown in ***Figure 10***. Six resonances are clearly detected and easily distinguishable and show good agreement between measurements and the simulation.

The theoretical RCS definition is independent of the distance (r)

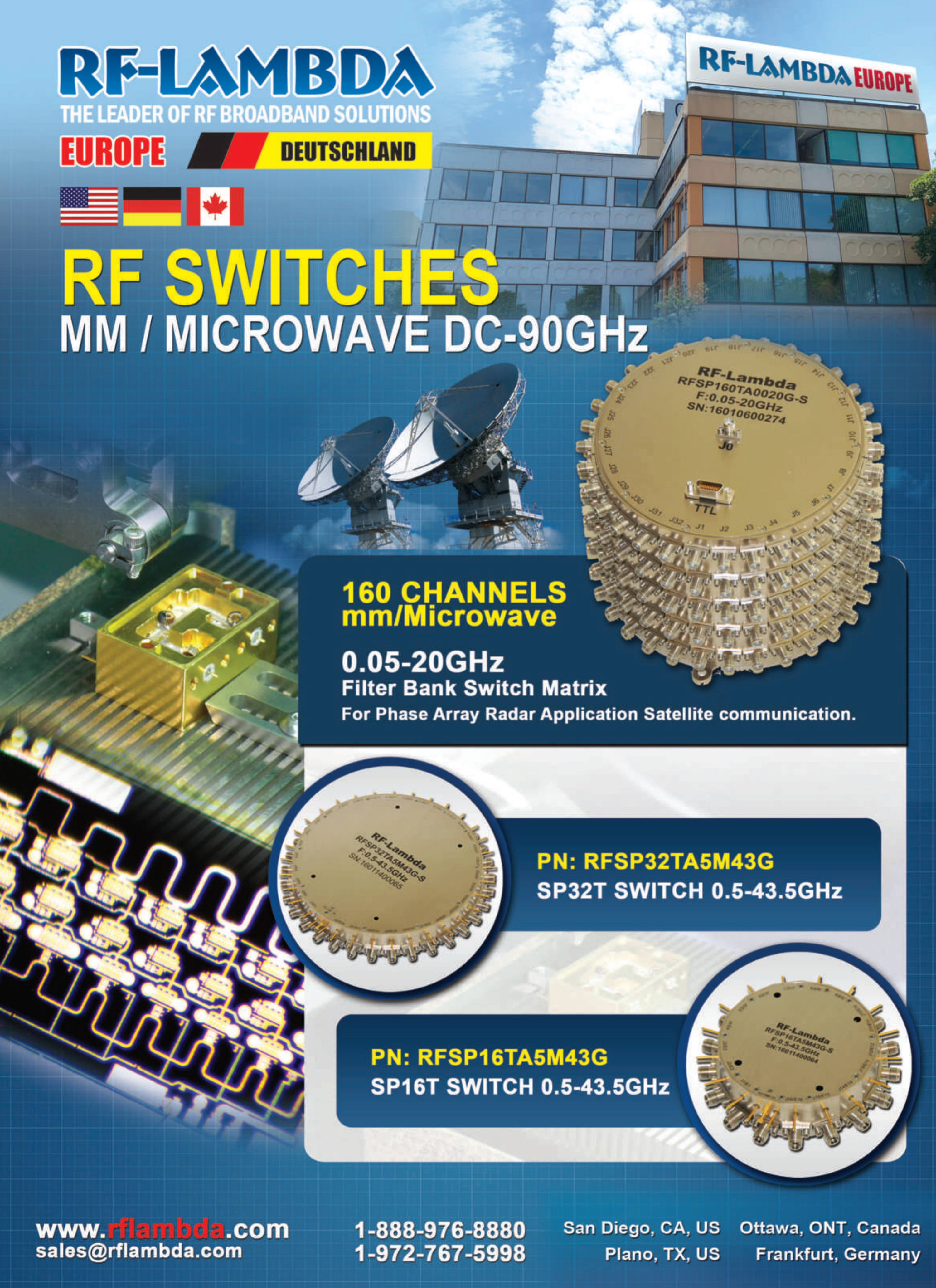
RF-LAMBDA
THE LEADER OF RF BROADBAND SOLUTIONS
EUROPE
DEUTSCHLAND
RF-LAMBDA EUROPE
RF SWITCHES
MM / MICROWAVE DC-90GHz
RF-Lambda
RFSP160TA0020G-S
F:0.05-20GHz
SN:16010600274
J0
TTL
160 CHANNELS
mm/Microwave
0.05-20GHz
Filter Bank Switch Matrix
For Phase Array Radar Application Satellite communication.
PN: RFSP32TA5M43G
SP32T SWITCH 0.5-43.5GHz
PN: RFSP16TA5M43G
SP16T SWITCH 0.5-43.5GHz
www.rflambda.com
sales@rflambda.com
1-888-976-8880
1-972-767-5998
San Diego, CA, US
Plano, TX, US
Ottawa, ONT, Canada
Frankfurt, Germany

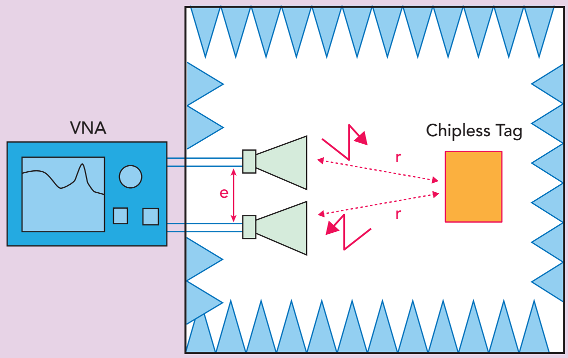

Fig. 6 Measurement setup using a VNA in an anechoic chamber.

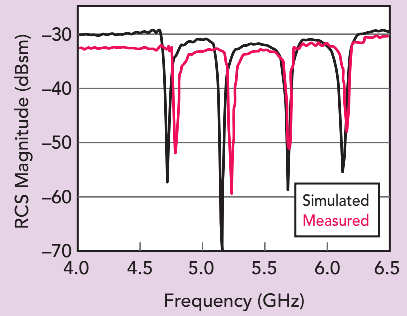

Fig. 7 Simulated vs. measured RCS magnitude of the 4-bit chipless tag.

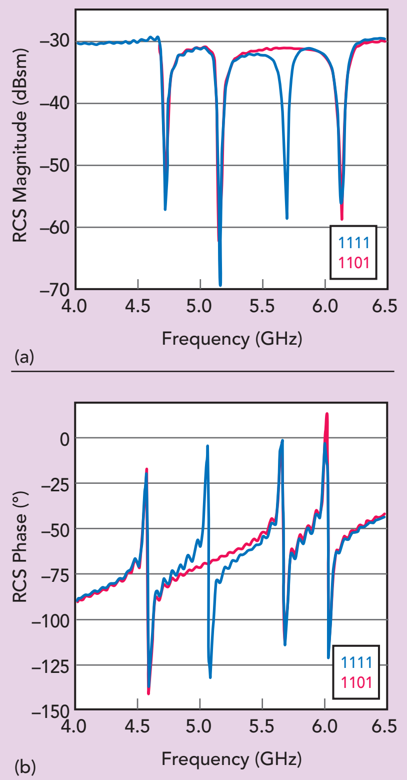

Fig. 8 Simulated vs. measured RCS magnitudes (a) and phase (b) for two tags with different IDs.

between the tag and the antenna.[26] In practice, the measured quantity is the backscattered power received at the antenna, which is highly dependent on the measurement setup. The Agilent PNA-N5221A VNA in a bistatic configuration is used to measure vertically polarized radiation in the frequency domain. In the frequency range of 2 to 8 GHz, the VNA delivers 0 dBm of power. Over the frequency band of interest, the two horn antennas each have a gain of 12 dBi. In the setup shown in Figure 6, measurements are made with e = 30 cm and r = 20 and 30 cm. With r at 30 cm, the notch at the highest frequency is not well defined, which implies degraded performance be-

yond that range (see ***Figure 11***).

The chipless tag yields 6-bit data with a unique frequency signature. Comparing the results of the blue curve with those of the red curve in ***Figure 12a***, the fourth notch disappears, creating a tag response with ID "111011." Six phase transitions are seen in the phase response for the tag with ID "111111" in the blue curve, while only five are visible in the red curve in ***Figure 12b***.

A comparison of this with other reported work is shown in ***Table 1***.

CONCLUSION

A chipless RFID tag operating from 4.5 to 6.2 GHz transmits and recovers multi-bit data. Rectangular shaped resonators increase the bit-encoding capacity. Multi-patch RFID chipless tags use narrowband resonant structures to create notch frequencies. Although 6-bit data is encoded in the proposed tag, a higher capacity data structure can

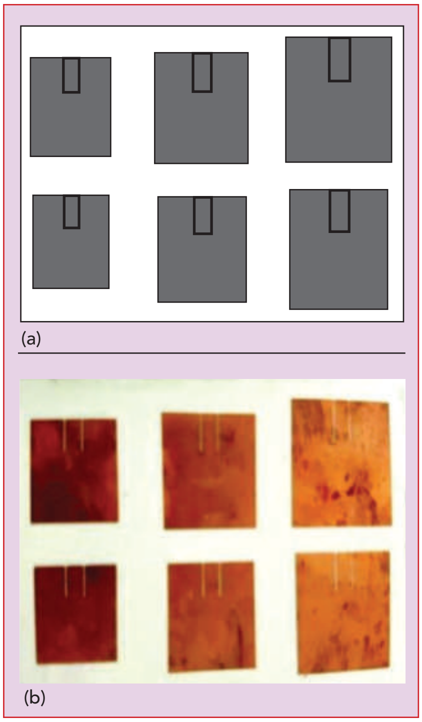

Fig. 9 Layout (a) and manufactured (b) patch tags designed to return the ID 111111.

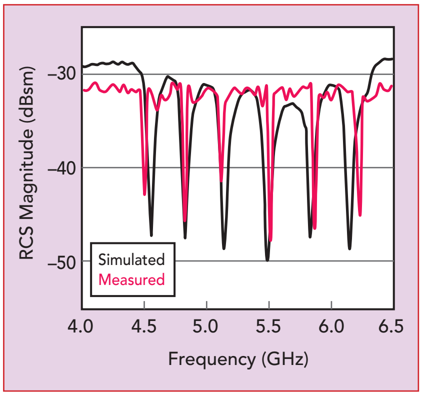

Fig. 10 Simulated vs. measured RCS magnitude of the 6-bit chipless tag.

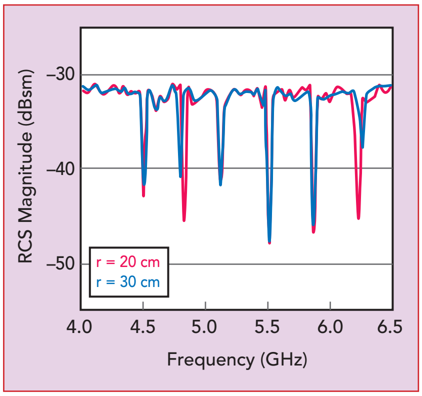

Fig. 11 RCS magnitude of the 6-bit chipless tag placed at 20 and 30 mm from the transmit and receive horn antennas.

be designed by adding more resonators while maintaining the same operating bandwidth. The low-cost single-sided compact chipless RFID tag can be printed directly on many items. ■

References

1. K. Athauda and N. Karmakar, "Chipped Versus Chipless RF Identification," *IEEE Microwave Magazine*, Vol. 20, No. 9, August 2019, pp. 47–57.
2. K. Mekki, O. Necibi, C. Boussetta and A. Gharsallah, "Miniaturization of Circularly Polarized Patch Antenna for RFID Reader Applications," *Engineering, Technology and Applied Science Research*, Vol. 10, No. 3, June 2020, pp. 5655–5659.
3. K. Mekki, O. Necibi, C. Boussetta and A. Gharsallah, "Design of a Miniaturized Dipole RFID Tag Antenna," *Indian Journal of Science and Technology*, Vol. 13, No. 30, August 2020, pp. 3103–3112.
4. A. Attaran and R. Rashidzadeh, "Chipless Radio Frequency Identification Tag for IoT Applications," *IEEE Internet Things Journal*, Vol. 3, No. 6, December 2016, pp. 1310–1318.
5. M. E. Jalil, M. K. A. Rahim, N. A. Samsuri, R. Dewan and K. Kamardin, "Flexible Ultra-Wideband Antenna Incorporated with Metamaterial Structures: Multiple Notches for Chipless RFID Application," *Applied Physics A*, Vol. 123, No. 1, January 2017.

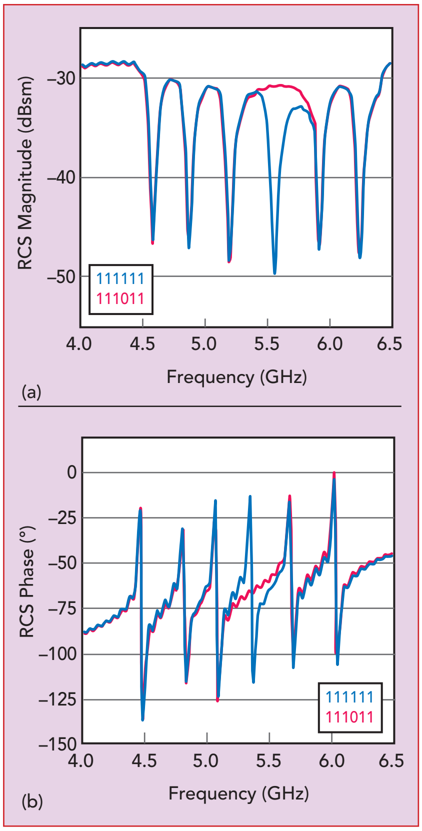

Fig. 12 RCS magnitude (a) and phase (b) responses for tags with IDs of 111111 and 111011.

6. A. El-Awamry, M. Khaliel, A. Fawky and T. Kaiser, "Adaptive Spectrum Scanning Techniques for Reducing the Identification Time of the Frequency Coded Chipless RFID System," *Transactions on Emerging Telecommunications Technologies*, Vol. 28, No. 11, November 2017.
7. M. Pöpperl, A. Parr, C. Mandel, R. Jakoby and M. Vossiek, "Potential and Practical Limits of Time-Domain Reflectometry Chipless RFID," *IEEE Transactions on Microwave Theory and Techniques*, Vol. 64, No. 9, September 2016, pp. 2968–2976.
8. H. Zhu, X. Li and S. Jia, "Compact and Coding Expandable Chipless RFID Tag with Bending Arms," *ACES Journal*, Vol. 34, No. 9, September 2019, pp. 1359–1365.
9. I. Jabeen, A. Ejaz, M. A. Riaz, M. J. Khan, A. Akram, Y. Amin and H. Tenhunen, "Miniaturized Elliptical Slot Based Chipless RFID Tag for Moisture Sensing," *ACES Journal*, Vol. 34, No. 9, September 2019, pp.1366–1372.
10. M. Polivka, J. Havlicek, M. Svanda and J. Machac, "Improvement in Robustness and Recognizability of RCS Response of U-Shaped Strip-Based Chipless RFID Tags," *IEEE Antennas and Wireless Propagation Letters*, Vol. 15, April 2016, pp. 2000–2003.
11. A. Ramos, Z. Ali, A. Vena, M. Garbati and E. Perret, "Single-Layer, Flexible, and Depolarizing Chipless RFID Tags," *IEEE Access*, Vol. 8, April 2020, pp. 72929–72941.
12. D. Betancourt, K. Haase, A. Hübler and F. Ellinger, "Bending and Folding Effect Study of Flexible, Fully-Printed and Late-Stage Codified Octagonal Chipless RFID Tags," *IEEE Transactions on Antennas and Propagation*, Vol. 64, No. 7, July 2016, pp. 2815–2823.

TABLE 1 CHIPLESS RFID TAG COMPARISON					
Reference	*Resonator Type*	*Frequency Range (GHz)*	*Bits Encoded*	*Useful Range (cm)*	*Size (mm²)*
11	L-Shaped	3 – 6	6	25	83 × 50
14	Triangular Patch	4.5 – 6.1	4	30	40 × 60
15	Microstrip Line	2– 3	4	50	60 × 36
16	Shorted Dipoles Oriented at 45°	3.1 – 10.6	6	10	70 × 42
16	Dual-L	4.5 – 6.5	4	25	50 × 50
This Work	**Square Patch**	**4.5 – 6.2**	**6**	**20**	**60 × 40**

13. N. Tariq, M. A. Riaz, H. Shahid, M. J. Khan, M. S. Khan, Y. Amin, J. Loo and H. Tenhunen, "Orientation Independent Chipless RFID Tag Using Novel Trefoil Resonators," *IEEE Access*, Vol. 7, August 2019, pp. 122398–122407.
14. K. Mekki, O. Necibi, H. Dinis, P. Mendes and A. Gharsallah, "Investigation on the Chipless RFID Tag with a UWB Pulse Using a UWB IR-Based Reader," *International Journal of Microwave and Wireless Technologies*, Vol. 14, No. 2, March 2022, pp. 166–175.
15. Y. J. Zhang, R. X. Gao, Y. He and M. S. Tong, "Effective Design of Microstrip-Line Chipless RFID Tags Based on Filter Theory," *IEEE Transactions on Antennas and Propagation*, Vol. 67, No. 3, March 2019, pp. 1428–1436.
16. A. Vena, E. Perret and S. Tedjini, "A Depolarizing Chipless RFID Tag for Robust Detection and its FCC Compliant UWB Reading System," *IEEE Transactions on Microwave Theory and Techniques*, Vol. 61, No. 8, August 2013, pp. 2982–2994.
17. Y. Z. Ni, X. D. Huang and C. H. Cheng, "Improved Chipless Tag Based on Multifilters," *Microwave and Optical Technology Letters*, Vol. 59, No. 8, August 2017, pp. 1890–1896.
18. M. Forouzandeh and N. Karmakar, "Self-Interference Cancelation in Frequency-Domain Chipless RFID Readers," *IEEE Transactions on Microwave Theory and Techniques*, Vol. 67, No.5, May 2019, pp. 1994–2009.
19. M. Svanda, M. Polivka, J. Havlicek, J. Machac and D. H. Werner, "Platform Tolerant, High Encoding Capacity Dipole Array-Plate Chipless RFID Tags," *IEEE Access*, Vol. 7, August 2019.
20. C. Herrojo, F. Paredes, J. M. Contreras, S. Zuffanelli and F. Martín, "Multistate Multiresonator Spectral Signature Barcodes Implemented by Means of S-Shaped Split Ring Resonators (S-SRRs)," *IEEE Transactions on Microwave Theory and Techniques*, Vol. 65, No. 7, July 2017, pp. 2341–2352.
21. C. Herrojo, M. Moras, F. Paredes, A. Nunez, J. Mata, E. Ramon and F. Martin, "Time-Domain-Signature Chipless RFID Tags: Near-Field Chipless RFID Systems with High Data Capacity," *IEEE Microwave Magazine*, Vol. 20 No. 12, December 2019.
22. M. A. Ashraf, Y. A. Alshoudokhi, H. M. Behairy, M. R. Alshareef, S. A. Alshebeili, K. Issa and H. Fathallah, "Design and Analysis of Multi Resonators Loaded Broadband Antipodal Tapered Slot Antenna for Chipless RFID Applications," *IEEE Access*, Vol. 5, October 2017, pp. 25798–25807.
23. A. Ramos, A. Lazaro, D. Girbau and R. Villarino, "Time-Domain Measurement of Time-Coded UWB Chipless RFID Tags," *Progress in Electromagnetics Research*, Vol. 116, January 2011, pp. 313–331.
24. N. C. Karmakar, "Tag, You're It Radar Cross Section of Chipless RFID Tags," *IEEE Microwave Magazine*, Vol. 17, No. 7, July 2016, pp. 64–74.
25. K. Mekki, C. Boussetta and A. Gharsallah, "Design and Miniaturization of UHF RFID Reader Antenna," *18th Mediterranean Microwave Symposium*, October 2018.
26. A. Vena, E. Perret and S. Tedjini, "Chipless RFID Tag Using Hybrid Coding Technique," *IEEE Transactions on Microwave Theory and Techniques*, Vol. 59, No. 12, December 2011, pp. 3356–3364.

Magnetically Tunable U-Slot Microstrip Patch Antenna Based on Nematic Liquid Crystal Materials

Adel Kouki, Fakher Sboui and Lassaad Latrach
University of Tunis El Manar, Tunis, Tunisia

A reconfigurable U-slot microstrip patch antenna uses a nematic state liquid crystal (LC) mixture operating at 5 GHz for wireless communications such as Wi-Fi. An external magnetic field from 0 to 1200 Oersted changes the relative permittivity of the LC to adjust the patch resonant frequency. A tuning range of 200 MHz in both measurement and simulation is demonstrated with a maximum gain of 4.05 dB. LC is considered a good candidate for reconfigurable antennas due to its low cost, low profile and performance.

Wireless communication has evolved to become a necessary aspect of our daily lives. At the same time, the growth of the market has led to an increase in the number of standards allocated to systems and terminals operating on different frequency bands. This multiplicity of communication standards typically requires the use of several antennas, each dedicated to a specific band. This, however, implies an increase in the physical size of the system with a significant impact on its cost, energy consumption and complexity. Alternatively, the use of a reconfigurable antenna operating over several frequency bands enables reduced size, power consumption and cost.

A patch antenna has many advantages, such as low weight, moderate cost and ease of manufacture. Nevertheless, for some applications, its bandwidth is too narrow. This limitation can be overcome by making it reconfigurable using lumped elements such as PIN diodes,[1] varactor diodes,[2,3] RF MEMS switches[4] or tunable materials such as ferroelectrics[5] and LC.[6-13] The possibility of changing the LC dielectric constant in its nematic state through an applied electric or magnetic field has attracted researchers in the microwave community for some decades.

In this work, a patch antenna is designed, using the characteristics of LCs to add reconfigurability. The nematic state LC mixture E7 is injected between the patch antenna and ground. Simulation and measurements demonstrate a tunable range of 200 MHz, with the application of a magnetic field, and a peak gain of 4.05 dB.

PROPERTIES OF LCS

The nematic state of a LC is generally used

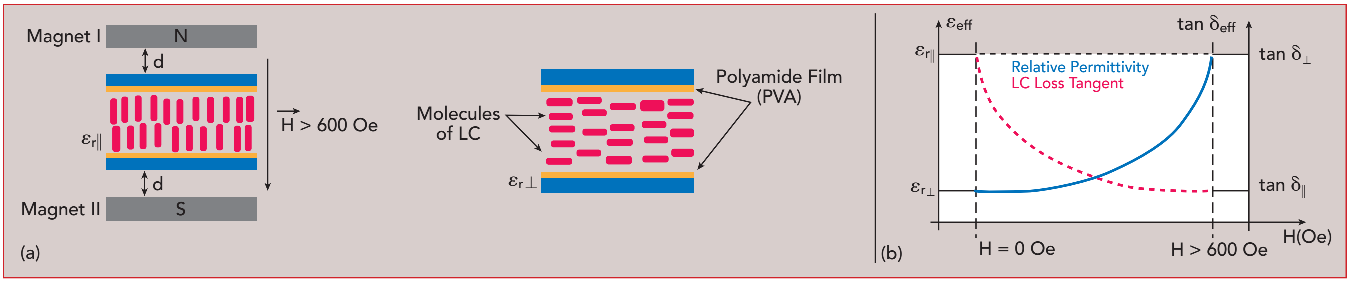

▲ Fig. 1 Parallel and perpendicular permittivity (a). Effective permittivity and loss tangent vs. applied bias magnetic field (b).[13]

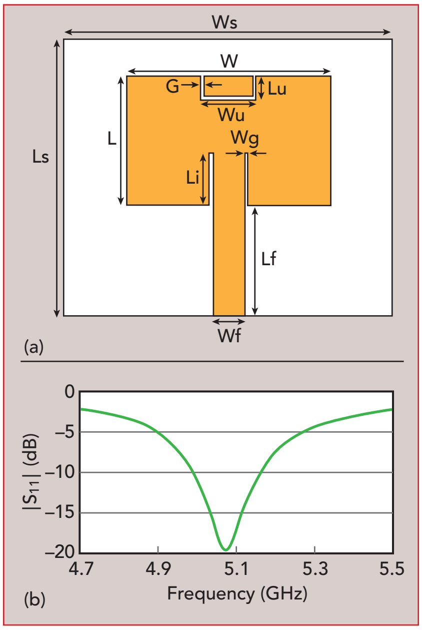

▲ Fig. 2 Microstrip patch antenna without LC (a) and simulated $|S_{11}|$ (b).

TABLE 1

DIMENSIONS OF ANTENNA WITHOUT LC

Description	Symbol	Dimension (mm)
Substrate Thickness	h	1.6
Substrate Width	Ws	30
Substrate Length	Ls	30
Patch Width	W	18.42
Patch Length	L	13.91
Inset Feed Length	Li	5.7
Inset Feed Gap	Wg	0.2
Microstrip Length	Lf	12.05
Microstrip Width	Wf	2.90
Slot Gap Width	G	0.2
Slot Width	Wu	5
Slot Length	Lu	2.7

in microwave and mmWave systems with the external application of an electric or magnetic field to change its dielectric constant. The use of an electric field to change the orientation of LC molecules is, by analogy, equivalent to the use of a magnetic field. In this work, a magnetic field is used to shift the frequency of a patch antenna. To switch on the magnetic field, two magnets are spaced 5 mm on either side; to switch off the magnetic field, the two magnets are removed.

The magnetic field applied to the LC must be greater than 600 Oe.[13] To ensure that the molecules of the LC are parallel to the applied magnetic field, the two magnets are positioned 5 mm from both sides of the antenna, where the total magnetic field strength equals 1200 Oe (see ***Figure 1***). The LC molecules are oriented according to the magnetic field applied. When no magnetic field is applied, alignment of the molecules is promoted by covering the lower and upper contact surfaces of the LC layer with a microscopic polyamide film. This achieves the perpendicular permittivity $\varepsilon_r\perp$. When the applied magnetic field is equal to 1200 Oe, the molecules are oriented in the same direction as the magnetic field, which achieves parallel permittivity $\varepsilon_{r\|}$. Martin et al.[7] used a foam substrate loaded with LC K15 to obtain a tunable frequency range of 140 MHz from 4.6 to 4.74 GHz and a tuning range of 4 percent, from 5.43 to 5.66 GHz, was achieved using LC E7.[13]

PATCH ANTENNA DESIGN

A 5 GHz antenna (see ***Figure 2a***) was designed using Equations 1 through 5.[14] The substrate was FR-4, with a relative permittivity ε_r = 4.4 and a thickness h = 1.6 mm. The patch dimensions were Ls = 30 and Ws = 30 mm. The inset feed Li and gap Wg = 5.7 and 0.2 mm, respectively. A 50 Ω microstrip line (Lf = 2.9 mm; Wf = 12.05 mm) was used to feed the patch on a grounded substrate. Design choices were based on simulations using the CST Studio Suite software. The width, W, was calculated using

$$W = \frac{1}{2f_c}\sqrt{\frac{2}{\varepsilon_{reff}+1}} \qquad (1)$$

where f_c is the center frequency and ε_{reff} is the effective permittivity. ε_{reff} is given by

$$\varepsilon_{reff} = \frac{\varepsilon_r+1}{2}+\frac{\varepsilon_r+1}{2}\left[1+12\left(\frac{h}{w}\right)\right]^{-1/2} \qquad (2)$$

where h is the thickness of the dielectric substrate.

ΔL, the extended incremental length of the patch, is calculated from

$$\frac{\Delta L}{h} = 0.412\frac{\left(\varepsilon_{reff}+0.3\right)\left(\frac{w}{h}+0.264\right)}{\left(\varepsilon_{reff}+0.258\right)\left(\frac{w}{h}+0.8\right)} \qquad (3)$$

The effective length is determined by

$$L_{eff} = \frac{c}{2f_c\sqrt{\varepsilon_{reff}}} \qquad (4)$$

The actual length of the patch is determined by

$$L = L_{eff} - \Delta L \qquad (5)$$

The final dimensions of the design are listed in ***Table 1***.

Figure 2b shows the simulated reflection coefficient, where $|S_{11}|$ reaches a value less than -19 dB at the resonant frequency of 5.07 GHz. The simulated radiation patterns

Dielectric Varactor

- New -

Tecdia's SMT analog varactors, made with unique voltage controlled dielectrics, are designed for controlling impedance inside analog phase shifters operational up to 100GHz.

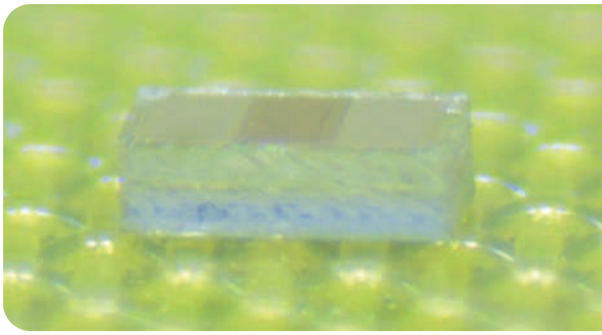

- Low ESR
- High Linearity
- Microsecond Switching Speed
- 0V Capacitance of 0.1pF or more
- 0201 SMT Solderable Form Factor

Applications

- Tunable Phase Shifters
- Tunable Matching Networks
- Tunable Filters
- Beamforming
- Voltage Controlled Oscillators

Final Markets

5G Backhaul and Small Cell
24GHz ~ 86GHz

Low Earth Orbit
26 ~ 40GHz

Radar
3GHz ~ 6GHz &
8GHz ~ 12GHz

Let's do this.
TECDIA

TECDIA Inc.
TEL +1-408-748-0100 FAX +1-408-748-0111 Email sales@tecdia.com

without the LC (see ***Figure 3***) show a maximum gain of 2.28 dB and a directivity of 6.80 dBi at 5.07 GHz.

The LC E7 mixture in its nematic state, i.e., as a liquid material, is injected into a cavity created above the ground with a depth of 1.5 mm on the substrate, and the upper and lower contact surfaces of the LC layer are covered by a microscopic polyamide film (see ***Figure 4***). Following a parametric study to determine the best position for the cavity, the LC layer is placed under the patch. The dimensions of the LC layer are listed in ***Table 2*** and its electrical characteristics are summarized in ***Table 3***.

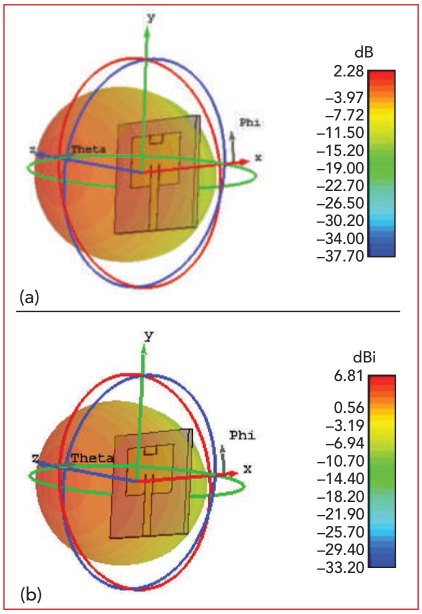

Fig. 3 Simulated 3D gain (a) and directivity (b) at the 5.07 GHz resonant frequency.

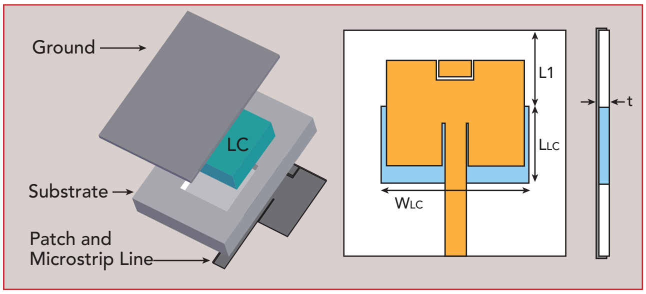

Fig. 4 Microstrip patch antenna loaded with LC E7.

TABLE 2

LC LAYER DIMENSIONS

	Parameter	Value (mm)
Length of LC Layer	L1	10
Width of LC Layer	W_{LC}	20
LC Layer Distance from Top	L_{LC}	10

SIMULATION AND MEASUREMENT

The fabricated prototype of the patch antenna is shown in ***Figure 5***, and ***Figure 6*** shows the measurement set-up for reflection measurements. ***Figure 7*** compares the simulated and measured reflection

TABLE 3

E7 LIQUID CRYSTAL ELECTRICAL CHARACTERISTICS AT 23°C AND 30 GHZ

$\varepsilon_{r\perp}$	2.72	$\tan\delta_{\perp}$	0.12
$\varepsilon_{r\parallel}$	3.17	$\tan\delta_{\parallel}$	0.02

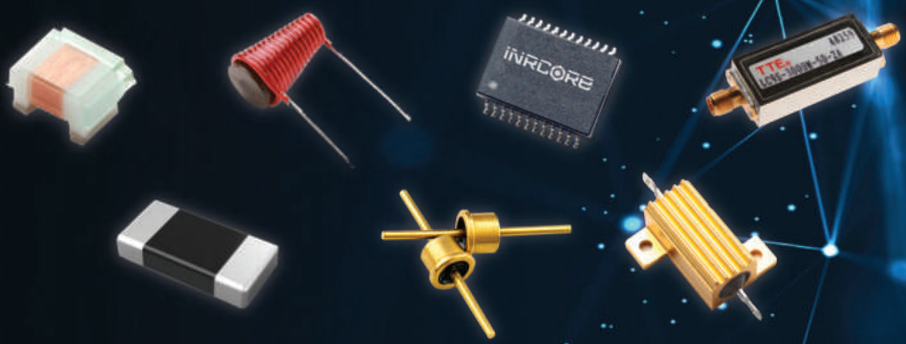
iNRCORE
TTE

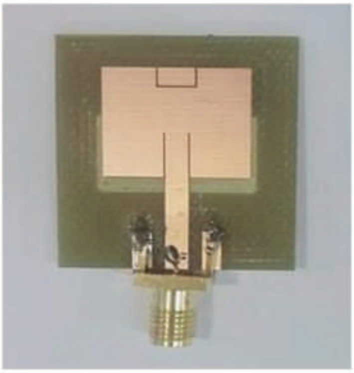

Fig. 5 Fabricated prototype antenna.

coefficients for LC E7 mixtures with two permittivities. Both the simulated and measured results show an adjustable frequency from 5.64 GHz with no magnetic field applied (H = 0 Oe, $\varepsilon_{r\perp}$ = 2.72 and tan(δ) = 0.12) to 5.44 GHz with the two magnets positioned 5 mm from each side of the antenna (H = 1200 Oe, $\varepsilon_{r\parallel}$ = 3.17 and tan (δ) = 0.02). The difference in resonant frequencies is ΔFr = 200 MHz, representing a 3.6 percent tunable range. The minimum simulated value of $|S_{11}|$ at 5.64 GHz is -26 dB improving when the 1200 Oe magnetic field is applied, which is linked to the decrease in tan(δ) from 0.12 to 0.02.

Figure 8 shows the test set-up for measuring the antenna patterns, both peak gain (see ***Figure 9***) and the E-plane patterns (see ***Figure 10***). The figures compare the simulated and measured results. The measured peak gains for the two cases are approximately 0.5 dB lower than the simulated values. The maximum gain of the patch antenna loaded with LC E7 is approximately 4.05 dB, with a radiation efficiency of 61 percent. The measured gain patterns are similar to the simulations, with the measured patterns more omnidirectional than predicted. The difference between measured and simulated is less in the case of no applied magnetic field, i.e., 5.64 GHz resonance (see Figure10a). At 5.4 GHz, with the antenna magnetically biased, the magnets disturb the gain pattern measurement (see Figure 10b). Not surprisingly, the metallic masses mounted to the sides and close to the aperture affect the pattern, scattering the radi-

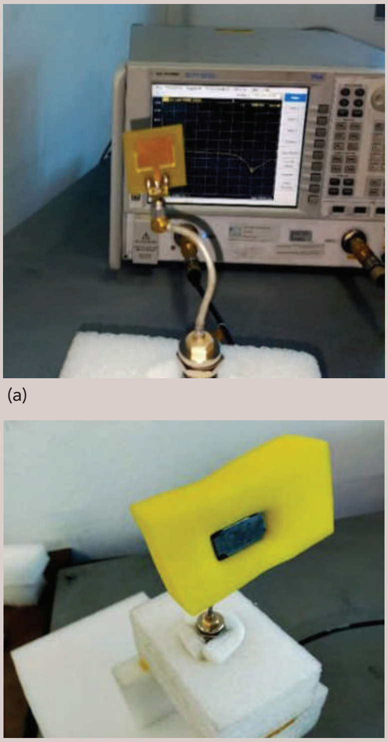

Fig. 6 Test set-up for the prototype antenna without (a) and with (b) an applied magnetic field.

Extend 5G Coverage. Everywhere.

Cellular signal repeaters for amplifying in-building and outdoor coverage.

Enterprise 1337R

3.7 to 3.8 GHz

- Amplify mid-band 5G operating on C-Band frequencies in-building
- Sync with network time-division duplexing
- Use dual-amplification paths (2x2 MIMO) or split mode
- Remotely manage the system with WilsonPro Cloud

Network 257

28 GHz

- Amplify high-band 5G operating on mmWave outdoors
- Efficiently amplifies signal using dielectric waveguide antennas
- Withstands rugged environments and extreme temperatures
- Remote management capability via LTE connectivity
- Rapidly deployable requiring only AC power and no fixed backhaul
- Low energy consumption

Call our experts at 800-871-1612 or visit wilsonpro.com to learn more about 5G and LTE solutions.

WILSONPRO™

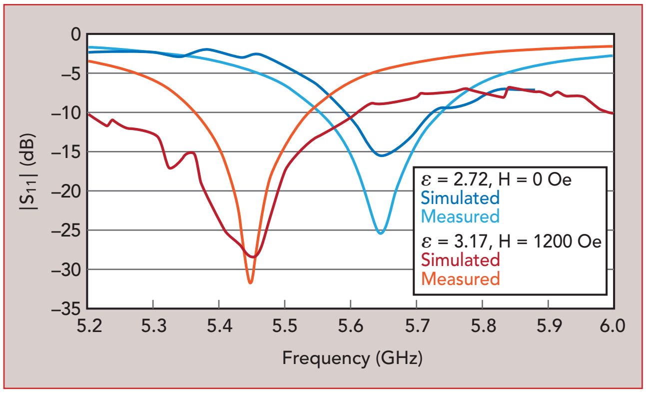

▲ Fig. 7 **Simulated vs. measured $|S_{11}|$ with two LC E7 mixture permittivities.**

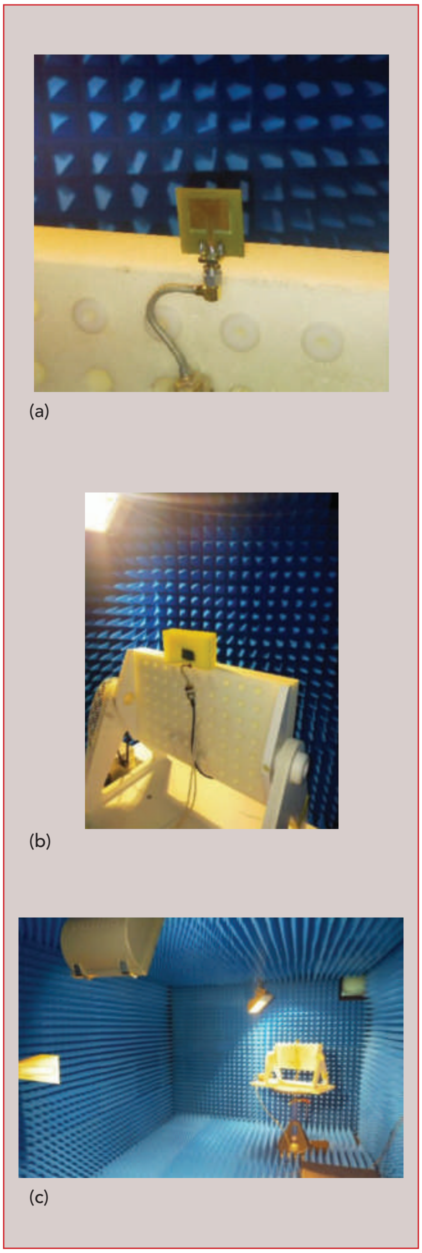

▲ Fig. 8 **Radiation pattern test set-up: antenna on a mount without magnets (a), antenna with magnets (b) and view of anechoic chamber (c).**

ation to the rear. To minimize this, an alternative method to create the magnetic field using Helmholtz coils[15] would likely minimize this effect.

The response time of the LC is relatively long—on the scale of milliseconds—after the application of the externally applied magnetic field. This is less of a concern with the discovery of new types of LCs that exhibit short response times and low losses at microwave and mmWave frequencies.

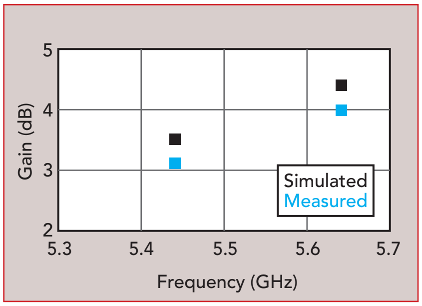

▲ Fig. 9 **Simulated vs. measured peak gain with two LC E7 mixture permittivities.**

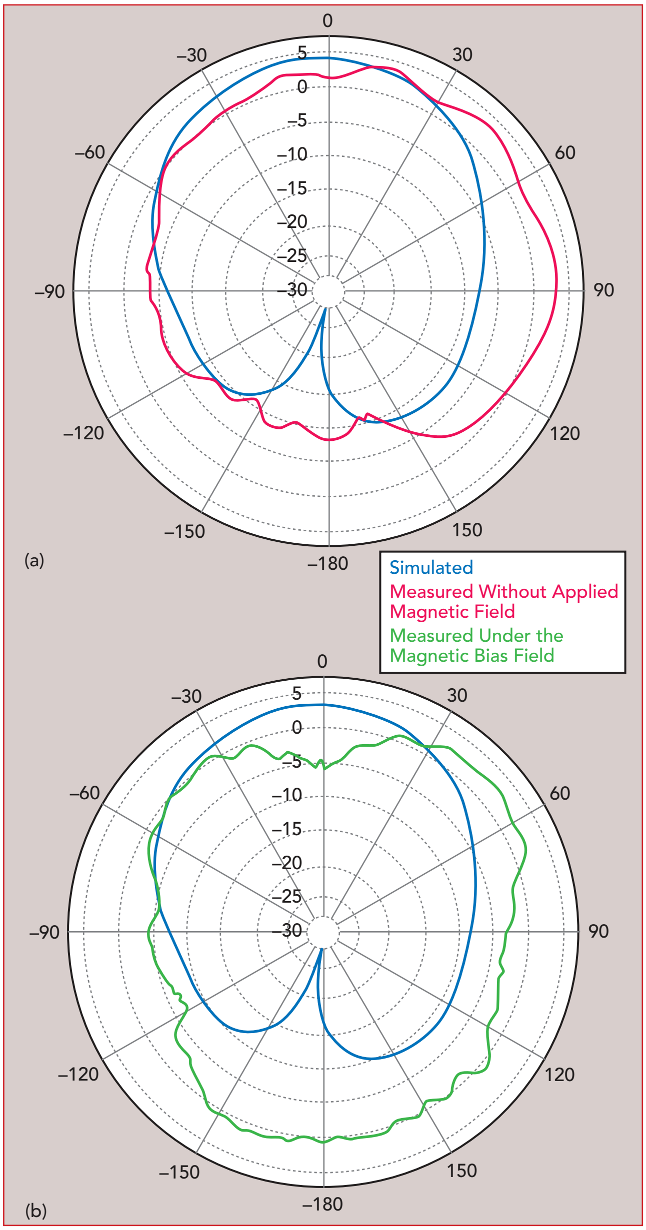

▲ Fig. 10 **Simulated vs. measured E-plane patterns: without applied magnetic field at 5.64 GHz (a) and with a magnetic field at 5.44 GHz (b).**

Table 4 compares the performance of this antenna with similar work. This design achieves a similar tuning range with higher gain and efficiency.

CONCLUSION

A microstrip patch antenna was fabricated with an LC E7 dielectric layer using a new method for adjusting the resonant frequency: magnets spaced 5 mm on either side of the antenna, applying a magnetic field of 1200 Oe. The magnetic field changes the LC permittivity, shifting the antenna's resonant frequency from 5.64 to 5.44 GHz, which is suitable for Wi-Fi applications. The measured radiation patterns are stable over the tuning range. In addition to the performance, the LC reconfigurable antenna has a low profile and is low cost to manufacture. ■

TABLE 4 COMPARISON WITH SIMILAR WORK

Ref	Matching (dB)	Agility Technique	Tuning Range (GHz)	Maximum Gain (dB)	Efficiency (%)
6	-22	LC 5CB (K15)	4.6–4.74 ΔFr = 140 MHz 2.95%	—	—
9	-12	LC 5CB (K15)	4.6–4.745 ΔFr = 145 MHz 3%	≤ 0	0
10	-28	LC E7	5.43–5.66 ΔFr = 230 MHz 4%	1.05	35
11	-30	LC E7	5.43–5.66 ΔFr = 230 MHz 4%	—	40
This Work	-28	LC E7	5.44–5.64 ΔFr = 200 MHz 3.5%	4.05	61

References

1. A. -F. Sheta and S. F. Mahmoud, "A Widely Tunable Compact Patch Antenna," *IEEE Antennas and Wireless Propagation Letters*, Vol. 7, March 2008, pp. 40–42.
2. F. Sboui, J. Machac and A. Gharsallah, "Tunable Slot Antenna Backed by Substrate Integrated Waveguide Cavity," *International Journal of RF and Microwave Computer-Aided Engineering*, Vol. 28, No. 9, October 2018.
3. F. Sboui, J. Machac and A. Gharsallah, "Low-Profile Slotted SIW Cavity Backed Antenna for Frequency Agility," *Radioengineering*, Vol. 28, No. 2, June 2019, pp. 386–390.
4. K. Topalli, E. Erdil, O. A. Civi, S. Demir, S. Koc and T. Akin, "Tunable Dual Frequency RF MEMS Rectangular Slot Ring Antenna," *Sensors and Actuators A: Physical*, Vol. 156, No. 2, December 2009, p. 373–380.
5. M. Sazegar, Y. L. Zheng, H. Maune, C. Damm, X. H. Zhou, J. Binder and R. Jakoby, "Low-Cost Phased-Array Antenna Using Compact Tunable Phase Shifters Based on Ferroelectric Ceramics," *IEEE Transactions on Microwave Theory and Techniques*, Vol. 59, No. 5, May 2001, pp. 1265–1273.
6. N. Martin, P. Laurent, C. Person, P. Gelin, and F. Huret, "Patch Antenna Adjustable in Frequency using Liquid Crystal," *33rd European Microwave Conference*, October 2003, Vol. 3, pp. 1417–1420. DOI: 10.1109/EUMC.2003.177573.
7. N. Martin, P. Laurent, C. Person, P. Gelin and F. Huret, "Size Reduction of a Liquid Crystal-Based, Frequency-Adjustable Patch Antenna," *Proceedings of the 34th European Microwave Conference*, Vol. 2, November 2004, pp. 825–828.
8. F. Sboui, J. Machac, L. Latrach and A. Gharsallah, "Triple Band Tunable SIW Cavity Antenna with Cristal Liquid Materials for Wireless Applications," *IEEE 19th Mediterranean Microwave Symposium*, October 2019.
9. N. C. Papanicolaou, M. A. Christou and A. C. Polycarpou, "Frequency-Agile Microstrip Patch Antenna on a Biased Liquid Crystal Substrate," *Electronics Letters*, Vol 51, No. 3, February 2015, pp. 202–204.
10. A. C. Polycarpou, M. A. Christou and N. C. Papanicolaou, "Tunable Patch Antenna Printed on a Biased Nematic Liquid Crystal Cell," *IEEE Transactions on Antennas and Propagation*, Vol. 62, No. 10, July 2014, pp. 4980–4987.
11. L. Liu and R. J. Langley, "Liquid Crystal Tunable Microstrip Patch Antenna," *Electronics Letters*, Vol. 44, No. 20, October 2008, pp. 1179–1180.
12. S. Missaoui, S. Missaoui and M. Kaddour, "Tunable Microstrip Patch Antenna Based on Liquid Crystals," *XXIst International Seminar/Workshop on Direct and Inverse Problems of Electromagnetic and Acoustic Wave Theory*, September 2016.
13. L. -C. Huang, C. -M. Fu, C. -W. Lee and A. -C. Sun, "Magnetic Field Effects on the Electric Modulus Properties of Nematic Mixture E7," *Current Applied Physics*, Vol. 14, No. 1, January 2014.
14. C. A. Balanis, *Antenna Theory: Analysis and Design*, Third Edition, Wiley, 2005.
15. G. Podaru, J. Moore, R. K. Dani, P. Prakash and V. Chikan, "Nested Helmholtz Coil Design for Producing Homogeneous Transient Rotating Magnetic Fields," *Review of Scientific Instruments*, Vol. 86, No. 3, March 2015.

MiCable

NEW

0.4-8GHz HIGH POWER Directional & Dual-Directional Coupler

- High power handling : up to 600W
- Low VSWR & insertion loss
- Excellent coupling, flatness and directivity which will significantly improve the signal acquisition accuracy
- Environment conditions meet MIL-STD-202F

P/N	CW Power Max.(W)	Nominal Coupling (dB)	Main Line VSWR	Coupling VSWR	Insertion Loss*	Coupling	Flatness	Directivity Min.(dB)
			Max.(:1)		Max.(dB)			
0.4-8GHz Directional Coupler								
D3002H004080	120	30	1.3	1.3	0.8	30±1.0	±0.8	18
D4002H004080	120	40	1.3	1.3	0.8	40±1.0	±0.8	18
D3005H004080	250	30	1.4	1.4	0.6	30±0.9	±1.3	14
D4005H004080	250	40	1.4	1.4	0.6	40±1.0	±1.4	14
D3008H004080	400	30	1.4	1.4	0.6	30±0.9	±1.3	14
D4008H004080	400	40	1.4	1.4	0.6	40±1.0	±1.4	14
D3012H004080	600	30	1.4	1.4	0.6	30±0.9	±1.3	14
D4012H004080	600	40	1.4	1.4	0.6	40±1.0	±1.4	14
0.4-8GHz Dual-Directional Coupler								
D3002HB004080	120	30	1.3	1.3	0.8	30±1.0	±1.0	18
D4002HB004080	120	40	1.3	1.3	0.8	40±1.0	±1.0	18
D3005HB004080	250	30	1.4	1.4	0.7	30±0.9	±1.5	14
D4005HB004080	250	40	1.4	1.4	0.7	40±1.0	±1.6	14
D3008HB004080	400	30	1.4	1.4	0.7	30±0.9	±1.5	14
D4008HB004080	400	40	1.4	1.4	0.7	40±1.0	±1.6	14
D3012HB004080	600	30	1.4	1.4	0.7	30±0.9	±1.5	14
D4012HB004080	600	40	1.4	1.4	0.7	40±1.0	±1.6	14

*Theoretical I.L. Included

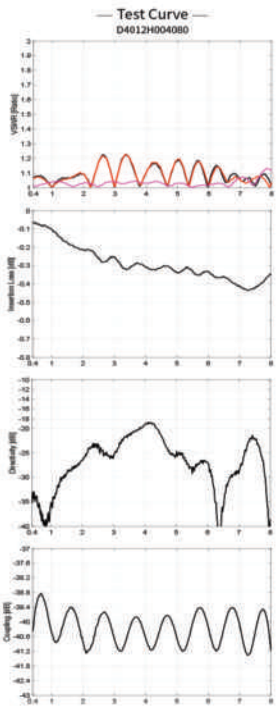

More Information-
Scan the QR Code

Fujian MIcable Electronic Technology Group Co.,Ltd

Tel: +86-591-87382856 Email: sales@micable.cn Website: www.micable.cn

INVITED PAPER

Overcoming C-V2X Compliance Challenges

Dylan McGrath
Keysight Technologies, Santa Rosa, Calif.

More than 1.3 million people are killed in auto accidents each year. The U.S. National Highway Transportation Safety Administration estimates that human error is responsible for 94 to 96 percent of these fatalities. Other estimates are even higher—as much as 98 percent. Improving automotive safety, reducing or even eliminating auto fatalities and accidents, is one of the primary motivations behind the rise of cellular vehicle-to-everything (C-V2X) communications. C-V2X is a wireless technology that promotes higher levels of autonomous operation in vehicles by enabling vehicles to communicate continuously, in real time, with other vehicles, as well as other parts of the traffic system, including roadside infrastructure, bicyclists and pedestrians.

The use of 5G C-V2X technology will multiply in the coming years as automotive manufacturers increasingly make it available in new vehicles to promote safety, efficiency, mobility and quality of life. However, incorporating C-V2X into vehicles and vehicle modules poses challenges. These challenges include RF propagation complications associated with moving vehicles, congested roadways and metal objects. C-V2X is also complicated by an abundance of standards created by different organizations and regional differences in standards, traffic safety laws and policies.

This article describes the status of C-V2X technology and its adoption, including the newest updates in the 3GPP's Release 17. It also delves into the major challenges associated with C-V2X validation and testing, including those associated with regional variance in technology implementation and standards and offers some practical advice for navigating the pitfalls of C-V2X certification.

C-V2X HISTORY

The roots of V2X technology date back to the 1970s with research in the U.S. and Japan. However, in 2016, the first mass-produced vehicles equipped with V2X communications began. Early V2X vehicles did not use cellular technology; instead, these vehicles in the U.S. and Japan used a WLAN-based technology called direct short-range communication (DSRC). V2X first made it into cellular standards with 3GPP Release 14 in 2017. The first commercial C-V2X chipsets, which supported LTE-based C-V2X, were introduced in 2018. In 2020, the first mass-market vehicles that incorporated C-V2X rolled off the assembly line in China.

The first 5G new radio (NR) C-V2X specifications were included in 3GPP Release 15, the initial 5G standards, which achieved ASN.1 freeze in mid-2019. Following that, 3GPP Release 16 added a significant number of enhancements supporting C-V2X, including sidelink. Sidelink enables user

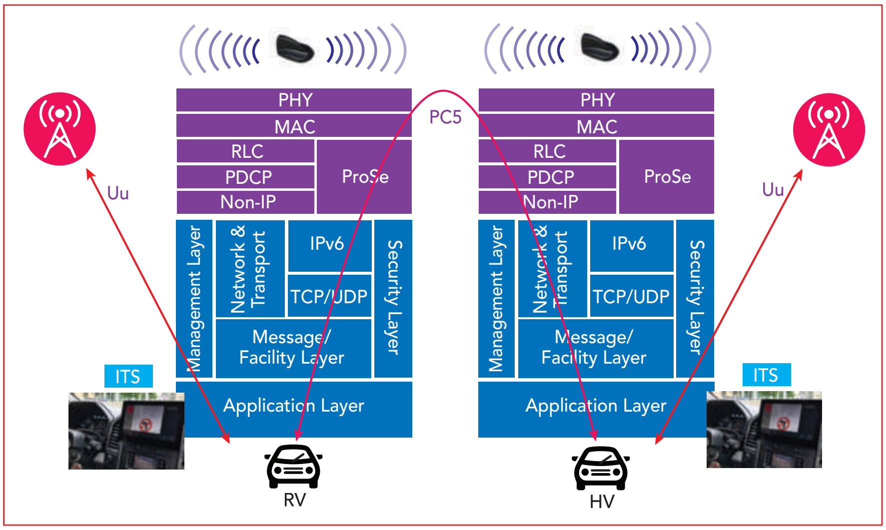

Fig. 1 C-V2X ITS stack.

equipment (principally vehicles) to communicate directly without involving the network, facilitating the sharing of real-time sensor data. Sidelink is a major component of C-V2X because direct vehicle-to-vehicle and vehicle-to-infrastructure communications enable vehicles to understand real-time traffic and road conditions, access non-line-of-sight data sensing to see around corners and warn each other of driving hazards. Other significant enhancements contained in Release 16 that enable and enhance C-V2X functionality are:

- scalable OFDM interfaces
- self-contained slot structures with immediate feedback enabling a very reliable communication system with low latency
- advanced channel coding improving reliability with low complexity
- wideband carrier support
- support for massive MIMO for higher data rates, increased range and increased reliability.

Release 17, which achieved ASN.1 freeze earlier this year, built off the functionality in Release 16, including the addition of several sidelink enhancements such as network-controlled interactive service (NCIS), enhanced relays for energy efficiency and extensive coverage (REFEC) and audio-visual service production (AVPROD).

Fig. 2 Typical freeway scene.

REGIONAL VARIATIONS

One of the major complexities that makes the design and test of C-V2X modules challenging is the intelligent transport system (ITS), a comprehensive system that aims to enhance traffic management in many countries and regions. Most countries have designated the 5.9 GHz frequency band as the official ITS frequency band.

The ITS stack is comprised of several elements that sit above the physical layer (see ***Figure 1***). The stack has been inverted to reflect the more practical arrangement. For example, the physical layer, typically connected to antennas on the rooftops of vehicles, is shown at the top of the diagram. ITS stack elements include the transport, messages and applications layers, with each layer possessing management capability and security. Although the physical layer of C-V2X is based on cellular technology and differs from other V2X systems such as DSRC, each layer in the ITS stack is adapted from standards created by many organizations, including SAE International, the European Telecommunications Standards Institute (ETSI), the Car 2 Car Communication Consortium, China Communications Standards Associations (CCSA), China Society of Automotive Engineers and others. Even though the layers of the ITS stack are based on standards and reused, the upper layers of the stack contain regional differences. The regional ITS layer differences can be attributed mainly to North America, Europe and China. Each layer performs similar functions, regardless of regional variance. The C-V2X module design must consider the different standards of each region where the product will be sold. Test equipment and test processes must reflect these differences as well, meaning different design and test tools and test methodologies may be required for every C-V2X module or vehicle being sold in multiple regions.

Figure 1 illustrates the importance of verifying that the remote vehicle (RV) can send and receive messages from the host vehicle (HV). For example, if a message such as an electronic emergency brake light warning is initiated by one vehicle, it is important to ensure this warning message goes up through the layers of the physical stack over the air and is received and decoded back through the application layer. The figure shows a logical understanding of how the message is initiated in one vehicle, travels up through the layers to the antenna, is received by the other vehicle through its antenna and is then processed and decoded back down. For C-V2X certification purposes, proper testing of this func-

Fig. 3 A future of cars and infrastructure connected using multiple wireless technologies.


Portable Handheld Field Solutions
Expand your signal analysis capabilities
to 6G Research, Development & Deployment
90 GHz to 220 GHz and Beyond
M08H4BDC
90 GHz to 140 GHz
M06H6BDC
110 GHz to 170 GHz
M05H6BDC
140 GHz to 220 GHZ
Innovation in Millimeter Wave Solutions
www.omlinc.com
(408) 779-2698
OML

tionality requires accurately measuring this interchange and accounting for regional variance.

STRESS TESTING

One of the most important attributes of C-V2X is reliability. Because passenger safety and lives are on the line, it is critical that the technology is available in all road and traffic conditions. One of the most challenging conditions for the design and testing of C-V2X modules is heavy congestion, a situation arising daily for vehicles traveling—and sometimes sitting in traffic—on the highways of the world (see ***Figure 2***). C-V2X modules must transmit and receive messages containing critical safety information, even in environments with hundreds or thousands of cars in the same immediate area that are also relaying and receiving C-V2X messages. Because the sharing of resources on the ITS band can be a challenge, congestion control stress testing is a requirement. Conducting a congestion control stress test involves placing a device in a congested environment, such as dense traffic situations with many C-V2X modules and other ITS stations.

Properly functioning congestion control algorithms are required to coordinate the appropriate usage of the channels. Algorithms have been developed to mitigate the impact of these situations, such that resources are shared equally to keep the channels as unsaturated as possible. The standard defines two metrics that characterize the state of the channels. These are channel busy ratio (CBR) and channel occupancy ratio (COR). C-V2X modules will sense the environment for 1000 milliseconds and try to determine which resource blocks, each made up of subframes and subchannels, are transmitted by neighboring vehicles. The device then determines if there is a spare resource block at a certain frequency or a certain channel and then decides when to transmit at the least used or lowest energy segment of the spectrum. Decisions are made based on COR and CBR information that comes over the control plane, and resources are consequently allocated and transmitted.

In addition to the CBR and COR, congestion control algorithms make decisions based on various metrics and parameters, including power, channel quality indicator and range. There are various techniques the station or the device can use depending on the inputs to the algorithm. Some of the techniques that can be used are:

- Drop packet retransmission: If the retransmission feature is enabled, the station can disable it
- Drop packet transmission: The station simply drops the packet transmission, including the retransmission if enabled; this is one of the simplest techniques
- Reduce packet transmission periodicity: Extend the packet transmission interval
- Adapt transmission power: The station can reduce its transmission power; consequently, the

DALIAN DALICAP TECH. CO.,LTD.

Professional Manufacturer for RF/ Microwave Ceramic Capacitors

DLC70 SERIES HIGH Q RF/MICROWAVE MLCC

Features: High Q/Zero TCC/Low ESR/ESL
Ultra-Stable Performance/Extended WVDC

Size: 0402,0603,0505,0805,0710,1111,2225,3838 for RF/Microwave
6040,7575,130130 for High RF Power

Typical Applications:

Filters,RF Power Amplifiers,Antenna Tuning,
Plasma Chambers,Medical(MRI Coils) and Transmitters

DLC75 SERIES ULTRA-LOW ESR,RF/MICROWAVE MLCC

Features: Ultra-Low ESR, High Working Voltage,
High Self-Resonance Frequency

Typical Applications:

Cellular Base Stations
Wireless Communications
Trunked Mobile Communication System.

MICRO-STRIP/LEAD MLCC

Features:
- Originated from DLC70 series
- Suitably soldering in various surface mount and leaded style
- Available sized above 1111(B SIZE)
- Available for customized products

Axial Wire | Radial Wire | Axial Ribbon | Custom Microstrip

HIGH POWER ASSEMBLY

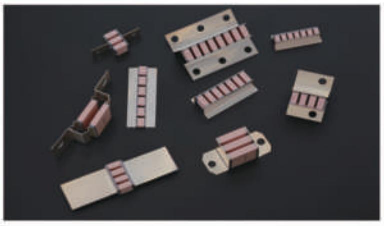

Features:
- Capacitance and space matched well
- Fully customized for high power application
- Easy to solder
- Highly integrated and easy to handle

SINGLE LAYER CAPACITOR

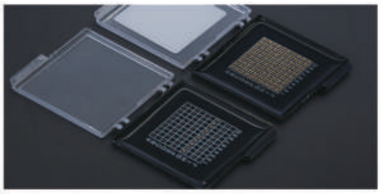

Features:
- Broadband application up to 100GHZ
- Standard capacitance range 0.05pF to 10,000pF
- Voltage rating up to 100WVDC
- Minimum dimension size 10mil × 10mil
- Custom value and size are available

DALICAP

Phone: 86-411-87632359 Fax: 86-411-87613784
E-mail: dalicap@dalicap.com.cn
Web: WWW.DALICAP.COM

overall CBR in the area will be reduced, and the value of the CBR limit might be increased.

Because the standards do not mandate which techniques to use, it may be beneficial to place the device under test in a crowded environment to see which mechanisms are triggered and how the device handles the messages and reacts accordingly. Testing how well the congestion control algorithms work is critical.

COEXISTENCE & INTERFERENCE TESTING

In addition to congestion stress testing, coexistence and interference testing is required to ensure the C-V2X will coexist with all the many other wireless technologies operating in and around modern vehicles (see ***Figure 3***). 5G NR's Frequency Range 1 (FR1) includes the frequency bands from 410 MHz to 7.125 GHz, including spectrum used by or adjacent to existing wireless communications systems, Wi-Fi and Bluetooth. Again, given the safety implications of C-V2X communications, it is critical that 5G C-V2X modules operate in this spectrum range without interference.

Comprehensive interference testing involves testing in-band and out-of-band emissions and testing the impact of the C-V2X signals on other radio signals to ensure that the 5G C-V2X signal does not cause interference with other radios in the same vehicle or other radio signals in the channel or adjacent spectrum. Interference from out-of-band emissions can degrade the reliability of C-V2X communications, directly impacting transportation safety. A U.S. Department of Transportation technical assessment found that out-of-band interference from DSRC, Wi-Fi and LTE C-V2X operating in adjacent channels can leak into the adjacent spectrum, causing concern about the reliability of C-V2X communications. C-V2X modules must operate in a shared spectrum environment without negatively impacting bandwidth. Sharing airwaves increases the responsibility of semiconductor manufacturers, automakers and equipment manufacturers to ensure the C-V2X system will coexist with existing commercial wireless infrastructure.

Much like congestion control algorithms, C-V2X systems require complex algorithms to monitor and detect other users in the spectrum and adjust the transmission and reception of signals accordingly.

MMWAVE QUALITY

5G NR's Frequency Range 2 (FR2) extends from 24.25 to 71 GHz. Extending to mmWave frequencies enables 5G NR to access a larger contiguous bandwidth, meaning access to much more data related to traffic and road hazards to and from the cloud or to nearby vehicles. But the smaller wavelength of mmWave introduces challenges to signal quality and link budget. Factors impacting mmWave signal quality include baseband signal processing, modulation, filtering and up-conversion. Also, C-V2X modules will face signal impairments more problematic at higher frequencies and the wider channel bandwidths.

The orthogonal properties inherent in OFDM systems prevent interference between overlapping subcarriers. However, issues such as I/Q impairments, phase noise, linear (AM to AM) and nonlinear (AM to PM) compression and frequency error cause distortion in the modulated signal. Phase noise is one of the most challenging: high phase noise results in high error vector magnitude and subcarrier interference, impairing demodulation.

Operating at mmWave introduces challenges from path loss, blockage and signal propagation. Because of the shorter wavelengths at mmWave, physical obstacles in the channel—including other vehicles—will block the signal, with the severity compounded by vehicle-mounted antennas. Beamforming is a key technology for overcoming these propagation issues, making FR2 transmissions highly directional and requiring higher gain active antennas that are electrically steerable. The body of the vehicle acts as a large ground plane located near the antenna, creating a host of additional antenna testing challenges and link budget management complexities.

Overcoming the physical challenges associated with mmWave signals in C-V2X modules requires test solutions that measure and characterize signal quality accurately, without introducing new issues, to validate the C-V2X quality of service and performance on the network.

USE CASES

Organizations such as the 5G Automotive Association (5GAA) have created basic safety use cases for testing C-V2X devices and applications. Some of the most prominent are:

- **Emergency brake light (EEBL)**: When a vehicle's brakes are activated, a warning signal is sent to nearby vehicles
- **Signal phase and timing from traffic lights**: This is useful to determine the appropriate speed as a vehicle approaches a traffic light
- **Intersection collision warning**: A vehicle may send an EEBL message to warn of a potential collision risk
- **Across traffic turn collision risk warning**: A vehicle may send an EEBL message to warn of a potential collision risk
- **Vulnerable road user protection**: This alerts pedestrians or other non-vehicle users of a potential collision risk using their smartphones
- **Slow vehicle warning or stationary vehicle**: This provides alerts of a potential vehicle collision while in traffic jams or with other parked or stationary vehicles.

In addition to these basic safety use cases, other use cases known as "day one use cases" cover basic safety concerns. Every region has its own list of day one use cases. For example, China has approximately 17 to 20 specific to that region. Other regions may have similar col-

lections, but they are not always identical. Various day one use cases may include forward collision warnings, left turn assist and blind spot warnings.

CERTIFICATION CHALLENGES

Like so much of 5G C-V2X technology, certification of C-V2X modules is challenging because of the evolving nature of the standards and the many organizations involved in the standardization of the technology, including 3GPP, SAE, ETSI, CCSA, IEEE, Institute of Transportation Engineers, National Electrical Manufacturers Association and European Telecommunications. ITS organizations and road operator regulators need to meet the performance criteria set by the respective standards development organizations, telecom and automotive industry governing bodies.

Typically, a C-V2X device requires Global Certification Forum (GCF) RF/protocol certification according to global cellular standards. Depending on the region where the device will operate, it likely needs to be tested to the ITS upper layer standards, such as IEEE 1609.2/3/4, SAE J2945 for North America and the applicable regional standards in Europe and China. In addition, devices likely need to pass region-specific test cases currently being developed for the ITS application layer.

Manufacturers may conclude that purchasing test equipment capable of testing future expansions of 5G NR is too great an investment. This should not be an obstacle to success. Fully audited test houses provide technical expertise and the most state-of-the-art testing technologies. Using an outside resource ensures each device being tested meets the evolving standards of C-V2X. Given the dynamic nature of C-V2X standards and test requirements, using an independent test house can help companies ensure products are tested using the latest guidelines and meet all requirements. Using a testing and certification body such as the OmniAir Consortium is one method for gaining certification for a C-V2X device in a timely and cost-effective manner, regardless of whether the testing is conducted in-house or through an independent third-party laboratory. Using an audited state-of-the-art facility for bench, field and security test ensures conformance with the latest test standards. Once the lab reports are complete, the governing body approves the findings and the device receives a certification mark to prove conformance.

CONCLUSION

As with everything else in the 5G realm, the importance of testing and validation for C-V2X cannot be overstated. Only fully audited test equipment for current and future 5G and C-V2X standards and strict adherence to the specifications will ensure certification and, ultimately, the successful performance of 5G NR C-V2X modules. While the obstacles to widespread deployment of C-V2X are not insignificant, they are surmountable with proper test equipment and methodologies. Addressing these obstacles is a critical step on the road to safer, greener and more efficient transportation—leading to fully autonomous vehicles in the future. ■

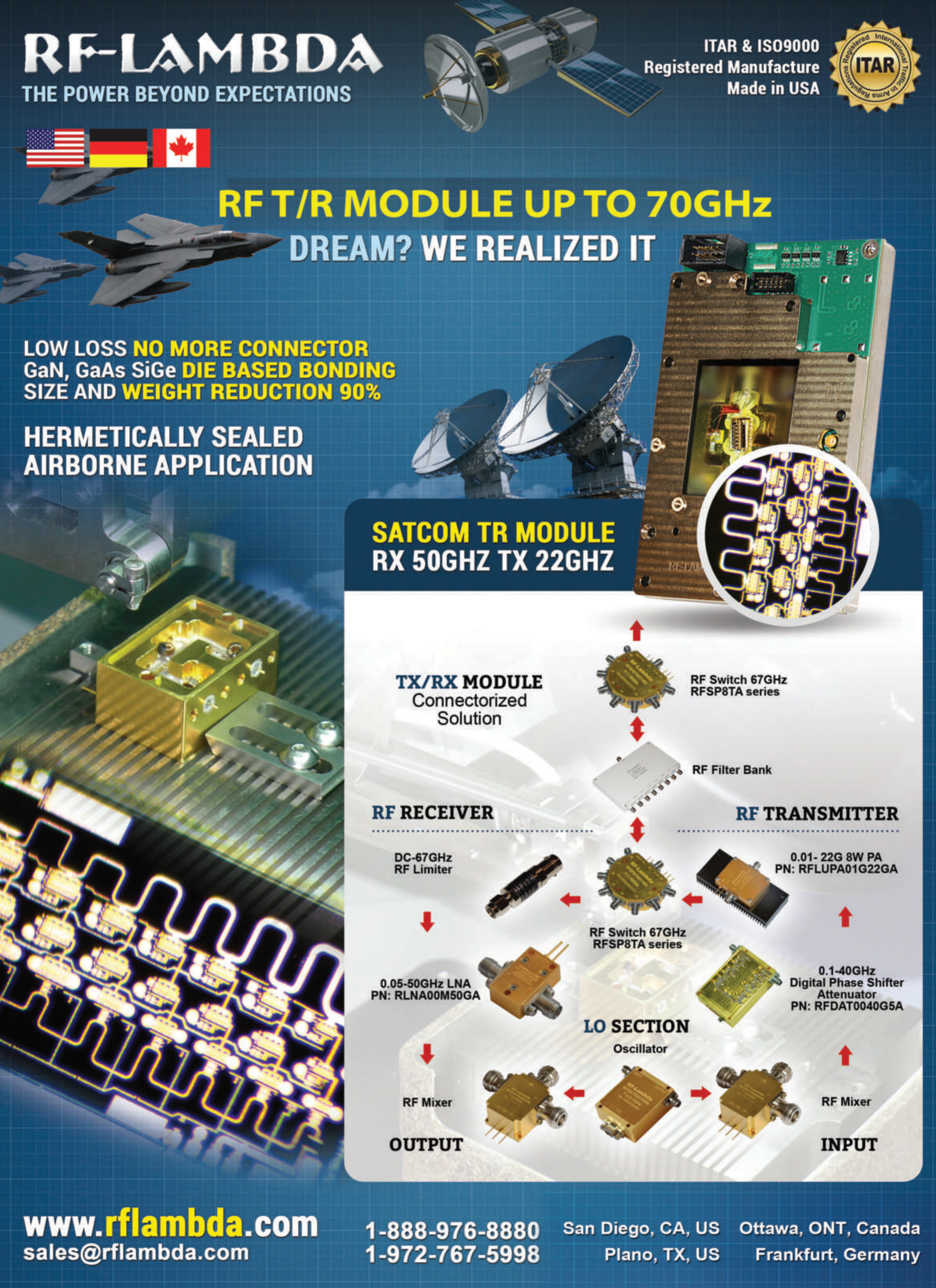
RF-LAMBDA
THE POWER BEYOND EXPECTATIONS
ITAR & ISO9000
Registered Manufacture
Made in USA
ITAR
Registered International Traffic in Arms Regulations
RF T/R MODULE UP TO 70GHz
DREAM? WE REALIZED IT
LOW LOSS NO MORE CONNECTOR
GaN, GaAs SiGe DIE BASED BONDING
SIZE AND WEIGHT REDUCTION 90%
HERMETICALLY SEALED
AIRBORNE APPLICATION
SATCOM TR MODULE
RX 50GHZ TX 22GHZ
TX/RX MODULE
Connectorized
Solution
RF Switch 67GHz
RFSP8TA series
RF Filter Bank
RF RECEIVER
RF TRANSMITTER
DC-67GHz
RF Limiter
0.01- 22G 8W PA
PN: RFLUPA01G22GA
RF Switch 67GHz
RFSP8TA series
0.05-50GHz LNA
PN: RLNA00M50GA
0.1-40GHz
Digital Phase Shifter
Attenuator
PN: RFDAT0040G5A
LO SECTION
Oscillator
RF Mixer
RF Mixer
OUTPUT
INPUT
www.rflambda.com
sales@rflambda.com
1-888-976-8880
1-972-767-5998
San Diego, CA, US
Plano, TX, US
Ottawa, ONT, Canada
Frankfurt, Germany

INVITED PAPER

Fast, mmWave Over-the-Air Testing

Su-Wei Chang, Ethan Lin, Andrew Wu and Jackrose Kuo
TMYTEK, New Taipei City, Taiwan

This article describes the design of a mmWave phased array antenna test system that can be integrated with a handler for mass production over-the-air (OTA) testing. The test system dramatically speeds the measurement of beamforming systems.

A phased array antenna aggregates many antenna elements to form a large array that uses beamforming to increase the directional gain, with the effective isotropic radiated power (EIRP) characterizing the power and reach of the phased array. The directional gain compensates for signal fading, enabling applications to benefit from mmWave's high bandwidth and low latency. As such, phased arrays have been widely adopted for 5G and satcom applications, with MIMO, multi-user MIMO (MU-MIMO) and massive MIMO (mMIMO) architectures enabled by beamforming and beam steering technologies to increase network capacity and improve the user's experience.

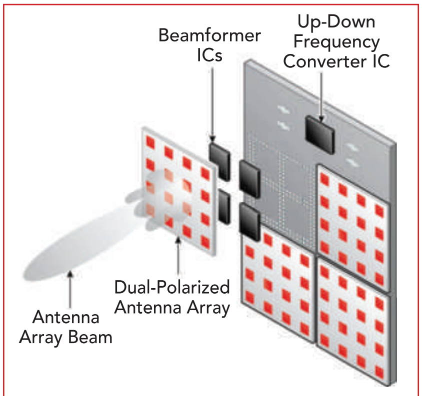

Fig. 1 AIP system construction.

To minimize size and achieve the best performance, many systems adopt the compact antenna-in-package (AiP) architecture, where the phased array antenna and components such as beamformers, power amplifiers and up- and down-converters are all integrated (see ***Figure 1***). The only way to test a mmWave AiP system is OTA, since the AiP system is a single, compact package with many RF channels and no RF connectors at the antenna elements. Beam steering is a key factor for successful performance. To guarantee beam steering performance, OTA testing must evaluate the AiP's characteristics, such as radiation pattern and the relative gain and phase of the elements.

TRADITIONAL OTA TESTING

With the adoption of 5G and satcom, more systems and devices are moving to mmWave frequencies. Depending on the system architecture and antenna design, devices for these applications have varying sizes and shapes; OTA measurement of the antenna system requires an anechoic test chamber, where the size of the chamber depends on the size of the device. For 5G systems, several measurement options are defined by 3GPP:

Far-Field Measurement Options

The 3GPP TR 38.810 specification defines the direct far-field (DFF) technique, which requires a minimum measurement distance (see ***Figure 2***), where the spherical wave from the source is transformed into a plane wave for radiation pattern measurements. The DFF method generally requires larger

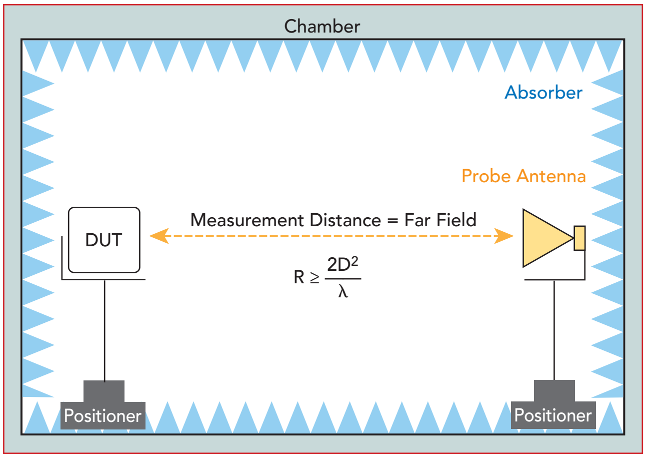

Fig. 2 Direct far-field test setup.

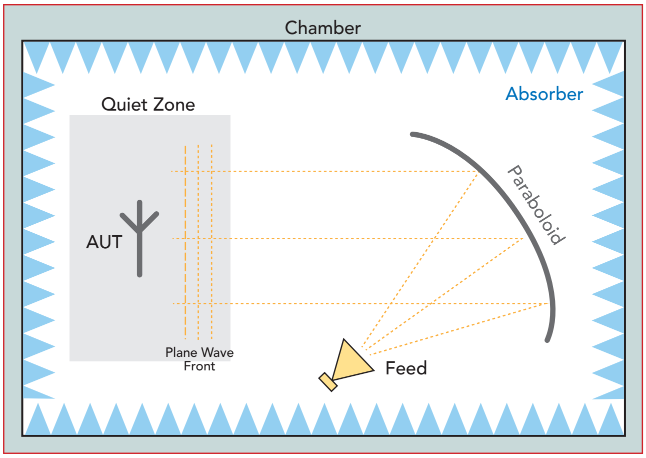

Fig. 3 Indirect far-field test setup using a CATR.

test chambers based on the diameter and operating wavelength of the AiP module. For example, a 28 GHz device with an antenna dimension of 15 cm requires a 4.2 m chamber to achieve far-field measurements. The larger the chamber, the higher the cost, the greater the space and added test time due to the mechanical operation of the chamber.

A compact antenna test range (CATR) uses the indirect far-field (IFF) method to reduce the size of the test chamber (see ***Figure 3***). The CATR system uses a parabolic reflector to parallelize the wave from the feed horn to create a far-field test environment. Although the distance between the device under test (DUT) and the feed antenna is essentially halved, the entire CATR system still requires a chamber box of significant dimensions. In addition to chamber size, the CATR setup slows measurement time, typically taking 10 to 20 minutes.

To measure a 3D sphere radiation pattern, the testing methods for traditional DFF chambers and IFF CATR include rotating the DUT in azimuth and elevation to obtain full pattern measurements. This requires the DUT to be mounted on a rotating table stepped by electric motors, often taking hours to generate a complete 3D antenna pattern—with the potential for interference or other limitations caused by the motors.

Horn Antenna Measurements

AiP testing using a horn antenna is faster and more cost-effective for mass production testing (see ***Figure 4***). However, it only measures the total radiation peak power at a fixed angle. Even with three horn systems, each horn in a different position, the testing angles and dimensions are limited. Since the AiP is a phased array with many antenna elements,

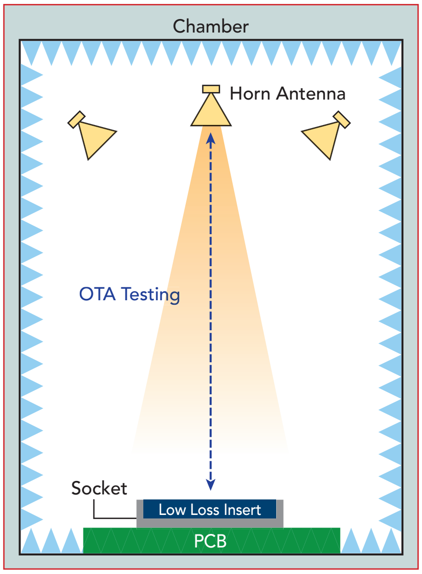

Fig. 4 OTA testing using a horn antenna.

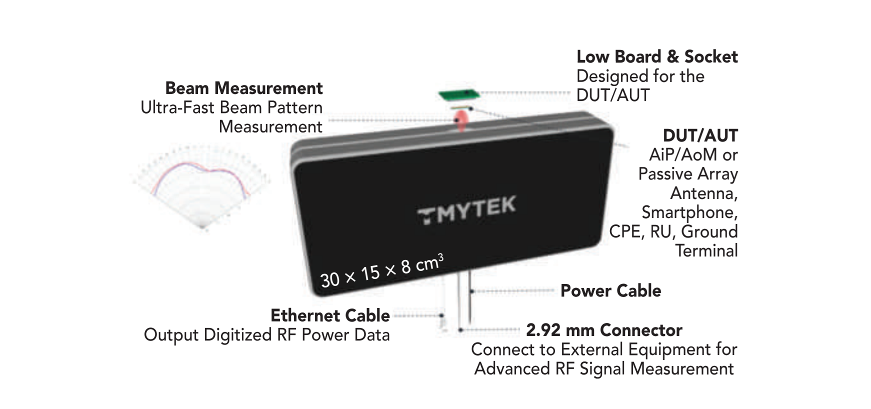

Fig. 5 XBeam 2D test system.

each with configurable gain and phase, only measuring the gain in a few directions yields uncertainty in assessing the antenna pattern and guaranteeing the performance of an AiP system.

OTA testing requires a stable and well-calibrated testing environment. As noted, available chamber-based test solutions provide comprehensive measurements, but the chamber is bulky and costly, and the tests are time consuming. The rotation of the turntable is slow, susceptible to interference and may be limited. This doesn't make sense for production lines. While the horn test approach is widely adopted in production, assessing the spatial coverage of the AiP is a significant gap.

INNOVATIVE OTA TESTING SOLUTION

To address these shortfalls, TMYTEK has developed a phased array antenna testing method that is fast, has a small footprint and measures both power and phase. Since the antenna pattern is a critical element of a phased array antenna, identifying any gain loss or phase differences among elements is important, an aspect that traditional testing methods cannot perform efficiently in production.

TMYTEK's XBeam system is available in two versions that scan antenna patterns in 2D and 3D in under 10 seconds—100x faster than other commercial test methods. It is compact and fully electronic, with no motors to limit measurements or cause interference. The small footprint makes it easy to integrate with other test elements such as handlers, and its application programming interface (API) and drivers support integration with existing test program configurations. Using TMYTEK's UD Box up- and downconverter enables use of sub-6 GHz analyzers, eliminating the need for mmWave instrumentation. The innovative hardware and software design enables the system to provide an affordable total cost of ownership (TCO).

XBeam 2D

The XBeam 2D is the more economical version of the XBeam family, suitable for production line testing (see ***Figure 5***). It is usually used for the small arrays used in mobile phones or customer premise equipment and also supports 2D testing of larger arrays, such as 5G radio unit and satcom terminals. The XBeam 2D receives and analyze one cut of the beam, generating a 2D pattern at ±5 degrees within 1 second. The

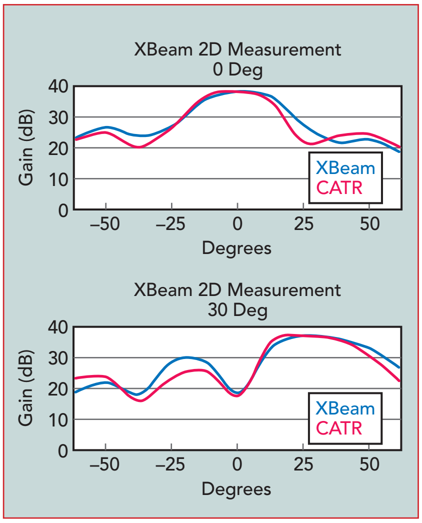

Fig. 6 Pattern measurement comparison: XBeam 2D vs. the CATR.

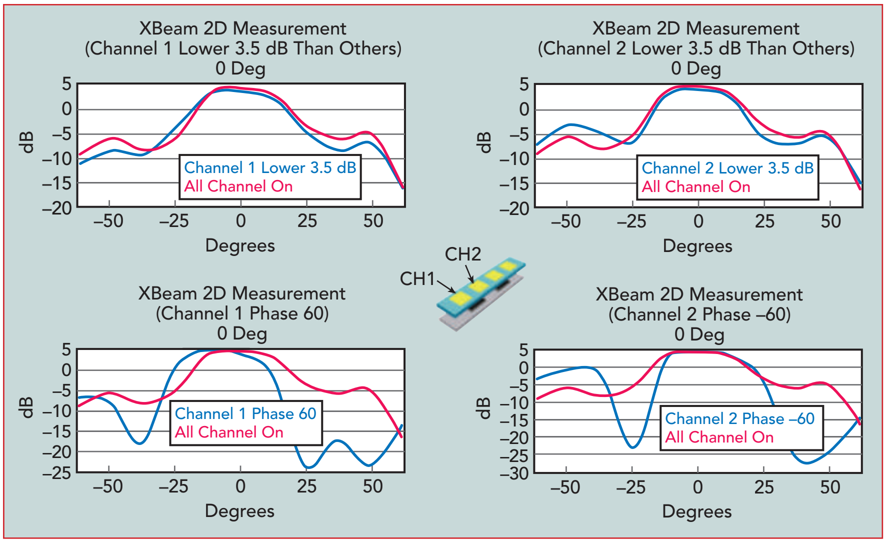

Fig. 7 Measurements showing low gain and phase offset effects.

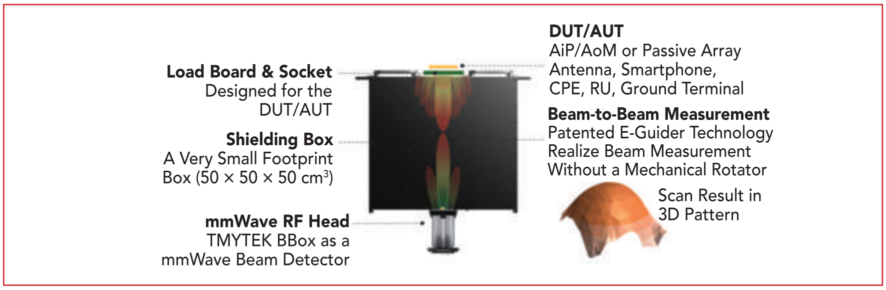

Fig. 8 XBeam 3D test system.

radiation pattern is digitized, and the RF power data can be retrieved via the ethernet interface. For measuring other RF parameters, such as error vector magnitude (EVM), the XBeam 2D can be connected to a spectrum analyzer or universal auto tester via a 2.92 mm connector. The small box measures 30 × 15 × 8 cm.

To confirm the XBeam 2D's measurement quality, TMYTEK tested and compared the XBeam 2D with a CATR under the same conditions using the mmWave New Radio beamforming development tool, BBox. The results (see ***Figure 6***) show the peak gain and radiation patterns are similar, sometimes equal, whether the beam is at boresight or offset to a steering angle. The data confirms the XBeam 2D's measurement method and results agree with the results achieved with a CATR.

A key feature of an AiP is beam steering, which has a baseline with all elements or channels having equal gain and phase. The OTA measurement system should be able to detect variations among the channels, which may indicate failures or the need for system calibration. To illustrate XBeam 2D's ability to identify such issues, a 1 × 4 channel AiP module was measured with channels 1 and 2 purposefully adjusted for 3.5 lower gain and a -60-degree phase offset to simulate a defect. ***Figure 7*** shows the measurement results, comparing the failures and good sections under the same test conditions. A single horn measurement system, which only measures peak gain at 0 degrees, would be unable to screen the non-functional components. By performing a full 2D pattern scan, gain differences can be noted when channel power is lower and the specific channel identified. With the phase offset, the beam has clearly shifted, and the AiP unit can be flagged by the test system.

TMYTEK XBeam 3D

XBeam 3D extends the measurement capability to two dimensions, e.g., azimuth and elevation. The system comprises a specially designed shielding box and the TMYTEK BBox radio detector head

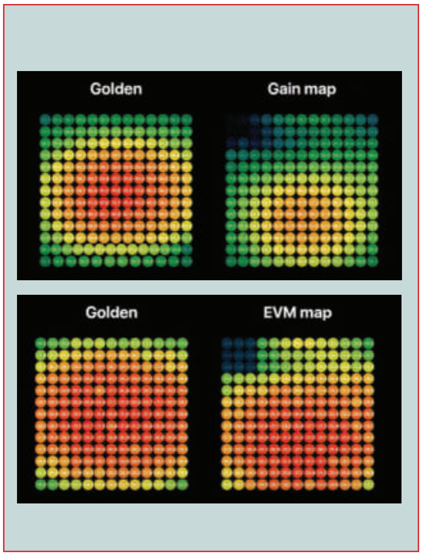

Fig. 9 Parameter maps generated by the software engine.

in a 50 × 50 × 50 cm testing cube (see ***Figure 8***). This first-generation module tests 28 GHz systems across ±50 degrees in 10 seconds.

The software developed for XBeam includes:

- BeamPicasso™, which measures beams at various angles
- mmWatson™, which measures and identifies faulty AiP modules
- OTACali™, which efficiently calibrates a phased array OTA.

The software can transform parameter measurements into visual bitmaps (see ***Figure 9***). Piece-by-piece calibration and statistical analysis matures the database, improving the capability to identify defects accurately and quickly.

To further improve capability and flexibility, handler APIs supporting popular wireless tester drivers enable the XBeam 3D to be fully automated in a mass production test system. ***Figure 10*** shows test results with the XBeam 3D integrated with one auto tester. Gain and EVM were measured at three beam angles in under 2 seconds, with the beam pattern analyzed in real time to identify failures, so defective components can be flagged. Testing speed enables the measurement data to be collected and fed to a database for artificial intelligence (AI) modeling and intelligent analysis, correlating production batches with the characteristics of array elements, for example. Real-time processing

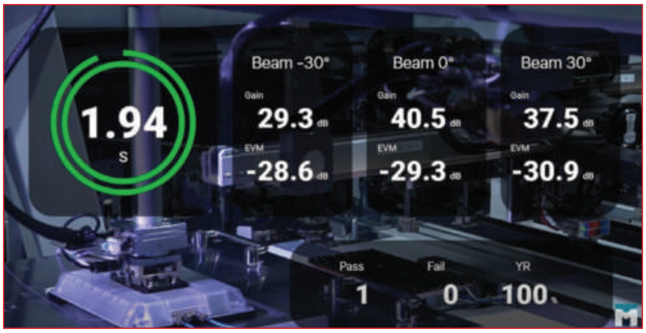

Fig. 10 **Demonstration measurements of the XBeam 3D integrated with auto tester.**

improves production efficiency and provides feedback to design engineering teams.

Like the XBeam 2D, the 3D cube can be customized for testing different modules with various form factors and operating frequencies based on the same testing approach. Both version of XBeam are software driven and powered by AI. ***Table 1*** summarizes the capabilities of the 2D and 3D versions of XBeam, and ***Table 2*** compares the capabilities of XBeam to the CATR and horn antenna testing configurations.

SUMMARY

The AiP is a key architecture for mmWave systems and devices, and the XBeam 2D and 3D test solutions offer a comprehensive way to test these systems. They can evaluate system performance—antenna patterns, EIRP, EVM—with the efficiency needed for production environments. Test times are typically 100x faster than can be achieved by traditional methods. With up- and down-conversion, the XBeam family interfaces with sub-6 GHz measurement instruments, further improving TCO. The XBeam test modules are compact and compatible with production handlers, and the AI-driven system software helps gain insight into AiP performance. ■

TABLE 1

COMPARISON OF XBEAM 2D AND XBEAM 3D

	XBeam 3D	*XBeam 2D*
Radiation Pattern Measurement	2D & 3D	2D
Measurement Speed	1 s for 2D Pattern 10 s for 3D Pattern	1 s for 2D Pattern
Elevation Steering Measurement	•	
Azimuth Steering Measurement	•	•
Size (28 GHz)	0.12 m^3	0.02 m^3
Weight	Heavy	Light

TABLE 2

COMPARISON OF OTA OPTIONS

	CATR	*XBeam 3D*	*XBeam 2D*	*Horn*
Measurement Speed	Slow	Fast	Very Fast	Fast
Pattern Measurement	•	•	•	
Elevation Steering Measurement	•	•		
Azimuth Steering Measurement	•	•	•	
Size (Same Frequency)	Big	Small	Very Small	Small
AiP Optimized		•	•	

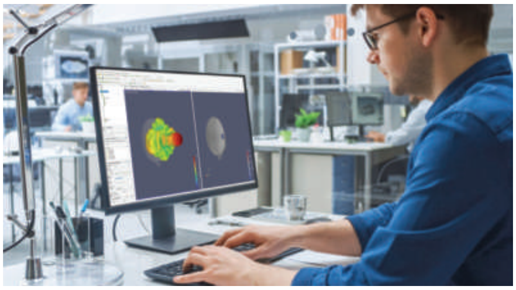

Powerful, Affordable 3D EM Simulation

CENOS
Riga, Latvia

RF engineers often lack the time to conduct thorough studies to select the best simulation software for antenna design, so they opt for a well-known platform, which can be overwhelming to learn and quite expensive. If the design team is part of a big corporation, cost is likely not a major consideration; broad capability and accuracy are most important. However, for a small to medium-sized organization with a limited budget and a design team of just a few engineers who want to learn quickly, is there a better option?

CENOS™ RF simulation software was developed for engineers in small and medium-sized organizations who expect simple and basic functions for simulation. CENOS RF enables them to perform antenna design and optimize antenna placement on a larger structure—even without having prior simulation experience. The platform is easy to learn, and its capabilities handle most antenna design and placement scenarios on systems as varied as drones, satellites, GPS trackers, IoT devices, robots, medical devices and other sensors.

CENOS RF is reasonably priced and offers free onboarding, which enables new users to get results quickly. Also, it is unique among simulation software with its immediate support via a live chat capability built in the software.

CENOS COMPARED TO OTHER SOFTWARE

CENOS RF stands out from the leading software platforms such as CST and Ansys HFSS with its ease of use, self-paced learning and immediate support from a dedicated contact person. Although software like CST and HFSS have wider functionality that is designed to satisfy almost every application, even niche ones, CENOS' functionality was focused on the most common applications, with ease of use prioritized.

The simulation platform comes with predefined simulation groups for components, such as waveguide, filters, couplers and multi-port networks and antennas, such as microstrip/PCB, horns, reflectors, wire and patch arrays (see ***Figure 1***). Its analysis capabilities enable optimizing the placement of an antenna within a device or system to maximize the radiation pattern while using the least amount of space. CENOS RF's visualization tools help users optimize performance and then share the results (see ***Figure 2***).

FEATURES

CAD file support — Users can upload STEP files and, in most cases, the mesh is created automatically (see ***Figure 3***). Recent tests yielded 75 percent conversion of all CAD fields; the remaining 25 percent needed manual meshing.

Recalculation and analysis — All settings are kept if a user wants to recalculate the model with changed parameters. If a geometric parameter is changed, the CAD file can be reloaded; all model parameters are retained, and the mesh is automatically

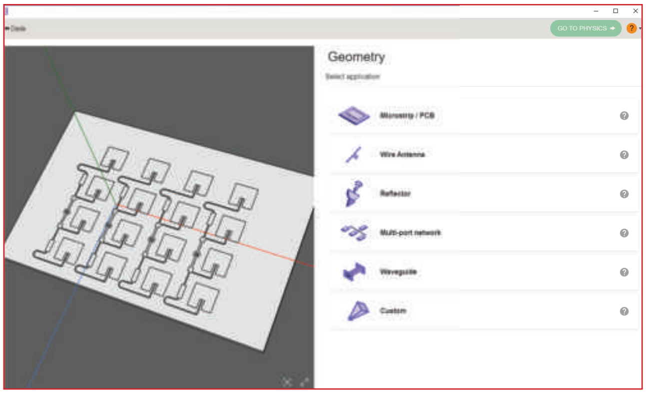

Fig. 1 Antenna types predefined in CENOS.

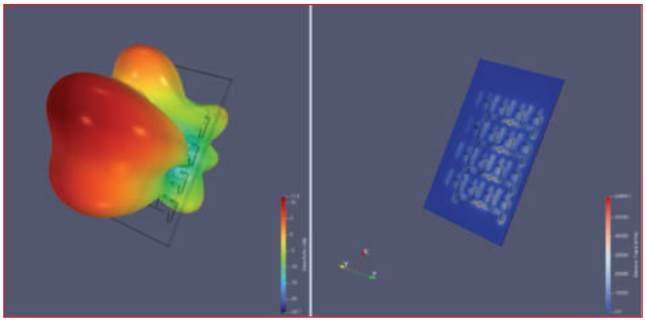

Fig. 2 CENOS visualization capabilities include the structure's geometry and EM fields. A patch array is shown.

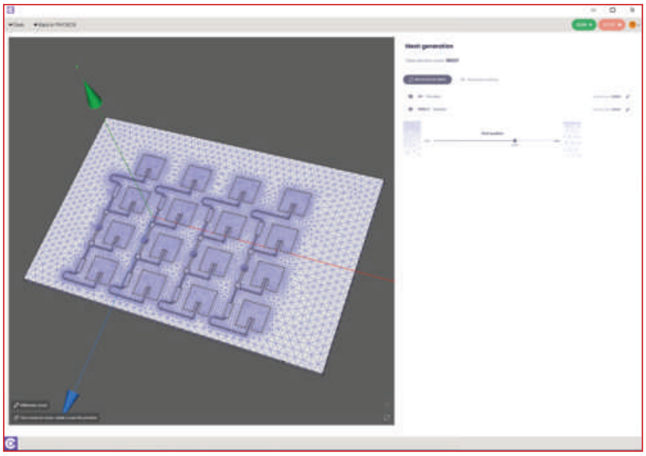

Fig. 3 Mesh generation screen. The mesh is automatically created from most imported STEP files.

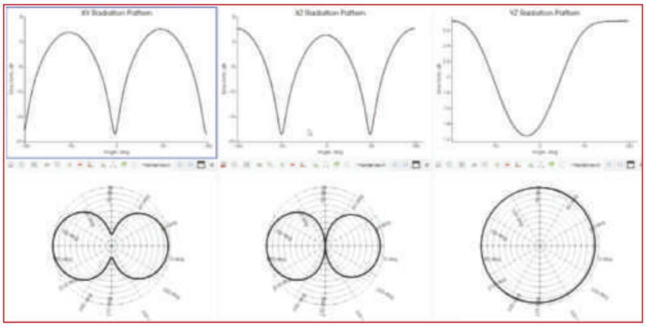

Fig. 4 Simulation results are easily summarized in a PDF report.

rebuilt, whether generated by CENOS or controlled manually.

Reporting of simulation results — Following simulation, CENOS RF provides a PDF report of the simulation results, a one-page summary of the analysis that is easily shared (see ***Figure 4***).

CENOS' RF simulation software was developed for engineers looking for a powerful and time-efficient simulation with advanced instant support that comes with an affordable price tag. Its pricing enables small to medium-sized organizations to have an internal EM simulation capability and not rely on outside consultants. Additionally, users praise two capabilities: 1) instant 24/7 support via the in-software chat, one of the most appreciated features because it keeps users from getting "stuck" and 2) the PDF reports.

CENOS, Riga, Latvia
www.cenos-platform.com

110 GHz DC Blocks and Bias Tees

HYPERLABS is expanding its 100+ GHz components by introducing DC blocks (DCBs) and bias tees (BTs) operating to 110 GHz. The HL9439 DCB and HL9449 BT operate from 160 kHz to 110 GHz. The devices are also offered as 95 GHz versions with part numbers HL9438 for the DCB and HL9448 for the BT. All four products support 200 Gbps PAM4 communications systems, high speed analog-to-digital conversion, frequency response testing for differential devices and many other ultra-broadband applications.

Both the 110 GHz DCB and BT are available with 11 or 30 V breakdown voltage, with the BT having a maximum DC current rating of 175 mA. The DCBs and BTs are available as matched pairs, offering optimized phase and amplitude matching for the best differential signaling.

With connectors, the standard housing for the HL9438/9 DCBs measures 1.067 x 0.525 x 0.535 in., and the standard housing for the HL9448/9 BTs measures 1.95 x 1.30 x 0.53 in. Both the DCB and BT have 1.0 mm connectors at each port, alternate connectors are available. Every unit is hand built and tested in Louisville, Colo. S-parameter data and demonstration units are available, either directly from HYPERLABS or from your local sales representative.

In addition to these 100+ GHz offerings, HYPERLABS is revising its entire component product line to cover 110 GHz. Founded in 1992 and privately owned, HYPERLABS sells ultra-broadband components reaching 110+ GHz, including power splitters, BTs, pickoff tees, DCBs and transition time converters. HYPERLABS' instrumentation line includes the industry's first USB powered and controlled time domain reflectometry instruments, controlled impedance analyzers, signal path analyzers, samplers and harmonic mixers.

HYPERLABS INC.
Louisville, Colo.
www.hyperlabs.com

mmWave Semiconductor Production Test System Rivals "Big Iron" ATE

Marvin Test Solutions' GENASYS Semi is an advanced, open-architecture mmWave semiconductor test platform that delivers features and performance rivaling proprietary, "big iron" automatic test equipment (ATE) systems.

The GENASYS Semi TS-900e-5G series is the first production 5G mmWave semiconductor test solution capable of providing vector correlated, gap-free measurements across the frequency band to 53 GHz. Featuring Keysight's PXIe VNA instrumentation and capable of supporting up to 20 independent, parallel measurement channels, the TS-900e-5G delivers exceptional measurement performance, repeatably and scalability.

Its modular, open platform architecture is flexible when faced with changing test needs, simplifying digital, analog and RF test resource expansion and updates. The compact design can be configured as a benchtop system or with an integrated manipulator without affecting measurement performance or system throughput. The high performance test interface delivers proven and repeatable connectivity to the device under test, with configurable receiver interface pin blocks so users can easily upgrade the receiver interface as test needs change or add new applications.

GENASYS Semi solutions are compatible with industry probe stations, device handlers (Opus 3, TEL, Seiko Epson E8040/ E8080) and manipulators (Reid-Ashman OM-1069, inTest). This simplifies integration into existing production facilities to meet the high throughput production demands of outsourced semiconductor assembly and test.

The ATEasy® Test Executive and Integrated Development Environment is included with all GENASYS Semi systems. It's an easy-to-use software development environment with an integrated and customizable test executive for executing, sequencing, debugging and analyzing faults. It provides a full suite of digital and parametric test capabilities so users can quickly develop and maintain their test applications.

Marvin Test Solutions
Irvine, Calif.
www.marvintest.com

Complete Solution for mmWave 5G Radio Units

Discover the breadth of ADI's sub-6 GHz and mmWave 5G portfolio through a complete 28 GHz 4T4R 5G RU with ADI ICs and antenna IP.

Analog Devices Inc.

www.analog.com/en/education/education-library/videos/6311758639112.html

Post Quantum Hacks, Quantum Key Distribution for SmallSats and the Fully Entangled Future

In this Constellations Podcast, Kratos welcomed Dr. Mark Adams, associate professor of Electrical & Computer Engineering at Auburn University, to discuss the basics of quantum information processing, how QKD ups the game in data transmission security and moving from the BB84 scheme to fully entangled microwave sources for small satellites.

Kratos Defense

https://bit.ly/3BWZWcz

Microchip MMIC Amplifier Awareness

Meet your application's needs and integrate high linearity, low noise MMICs with Microchip's low noise RF amplifiers, prescalers and control products.

Microchip Technology Inc.

https://bit.ly/3ymyTpR

Qorvo Delivers 20 W Output Power for Ku-/K-Band SATCOM

Qorvo's QPA1724 GaN PA delivers breakthrough performance and 20 W power for commercial and defense SATCOM.

Qorvo

www.youtube.com/watch?v=GdZthq8UdMM

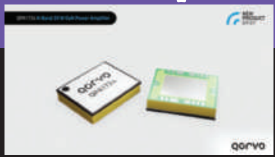

Rogers MCC in CPV Applications

In the latest Olivier's Twist blog post, Stefan Lutter presents two possible solutions using micro channel coolers (MCC) in concentrated photovoltaics (CPV) that could be used to better store renewable energy in the future.

Rogers Corp.

https://bit.ly/3f0MyvU

Optimom 2MP Turnkey Optical Modules

Powered by Teledyne's proprietary image sensor technology, Optimom has been designed to ensure there is minimum development effort required for vision-based embedded systems for robotics, logistics, drones or laboratory equipment. Watch the video to learn more.

Teledyne e2v

www.youtube.com/watch?v=4B0CELrxGVMwatch?v=GdZthq8UdMM

NEW PRODUCTS

FOR MORE NEW PRODUCTS, VISIT WWW.MWJOURNAL.COM/BUYERSGUIDE FEATURING VENDORVIEW STOREFRONTS

COMPONENTS

V-Band Transceiver
VENDORVIEW

Model SSC-6336337012-SFSF-S1-NU2 is a V-Band transceiver sub-assembly that transmits +12 dBm from 50 to 75 GHz through a horn antenna with 15 dBi gain to yield +27 dBm effective isotropic radiated power. The receiver includes a quadrature mixer and a low noise amplifier that achieves 18 dB conversion gain with 25 dB sideband rejection. The local oscillator uses an active ×6 multiplier with input signal power of -3 dBm. The receiver noise figure is 7 dB and the IF bandwidth covers 1 to 2 GHz.

Eravant
www.eravant.com

Wideband Power Dividers

The PD-8008-S-PM is an upgrade from the PD-8008-S that raises the bar for wideband power dividers with even tighter phase matching. The original PD-8008-S, is economically priced, a compact design, high-quality and an incredible value, but IFE created an even better part with ±3 degrees of phase balance across the same bandwidth. IFE still produces the same great PD-8008-S, but the PD-8008-S-PM will meet more requirements with just one part. Request information and a quote today.

I.F. Engineering
www.ifengineering.com

5G Tx/Rx Module

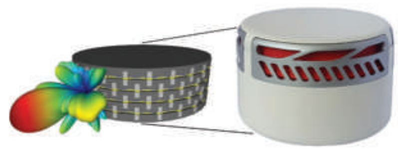

The innovative 5G Tx/Rx module, designed and manufactured by IMST, is a front-end module covering the 5G Ka-Band from 24.25 up to 29.5 GHz. The 24 beamformer ICs feed 2 × 96 antenna elements, all dual linear polarised. The module generates in standard configuration 48 beams with flexible polarization (LHCP, RHCP, dual linear, etc.) Four beams can be generated simultaneously. Scanning performance is 360 degrees in azimuth and ±45 degrees in elevation. The dual polarised antenna elements are based on a combined metal and dielectric waveguide design.

IMST GmbH
www.imst.com

mmWave Controlled Components

General Microwave Corporation is a key partner with major OEMs and primes, having been chosen for broad and comprehensive understanding of mmWave controlled components. General Microwave offers a wide range of mmWave products operating in the 18 to 40 GHz frequency range including catalog attenuators, switches and phase shifters as well as integrated microwave assemblies. If it's a standard catalog unit or a highly customized mmWave product designed specifically for high performance, General Microwave can provide products to support your requirements.

Kratos/General Microwave Corporation
www.kratosmed.com

Coaxial Frequency Mixer
VENDORVIEW

Mini-Circuits' model ZMDB-653H-E+ is a coaxial frequency mixer ideal for up-conversion and down-conversion in mmWave systems, with RF and LO frequency range of 20 to 65 GHz and IF range of DC to 20 GHz. It works with +15 dBm LO power and handles RF inputs to +21 dBm, with typical conversion loss of 11 dB. The mixer is supplied in a housing measuring 0.56 ×0.56 × 0.34 in. (14.22 × 14.22 × 8.64 mm) with three 1.85-mm female connectors.

Mini-Circuits
www.minicircuits.com

Switched Bit Attenuator
VENDORVIEW

Quantic PMI Model SBA-400M1400M-63DB-6B-SFF is a bi-directional switched bit attenuator operating from 400 to 1400 MHz. Designed to be switched between a low loss state and six set attenuation states. The attenuation range is 0 to 63 dB with 1 dB resolution. The settings are selected by six independent bit controls.

Quantic PMI
www.pmi-rf.com

CABLES & CONNECTORS

Conexctivity® Group

The Fischer family founded Conexctivity® Group to meet the connectivity challenges posed by the emergence of new cross-functional and scalable ecosystems, from locally interconnected devices and sensors to cloud-managed IoT platforms. The group's R&D department, which has doubled in size over the last five years, is strengthening its teams with new expertise, especially in signal integrity engineering, embedded electronics, the cloud and IoT. The family-owned technology group is accelerating the development of its two business activities, Fischer Connectors® and Wearin'®, towards the same entrepreneurial vision.

Fischer Connectors
www.conexctivity.com

Adaptor for VNAs
VENDORVIEW

MIcable NMD2.4MM female to NMD2.92MM male adaptors are suited for vector network analyzers (VNAs) with NMD2.4MM male or NMD2.92MM female ports, they have excellent electrical and mechanical performance with maximum VSWR at 1.15:1 at 40 GHz and durability at 5000 cycles minimum. They are used to protect the ports from accidental damage due to direct contact or wear caused by frequent DUT load and unload, and also avoid of the decline of testing accuracy and service life.

Fujian MIcable Electronic Technology Group Co.,Ltd
www.micable.cn

RF Cable Product Line
VENDORVIEW

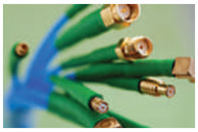

ExpressRF™ is Swift Bridge Technologies' most affordable RF cable product line. These cable assemblies are flexible and offer low signal loss across a broad frequency range, DC through 65 GHz. Cable sizes compatible with all connectors designed for RG402 and RG405 coax. These entry level cables provide an ideal solution for cost-sensitive applications which don't require the highest level of performance. Time delay matched pairs to within 1 ps available.

Swift Bridge Technologies
www.swiftbridgetechnologies.com

Important Information

Registration

https://apmc2022.org/b/registration.html

Technical Program

https://apmc2022.org/program/program_1.html

Conference Schedule

Tue, Nov. 29	Wed, Nov. 30	Thu, Dec. 01	Fri, Dec. 02
Workshops Short courses	Technical sessions -Oral sessions -Interactive forum Opening session -Keynote addresses Welcome ceremony	Technical sessions -Oral sessions -Interactive forum SDC Banquet	Technical sessions -Oral sessions -Interactive forum -Young Professionals -WIE/WIM Award Ceremony
	Microwave Exhibition 2022		

Organized and sponsored by
The Institute of Electronics Information and Communication Engineers (IEICE) of Japan

Supported by
Ministry of Internal Affairs and Communications

Special Collaboration with
Yokohama Convention & Visitors Bureau

Ministry of Internal Affairs and Communications

Technical Sponsors
IEEE MTT-S
IEEE AP-S
European Microwave Association (EuMA)
Union Radio-Scientifique Internationale (URSI)
IEEE MTT-S Japan/Kansai/Nagoya Chapters
IEICE Technical Committee on Microwaves
IEICE Technical Committee on Electronics Simulation Technology
IEICE Technical Committee on Integrated Circuits and Devices
IEICE Technical Committee on Electron Devices
IEICE Technical Committee on Antennas and Propagation
IEICE Technical Committee on Electromagnetic Compatibility
IEICE Technical Committee on Wireless Power Transfer
IEICE Technical Committee on Microwave Photonics and Terahertz Photonic-Electronics Technologies
Japan Society of Electromagnetic Wave Energy Applications
Japan Institute of Electronics Packaging
IEEJ Investigating R&D Committee on Innovative Advanced Application Technology of Electromagnetic Waves in the 5G/Beyond 5G Era
IEEJ Technical Committee on Communications
IEEJ Research Committee on MBSE / MBD / Digital Twin for Communications
IEEJ Research Committee on ICT-based Smart Technologies and Their Social Implementation
IEEJ Research Committee on Communication Technologies Promoting Ubiquitous Work
IEEJ Investigating R&D Committee on High-frequency Magnetics
JSPS R024 Electromagnetic-Wave-Excited Reaction Field
JSPS University-Industry Cooperative Research Committee 187th committee on Metamaterials
Wireless Power Transfer Consortium for Practical Applications

[Chair, Steering Committee] c/o Real Communications Corp. 3F Shinmatsudo S bldg., 1-409 Shinmatsudo, Matsudo 270-0034, Japan Phone: +81-47-309-3616, Fax: +81-47-309-3617, Email: mweapmc@io.ocn.ne.jp

UNITED STATES POSTAL SERVICE®

Statement of Ownership, Management, and Circulation (Requester Publications Only)

1. Publication Title: Microwave Journal	2. Publication Number: 3 9 6 _ 2 5 0	3. Filing Date: 9/30/22
4. Issue Frequency: Monthly	5. Number of Issues Published Annually: 12	6. Annual Subscription Price (if any): DOM $120 FOR $200
7. Complete Mailing Address of Known Office of Publication (Not printer) (Street, city, county, state, and ZIP+4®): Horizon House Publications, Inc. 685 Canton St., Norwood, MA 02062-2610		Contact Person: Barbara Walsh Telephone (Include area code): (781)769-9750 X2025

8. Complete Mailing Address of Headquarters or General Business Office of Publisher (Not printer)

Same as Above

9. Full Names and Complete Mailing Addresses of Publisher, Editor, and Managing Editor (Do not leave blank)

Publisher (Name and complete mailing address)
Carl S. Sheffres, Horizon House Publications, Inc., 685 Canton St., Norwood, MA 02062-2610

Editor (Name and complete mailing address)
Patrick Hindle, Horizon House Publications, Inc., 685 Canton St., Norwood, MA 02062-2610

Managing Editor (Name and complete mailing address)
Jennifer DiMarco, Horizon House Publications, Inc., 685 Canton St., Norwood, MA 02062-2610

10. Owner (Do not leave blank. If the publication is owned by a corporation, give the name and address of the corporation immediately followed by the names and addresses of all stockholders owning or holding 1 percent or more of the total amount of stock. If not owned by a corporation, give the names and addresses of the individual owners. If owned by a partnership or other unincorporated firm, give its name and address as well as those of each individual owner. If the publication is published by a nonprofit organization, give its name and address.)

Full Name	Complete Mailing Address
Horizon House Publications, Inc.	685 Canton St., Norwood, MA 02026-2610
William M. Bazzy, CEO	685 Canton St., Norwood, MA 02026-2610
Ivar A. Bazzy, President	685 Canton St., Norwood, MA 02026-2610
Jared M. Bazzy, Vice President	685 Canton St., Norwood, MA 02026-2610
Joan B. Eagan, EVP	685 Canton St., Norwood, MA 02062-2610

11. Known Bondholders, Mortgagees, and Other Security Holders Owning or Holding 1 Percent or More of Total Amount of Bonds, Mortgages, or Other Securities. If none, check box. → ☒ None

Full Name	Complete Mailing Address

12. Tax Status (For completion by nonprofit organizations authorized to mail at nonprofit rates) (Check one)
The purpose, function, and nonprofit status of this organization and the exempt status for federal income tax purposes:
☒ Has Not Changed During Preceding 12 Months
☐ Has Changed During Preceding 12 Months (Publisher must submit explanation of change with this statement.)

Publication Title: Microwave Journal		14. Issue Date for Circulation Data Below: YTD	September 30, 2022
Extent and Nature of Circulation: 50 K		Average No. Copies Each Issue During Preceding 12 Months	No. Copies of Single Issue Published Nearest to Filing Date
a. Total Number of Copies (Net press run)		25,399	26,988
b. Legitimate Paid and/or Requested Distribution (By mail and outside the mail)	(1) Outside County Paid/Requested Mail Subscriptions stated on PS Form 3541. (Include direct written request from recipient, telemarketing, and Internet requests from recipient, paid subscriptions including nominal rate subscriptions, employer requests, advertiser's proof copies, and exchange copies.)	16,987	18,157
	(2) In-County Paid/Requested Mail Subscriptions stated on PS Form 3541. (Include direct written request from recipient, telemarketing, and Internet requests from recipient, paid subscriptions including nominal rate subscriptions, employer requests, advertiser's proof copies, and exchange copies.)		
	(3) Sales Through Dealers and Carriers, Street Vendors, Counter Sales, and Other Paid or Requested Distribution Outside USPS®	6,314	6,726
	(4) Requested Copies Distributed by Other Mail Classes Through the USPS (e.g., First-Class Mail®)		
c. Total Paid and/or Requested Circulation (Sum of 15b (1), (2), (3), and (4)) ▶		23,300	24,883
d. Non-requested Distribution (By mail and outside the mail)	(1) Outside County Nonrequested Copies Stated on PS Form 3541 (include sample copies, requests over 3 years old, requests induced by a premium, bulk sales and requests including association requests, names obtained from business directories, lists, and other sources)	785	574
	(2) In-County Nonrequested Copies Stated on PS Form 3541 (include sample copies, requests over 3 years old, requests induced by a premium, bulk sales and requests including association requests, names obtained from business directories, lists, and other sources)		
	(3) Nonrequested Copies Distributed Through the USPS by Other Classes of Mail (e.g., First-Class Mail, nonrequestor copies mailed in excess of 10% limit mailed at Standard Mail® or Package Services rates)		
	(4) Nonrequested Copies Distributed Outside the Mail (Include pickup stands, trade shows, showrooms, and other sources)	1,285	1,013
e. Total Nonrequested Distribution [Sum of 15d (1), (2), (3) and (4)]		1,963	1,587
f. Total Distribution (Sum of 15c and e) ▶		25,264	26,470
g. Copies not Distributed (See Instructions to Publishers #4, (page #3)) ▶		135	518
h. Total (Sum of 15f and g)		25,399	26,988
i. Percent Paid and/or Requested Circulation (15c divided by 15f times 100) ▶		92.2%	94.0%

16. Electronic Copy Circulation	Average No. Copies Each Issue During Previous 12 Months	No. Copies of Single Issue Published Nearest to Filing Date
a. Requested and Paid Electronic Copies ▶		
b. Total Requested and Paid Print Copies (Line 15c) + Requested/Paid Electronic Copies (Line 16a) ▶		
c. Total Requested Copy Distribution (Line 15f) + Requested/Paid Electronic Copies (Line 16a) ▶		
d. Percent Paid and/or Requested Circulation (Both Print & Electronic Copies) (16b divided by 16c × 100) ▶		

☐ **I certify that 50% of all my distributed copies (electronic and print) are legitimate requests or paid copies.**

17. Publication of Statement of Ownership for a Requester Publication is required and will be printed in the November 2022 issue of this publication.

18. Signature and Title of Editor, Publisher, Business Manager, or Owner: Carl S. Sheffres, Publisher — *Carl S. Sheffres* — Date: 9/30/22

I certify that all information furnished on this form is true and complete. I understand that anyone who furnishes false or misleading information on this form or who omits material or information requested on the form may be subject to criminal sanctions (including fines and imprisonment) and/or civil sanctions (including civil penalties).

NewProducts

High Speed & High Density Multicoax Cable Assemblies

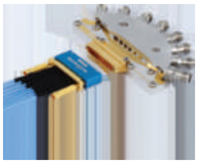

Withwave's high speed and high density multicoax cable assemblies (WMX Series) provide a wide range of multiple coax connectors and flexible cable assemblies. Specially, Board Edge Socket type is excellent signal integrity solutions at edge of PCB for benchtop testing and automated test equipment to meet increasing demands of semiconductor test equipment and optical testing industries.

withwave co. ltd
www.with-wave.com

AMPLIFIERS

X-Band Radar Solid-State Power Amplifier

COMTECH PST introduced a new GaN amplifier for ground or surface X-Band radar applications. The AB linear design operates from 9.2 to 9.7 GHz frequency range over an instantaneous bandwidth of 500 MHz. Development of this product is for a TWT replacement. The amplifier design features self-protection for load VSWR, duty factor, pulse width, temperature, as well as a graceful degradation in case of a RF power module failure. Comtech supports custom configurations and features are available as well as specific power levels up to 16 kW.

Comtech PST
www.comtechpst.com

Exodus AMP2026LC-1 KW

VENDORVIEW

Exodus AMP2026LC-1 KW is a rack-integrated powerhouse. Covering 2.0 to 6.0 GHz, produces 1000 W minimum output, 1500 W typical. Excellent gain flatness with a minimum power gain of 60 dB. Included are amplifier monitoring parameters for forward/reflected power in dBm and watts, VSWR, as well as voltage, current and temperature sensing on a large color touchscreen for optimum reliability and ruggedness. Unprecedented 18U total drawer height.

Exodus Advanced Communications
www.exoduscomm.com

SOURCES

Signal Generator

The RI8586 provides in a single TIM slot an ultra-low phase noise, continuous wave fast switching signal generator, tunable from 25 MHz to 24 GHz with 1 Hz resolution. This microwave source functions as a standalone instrument as well as a component of Roos' System RF (SyRf) core technology with multiple RF ports to support seamless system integration with Cassini's signal sources and test set TIMs. Fast phase settling enhances the speed and accuracy of vector-calibrated VNA measurements.

Roos Instruments Inc.
www.roos.com

SOFTWARE

Schematic Editor

VENDORVIEW

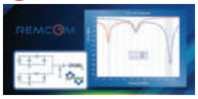

Remcom announced expanded capabilities within its schematic editor in the latest release of XFdtd® 3D EM Simulation Software, including support for diplex matched antennas and new efficiencies aimed at streamlining antenna design workflows and shortening design cycles. XFdtd's schematic

editor is a novel electromagnetic simulation tool that combines matching network analysis with full-wave results, making it ideal for complex antenna design applications involving multi-state and multi-port aperture or impedance tuners and corporate feed networks with digital phase shifters.
Remcom Inc.
www.remcom.com

ANTENNAS

Quad-Ridge Flared Horns

Quad-Ridge Flared Horns are antenna feeds designed for wideband microwave reflector antennas. The feeds exhibit a constant phase center and remains focused over a 6:1 frequency range. The lower frequency range starts at 0.5 to 4 GHz. Feeds are dual linear polarized designed for a given half-angle, HA, subtended by the reflector or sub-reflector facing the feed, specified for each feed. Operated at temperatures in the 4K to 350K range with minimal performance change.
Cosmic Microwave Technology, Inc.
www.cosmicmicrowavetechnology.com

TEST & MEASUREMENT

R140B 1-Port 14 GHz Analyzer

VENDORVIEW

Copper Mountain Technologies has launched the new R140B 1-port 14 GHz analyzer. R140B is an enhanced version of its predecessor—the R140 reflectometer—featuring faster measurement speeds, wider IFBW and an improved dynamic range. The R140B incorporates a new housing design similar to CMT's R60, taking advantage of enhanced heat exchange characteristics and a sturdy USB shroud. It will feature a new connector assembly, which includes four different port connector options (N male, female; 3.5 mm male, female).
Copper Mountain Technologies
www.coppermountaintech.com

Handheld Portable Source Module

OML offers mixer and sources that are specifically designed for handheld portable solutions for mmWave analysis measurement, maximizing portable field applications. Expand your signal analysis capabilities to 6G research, development and deployment 90 to 220 GHz and beyond. M08H4BDC covers 90 to 140 GHz, M06H6BDC 110 to 170 GHz and M05H-6BDC 140 to 220 GHz.
OML Inc.
www.omlinc.com

Bookend

Reviewed by: Doug Jorgesen

Bogatin's Practical Guide to Prototype Breadboard and PCB Design

Eric Bogatin

Eric Bogatin claims that his "Practical Guide to Prototype Breadboard and PCB Design" 'is for the casual user, not the power user.' His 521-page, 25-chapter opus to electronic subsystem development is definitely more than an introduction, however. It is practical as claimed, but provides tremendous depth and detail on both the general practices involved in designing the printed circuit board (PCB) and the electrical system intended to function on it. He begins with high level discussions on PCB architecture and electrical design topics, then moves to detailed discussions of a variety of PCB challenges including entire chapters on topics like 'Design for Bring Up.' In addition, PCB topics like trace routing and current handling, Bogatin devotes a significant portion to good component selection and system design processes. Throughout the book, the reader has the impression of having a conversation with a very experienced and eagerly helpful colleague that has seen it all before.

This is a valuable resource for the PCB designers among *Microwave Journal*'s readership (almost all of us), but there are two important limitations. First is that the book is so expansive it can be difficult to absorb the information in a timely manner. There are many great tips, but it wasn't clear how to extract them without reading through the entire book. Second, it is targeted primarily toward analog or high frequency system designers. The theory is couched in the terms of signal integrity and analog design rather than more familiar microwave terms (e.g. rise time degradation rather than lowpass filtering). For the most part this is a helpful perspective rather than distracting. If you have space for one book on PCB design on your shelf, "Practical Guide to Prototype Breadboard and PCB Design" is recommended.

ISBN 13: 9781630819620
Hardcover: $139
Digital download and online: $119
To order this book, contact:
Artech House
685 Canton St.
Norwood, MA 02062
800-225-9977
or
16 Sussex St.
London, SW1V 4RW, UK
+44 (0)20 7596 8750

Advertising**Index**

Sales Representatives

Eastern and Central Time Zones
Michael Hallman
Associate Publisher
(NJ, Mid-Atlantic, Southeast, Midwest, TX)
Tel: (301) 371-8830
Cell: (781) 363-0338
mhallman@mwjournal.com

Shannon Alo-Mendosa
Northeastern Reg. Sales Mgr.
(New England, New York, Eastern Canada)
Tel: (781) 619-1942
Cell: (978) 501-9116
salomendosa@horizonhouse.com

Submitting ad material?
Visit: www.adshuttle.com/mwj
(866) 774-5784
outside the U.S. call +1-414-566-6940

Pacific and Mountain Time Zones
Brian Landy
Western Reg. Sales Mgr.
(CA, AZ, OR, WA, ID, NV, UT, NM, CO, WY, MT, ND, SD, NE & Western Canada)
Tel: (831) 426-4143
Cell: (831) 713-9085
blandy@mwjournal.com

International Sales
Richard Vaughan
International Sales Manager
Tel: +44 207 596 8742
rvaughan@horizonhouse.co.uk

Ed Kiessling
(781) 619-1963
ekiessling@mwjournal.com

Germany, Austria, and Switzerland (German-speaking)
WMS.Werbe- und Media Service
Brigitte Beranek
Tel: +49 7125 407 31 18
bberanek@horizonhouse.com

France
Gaston Traboulsi
Tel: +44 207 596 8742
gtraboulsi@horizonhouse.com

Israel
Dan Aronovic
Tel: +972 50 799 1121
aronovic@actcom.co.il

Korea
Young-Seoh Chinn
JES MEDIA, INC.
Tel: +82 2 481-3411
corres1@jesmedia.com

China
Shenzhen
Annie Liu
ACT International
Tel: +86-0755-86-0755
anniel@actintl.com.hk

Shanghai
Linda Li
ACT International
Tel: 86-021-62511200
lindal@actintl.com.hk

Wuhan
Phoebe Yin
ACT International
phoebey@actintl.com.hk

Beijing
Cecily Bian
ACT International
Tel: +86 135 5262 1310
cecilyb@actintl.com.hk

Hong Kong, Taiwan, Singapore
Floyd Chun
ACT International
Tel: +86-13724298335
floydc@actintl.com.hk

Japan
Katsuhiro Ishii
Ace Media Service Inc.
Tel: +81 3 5691 3335
amskatsu@dream.com

Corporate Headquarters: 685 Canton Street, Norwood, MA 02062 • Tel: (781) 769-9750

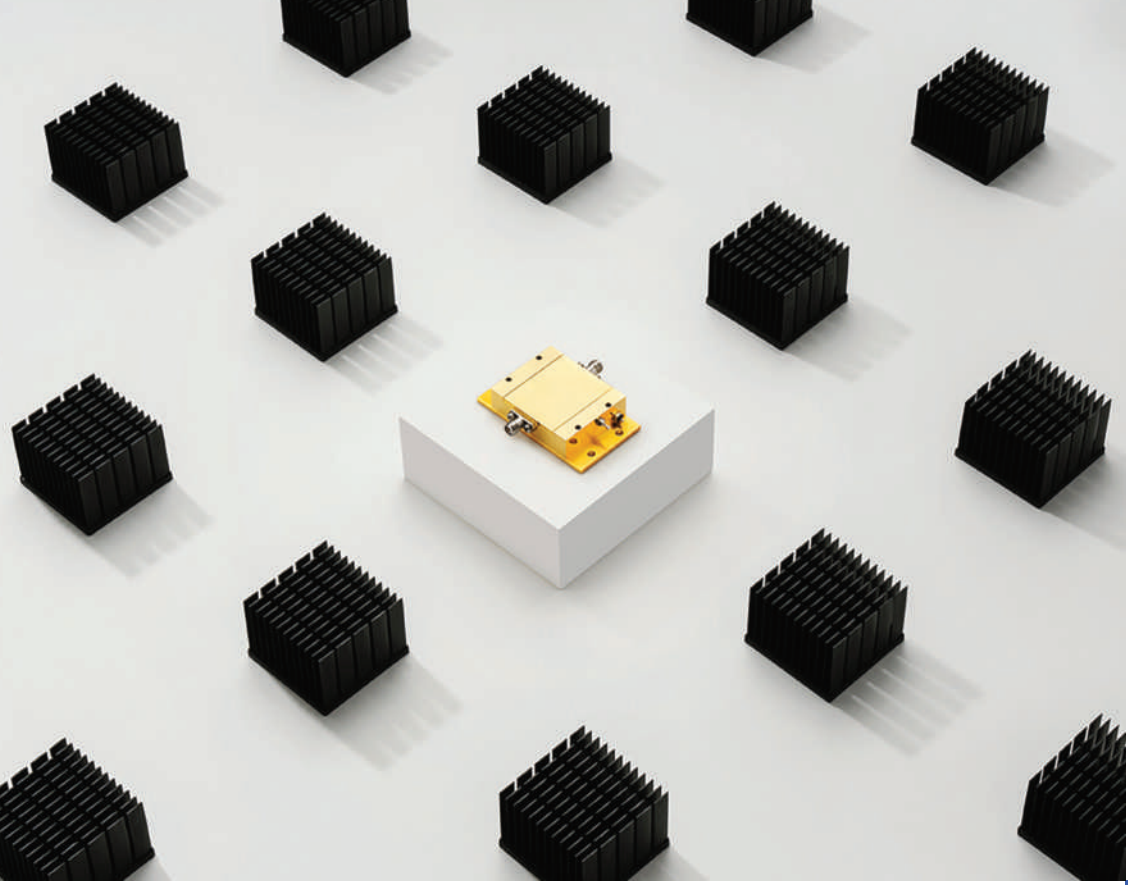

FABS and LABS

RLC Electronics: A 63-Year Commitment to Excellence in Passive Microwave Components

RLC Electronics is a classic example of the multi-generation family enterprises that helped create and sustain the U.S. microwave industry. Triggered by World War II, the U.S. government funded the development of technology and systems for radar, electronic warfare and military communications. This built the defense industrial base—companies such as GE, ITT, Raytheon, RCA—and these large firms created opportunities for entrepreneurial pioneers to supply the complex components needed by these systems. Alan Borck, a 1947 graduate of Rensselaer Polytechnic Institute who began his career at ITT, started RLC Electronics in 1959, the year after *Microwave Journal* was first published. His son Doug joined the company in 1978, followed by his grandson Jeff in 2011.

RLC Electronics designs and manufactures a wide-ranging portfolio of RF components developed for high performance, high reliability defense platforms—also well-suited for test and measurement applications. Highlighting the comprehensive product line are electromechanical switches and filters of all configurations, including cavity, microstrip, stripline, lumped element, tubular and suspended substrate. Myriad passive products complete the portfolio, including power dividers/combiners, couplers, hybrids, terminations, detectors, limiters and fixed or variable attenuators. High power and broadband versions of most products are available, an additional specialty of the company.

RLC encourages customers to bring their specific requirements and, with such a catalog and long heritage, RLC turns new designs quickly, supported by a dedicated prototype lab. The engineering team's experience averages 25 years per person and is complemented by the latest circuit and electromagnetic simulation software: HFSS, Keysight Genesys, PCFilt, Touchstone and internally designed tools. Using a consultive approach to product development, engineers work directly with customers to ensure timely communication.

RLC Electronics builds all products internally, sourcing purchased parts from U.S. suppliers. The capabilities at its 22,000 square-foot facility in Mount Kisco, N.Y., include assembly in a class 1000 clean room, machining, RF testing, environmental conditioning and qualification. RLC Electronics holds a Secret facility security clearance, AS9100D and ISO 9001:2015 certifications and is ITAR registered. It has the distinction of being the only switch manufacturer with products on the Qualified Product List of the U.S. Defense Logistics Agency.

To maintain its reputation for leadership, RLC Electronics continues to innovate. Its technology roadmap has several themes: 1) miniaturizing coaxial products while expanding the number of surface-mount designs, 2) extending the frequency coverage above 40 GHz (above 65 GHz for switches), 3) increasing power handling and 4) lowering cost by redesigning and reducing production time. To enable these changes, RLC is increasing the integration of its products, combining several technologies within a single package, and adding to its software tools to improve simulation accuracy and reduce development time.

RLC has an impressive set of customers. In defense, the list spans all the leading firms: BAE Systems, Boeing, General Atomics, Lockheed Martin, Northrop Grumman and Raytheon. In test and measurement, Keysight and Rohde & Schwarz are notable. However, the business is not restricted to the U.S., with products supporting Elbit Systems, IAI Elta, Indra, Leonardo and the defense ministries of allies.

63 years after Alan Borck started RLC Electronics, the company remains a successful, family run and globally renowned business, with a staff of some 40 committed to excellence. RLC fosters an environment of learning, opportunity and advancement for a team focused on customer satisfaction, growth and continued leadership in the RF/microwave components industry.

www.rlcelectronics.com

ENGINEERING EVOLVED

RADIAL COMBINERS

Multi-kW Power Levels ✦ **Low Loss Circuits** ✦ **Custom Designs Available**

Model	Type	Frequency (MHz)	Power (W CW)	Peak Power (W) 10% DC	Insertion Loss (dB)	VSWR	Connector Type
D9816	8-Way	330-530	10,000	50,000	0.25	1.30:1	3 1/8" EIA, N-Female
D8454	8-Way	370-450	10,000	50,000	0.25	1.30:1	3 1/8" EIA, N-Female
D5320	12-Way	470-860	500	5,000	0.30	1.30:1	All N-Female
D10119	4-Way	700-4200	2,000	15,000	0.30	1.35:1	13-30 DIN-Female, N-F
D10603	32-Way	900-925	50,000	150,000	0.15	1.25:1	WR975, 7/16-Female
D10795	32-Way	900-930	25,000	150,000	0.25	1.20:1	WR975, 4.3-10-F
D9710	8-Way	1000-2500	2,000	10,000	0.30	1.40:1	1 5/8" EIA, N-Female
D8182	5-Way	1175-1375	1,500	25,000	0.40	1.35:1	1 5/8" EIA, N-Female
D6857	32-Way	1200-1400	4,000	16,000	0.50	1.35:1	1 5/8" EIA, N-Female
D11896	4-Way	2000-2120	4,000	40,000	0.25	1.40:1	WR430, 7/16-Female
D11828	4-Way	2400-2500	3,000	25,000	0.20	1.25:1	WR340, 7/16-Female
D10851	8-Way	2400-2500	8,000	50,000	0.20	1.25:1	WR340, 7/16-Female
D11433	16-Way	2700-3500	2,000	20,000	0.30	1.35:1	WR284, N-Female
D11815	16-Way	2700-3500	6,000	40,000	0.30	1.35:1	WR284, N-Female
D12101	6-Way	2750-3750	2,000	20,000	0.35	1.40:1	WR284, N-Female
D9582	16-Way	3100-3500	2,000	16,000	0.25	1.50:1	WR284, N-Female
D12102	6-Way	5100-6000	850	4,500	0.35	1.35:1	WR159, N-Female
D12484	6-Way	8200-8600	600	700	0.35	1.25:1	WR112, SMA-Female
D12485	6-Way	9000-11,000	500	700	0.40	1.35:1	WR90, SMA-Female

Specifications subject to change without notice.

Werlatone, Inc. 17 Jon Barrett Road Patterson, NY 12563 845-278-2220 sales@werlatone.com www.werlatone.com